THEORETICAL INVESTIGATIONS OF THE BULK AND SURFACE PROPERTIES OF PRISTINE AND DOPED PUO_2

by

SHAFAQ AMDANI MOTEN

Presented to the Faculty of the Graduate School of

The University of Texas at Arlington in Partial Fulfillment

of the Requirements

for the Degree of

DOCTOR OF PHILOSOPHY

THE UNIVERSITY OF TEXAS AT ARLINGTON

May 2017

Acknowledgements

Dr. A. Ray who never gave up on me.

Dr. Weiss who always supported me.

Dr. Huda who mentored me through all small and big things. Not only was your support amazing academically but your advice and counsel were my saving grace many a times and for that I thank you from the bottom of my heart.

Defense Committee Members: Dr. Weiss, Dr. Zhang, Dr. Koymen, Dr. Musielak and Dr. Huda, I extend my deepest gratitude for sharing your time and considerable knowledge with me. Your guidance has been invaluable.

TACC computing services

UTA Computing services

UTA Physics department - The staff and the department are among the best.

Dedication

To my family for without you all, there is no me. Your unwavering support has been amazing.

My mother who is the best person I know and without whom this would not have been feasible. She never said no to any request and in fact made it so easy to take her for granted at times. Thank you.

My father always believed in me. He is the giant whose shoulder I stand on.

My sister in law or more accurately, the little sister I always wanted, Saman, who in conjunction with my mother, took care of my children when I was working or crashing and never said no when I needed her.

My brothers who always had my back even or especially at 2 in the morning. Faraz for his good cheer even in the midst of chaos and giving me another sister of my heart by marrying Uzma. Ahad for being my go-to-computer programmer and general tech. Yes I know, I have the most expensive tech for free. Moiz for being a jack-of-trades and master at being a great brother.

My in-laws for their prayers, support and words of encouragement.

My children who are my guiding light. Aayaan and Rayhan, the two of you will always be my angels even when you are determined to be little devils. Mama loves you!

My loving husband who only wanted my happiness and thus endured my crabbiness at times. You were my support day in and day out.

I love you all beyond all imaginings.

Above all, for Allah's blessing in all areas of my life, jazakallah.

April 17, 2017

Abstract

THEORETICAL INVESTIGATIONS OF THE BULK AND SURFACE PROPERTIES OF PRISTINE AND DOPED PUO_2

Shafaq Amdani Moten, PhD

The University of Texas at Arlington, 2015

Supervising Professor: Name Muhammad N. Huda

Plutonium oxides is of widespread significance due its application in nuclear fuels, space missions, as well as the long-termed storage of plutonium from spent fuel and nuclear weapons. The processes which refine and store plutonium bring many other elements in contact with the plutonium metal and thereby affect the chemistry of the plutonium. Pure plutonium metal corrodes to an oxide in air and the most stable form of this oxide is the stoichiometric plutonium dioxide, PuO_2. Defects such as impurities and vacancies can form in the plutonium dioxide before, during and after the refining processes as well as during storage. Studying the interaction between transition metals and plutonium dioxide is critical for better, more efficient storage plans as well as gaining insights to provide a better response to potential threats of exposure to the environment.

Using density functional theory, first the bulk and then the PuO_2 (111) surface of the pristine system have been investigated. The bulk results show that magnetic configurations of PuO_2 are still debatable and need to be tested further in surface slabs. The pristine periodic slab models of the 110 and the 111 surface were examined to find surface properties and slab size effects. Surface modelling of up to six molecular layers were conducted. Ferromagnetic (FM) and anti-ferromagnetic (AFM) configurations were considered with and without spin-orbit coupling for the 1x1 slab. Furthermore, the effects

of periodicity were explored between 1×1 and 2×2 super cell of the anti-ferromagnetic surface slabs. Results based on surface energies, work function, band gaps and density of states show that 5-6 molecular layer is sufficient for surface modelling. Except for the outer layer, the surface in general retains the Mott-insulator property.

Secondly the effects of impurity and defects in the bulk and then the PuO_2 (111) surface have been investigated. Our study explores the interaction of a few key metals within the plutonium dioxide structure which have a likelihood of being exposed to the plutonium dioxide powder. We explored a doped system of substituted metal impurity within PuO_2 supercell. We repeated the calculations with an additional oxygen vacancy. An impurity defect manifests itself at the bottom of the conduction band and affects the band gap of the unit cell. Our results reveal interesting volume contraction of PuO_2 supercell when one plutonium atom is substituted with a metal atom. The volume of the doped system was further contracted with the addition of a single nearby oxygen vacancy.

Extending the impurity dopant to a 5 molecular layer 2x2 surface, three layers were highlighted. The outer layer, exposed to the vacuum, the bulk layer in the middle of the slab and the subsurface layer sandwiched between the bulk and the outer layer. Oxygen vacancy in the outer layer is less favorable than the bulk-layer and effects the Pu-Pu distances beyond the layer that it resides in. Zirconium impurity tested on each highlighted layer, has negative formation energy and has minimal impact on the slab beyond its nearest neighbor atoms. The non-pristine slab contracts due to dopants and defects as well but retains the Mott-insulating character with a zirconium impurity within the PuO_2 (111) surface slab.

Table of Contents

List of Figures

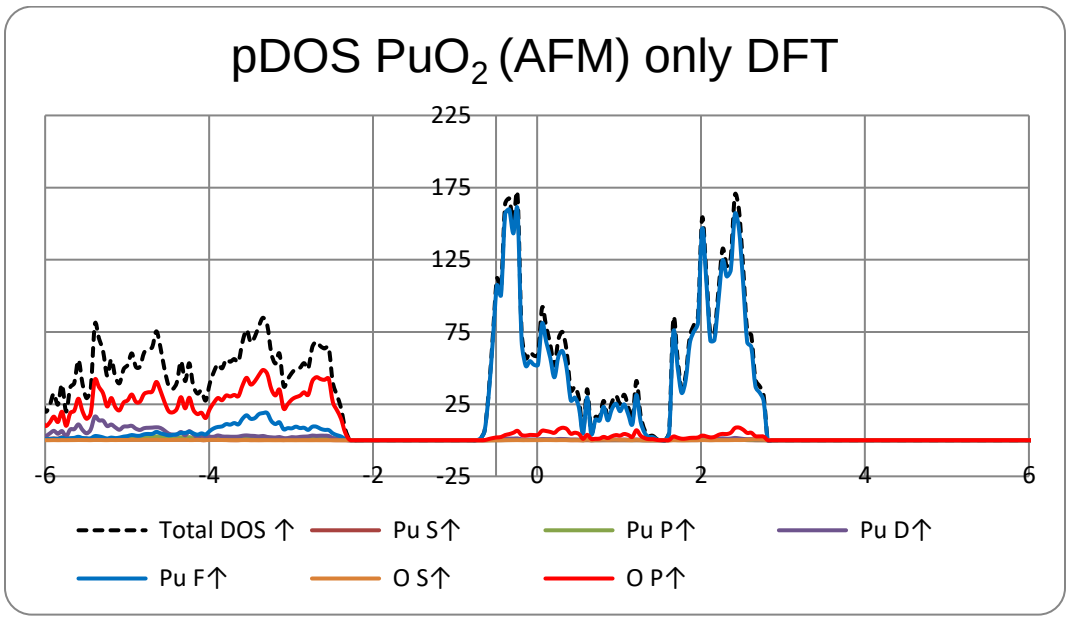

List of Tables

Chapter 1

Introduction

Plutonium oxides, especially PuO_2, is of widespread significance due it application as nuclear fuels, space missions, and it is the form that plutonium from spent fuel and nuclear weapons is stored in long-termed storage. The problem with experimentation arises because not only is PuO_2 radioactive and emits alpha particles but it has impurities and characteristics unique within each sample which makes reproducibility difficult.

As plutonium oxides are readily formed when plutonium is in contact with oxygen, it is the most abundant compound of plutonium in stock. While historically plutonium metal was produced in reactors, presently the feed material for preparation and refining of metallic plutonium is via the recycling of spent nuclear fuel, residues and scrap materials. Globally there are more than 90 tons of excess plutonium and about 500 tons of separated plutonium as of 2015 [1]. Plutonium metal is used for irradiation targets and fuels, for weapon components or stored directly. These processes in turn brings many other elements in contact with the plutonium metal and thus affecting the surface chemistry of the plutonium. Since this metal tends to corrode to an oxide when it encounters dry or moist air, it forms a powder of plutonium oxide. The most observable form of this oxide is plutonium dioxide, with the stoichiometric PuO_2 being the most stable[2]. PuO_2 is used within MOX fuels, heat sources and storage.

Plutonium dioxide while stable still has impurities due to the presence of other elements in the initial plutonium metal, the process it underwent and age. Some of these impurities are due to transition metal elements which may introduced within the plutonium dioxide before, during and after the refining processes as well as during storage.

NASA manages a Radioisotope Power system (RPS), which maintains its current and future space exploration endeavors. 238-Pu in form of plutonium dioxide is utilized in space missions as power and heat source for its RPS systems[3]. In those conditions, it is in close contacts with other materials including transition metals. If plutonium dioxide is released into the environment, the dioxide will come in contact with these elements in the immediate surrounding and can be exposed to living organisms which can be highly harmful due to radioactivity. Studying the interaction between transition metals and

plutonium dioxide is critical for better, more efficient storage plans as well as gaining insights in order to provide a better response to potential threats of exposure to the environment.

Plutonium Background

Plutonium is a radioactive, actinide element which is only found in trace amounts naturally and was not discovered until after systhesis of the element in 1940 by Seaborg, McMillan, Kennedy and Wahl. This element sits near the middle of the actinide series, thus having 5f electrons in its valence shell. Elements to the left have delocalized (bonding) electrons, while elements to the right of plutonium demonstrate more localized (nonbonding) character. Due to plutonium's position in the middle, the electrons seem to be in a unique state of being neither fully bonding nor localized. This leads to uniquely challenging electronic interactions and elusive physical and chemical behavior[4]. So far, the metal has exhibited six solid allotropes at ambient pressure and six chemical oxidation states. Plutonium is highly reactive and can be erratic with its changing density and phases in regards to temperature, pressure, chemical additions, and time. Plutonium can expand as it solidifies and the freshly machined surface will tarnish within minutes. It is a complex element whose mystery has not been fully solved and yet it is utilized every day around the world.

Plutonium was first produced by bombarding uranium with deutrons in a cyclotron at Berkeley. This initially produced neptunium:

$$^{238}_{92}U + ^{2}_{1}H \rightarrow \ ^{238}_{93}Np + 2^{1}_{0}n$$

Neptunium then decayed by beta emission, to form Pu-238:

$$^{238}_{93}Np + (\beta -) \underset{2.1d}{\longrightarrow} ^{238}_{94}Pu$$

with half-life of 88 years. Pu-239 was produced via bombardment of U-238 by neutrons to produce U-239 which decayed to Np-239 which further decayed to Pu-239 with half-life of 24,110 years. A single kilogram of Pu-239 can produce enough heat to generate 8 million kilowatt-hours of electricity and is most commonly formed in a typical nuclear reactor[5].

Today, a third of the energy produced in the nuclear plants comes from plutonium. Plutonium has fifteen isotopes, all of which are radioactive and are significant in fast neutron reactors as they are fissionable with neutrons.

The elemental Pu metal is in the actinide series, straddling a boundary between itinerant and localized 5f electrons states. While the light actinides' on the left of plutonium exhibit itinerant behavior, the heavier actinides on the right exhibit more localized 5f electron states[6]. Various theoretical[7–9] approaches have been applied to understand this complex behavior. However, the heavier actinides pose a challenge to correctly capture the effects of strong electron-electron interactions. Additionally, as plutonium metal oxidizes when exposed to air or moisture, the study of its oxides, notably the stoichiometric PuO_2, is necessary to gain insights into the plutonium-oxygen interaction process[10,11].

Plutonium dioxide Background

PuO_2, a fluorite type structure belonging to space group Fm-3m with an experimental lattice parameter of 5.396 Å[12], is toxic and highly reactive to exposed air or aqueous solution thereby making it problematic to store or use it as part of a mixed-oxide (MOX) fuel safely.

Plutonium oxidation is dependent upon metal surface area, particle size, oxygen concentration in the reaction zone, temperature, alloying and surface conditions such as oxide coating and surface imperfections. In general, the interactions of the actinide materials with environmental species begin on its surfaces. The theoretical and experimental studies of the electronic and other properties of the actinide surfaces are very important to understand the mechanism of surface corrosion in presence of environmental gases, and to find a suitably eco-friendly way of managing nuclear waste material. Thorough understanding of the properties of clean surfaces of Pu-oxides is a necessary first step to understand the surface interactions with other environmental species. Relevant past experimental and theoretical works are summarized here before focusing on the current ab initio modeling of the bulk and surface of pristine and doped PuO_2.

Although a plethora of bulk studies of PuO_2[13–19] have been done, only a few theoretical studies on PuO_2 surfaces [14,20–24] and some experimental studies[25–28] exist in literature. While recent studies [22–24] concluded that the (111) surface is the most stable is in agreement with ours, they did not for example, include spin-orbit coupling, which is necessary to accurately describe the Pu 5f electron behavior.

Plutonium and plutonium dioxide exposure to transition metal

Within nuclear fuel cycle, in Light water reactors (LWR) plutonium is exposed to zirconium alloys (containing other transition elements such Fe, Cr and Ni) which are utilized as cladding material to make

the fuel pin. Other transition elements such as Mo, Ru, Rh, Pd, Tc form small metal inclusions in the uranium oxide fuel. At the end of the process, spent nuclear fuel contains plutonium content which is the greatest source of plutonium inventory currently. Plutonium can form numerous compounds and complexes in the environment and during chemical processing.

Refining plutonium from the spent fuel can be divided into two major groups, aqueous and non-aqueous processes. The large-scale separation and purification of plutonium has been primarily attained using the Plutonium, Uranium, Reduction, Extraction (PUREX) liquid–liquid extraction process. This process separates uranium and plutonium from many other kinds of fuels and targets, including commercial power reactor fuels. The most significant transition element in this process is iron (Fe) which is used as part of the chain reaction in PUREX.

Aqueous processes dissolve plutonium contaminated items and impure plutonium dioxide in an acidic solution and passing the solution through various processes to end up with purified plutonium dioxide. The purified plutonium dioxide is then thermally treated to reduce moisture by high temperature (850 degree Celsius) calcination process. This may be followed by dry operations. In these processes, the plutonium comes in contact with other materials such as a Zr- alloy cladding, the MgO crucible, the Fe from the reactions, impurities within the feed which include a few transition metal elements of Cr, Mn, Fe, Ni, Cu, Zn, Mo, Rh, Ag, Ir, and Pt[2]. These purified dioxides inherently include some impurities. The plutonium dioxide material can be destined for further processing depending on its constituents and the destination of the sample. Plutonium dioxide can either sent for long-term storage, utilized in the as part of MOX (mixed-oxide) fuel in the nuclear cycle or be destined to be used as power source for space missions.

As mentioned above, plutonium dioxide can be an important fuel for heat and power sources for space exploration. For deep space heat source, pellet(s) of $^{238}PuO_2$ are packed within platinum-rhodium clad in LWRHU (Light Weight Radioisotope Heater Unit). Another example is the SNAP-19 and Transit systems fueled by $^{238}PuO_2$ with molybdenum cermets[29]. Voyager missions employed 24100-W heat sources of 238- PuO_2 each enclosed in an iridium shell. Current systems employ heat source generators fueled by a hot-pressed 150 g pellet of $^{238}PuO_2$ encapsulated in an iridium alloy (iridium-0.3% tungsten)

container. With these missions $^{238}PuO_2$ comes in contact with transition metals at the source but can potentially be released into the environment due to mechanical failures.

Environmental concerns of PuO_2 being accidently released into the earth's atmosphere are valid as once the plutonium dioxide is released in to the air, it can have long lasting detrimental effects. Generally, PuO_2 is insoluble but once in the environment, a small fraction of it can be transported to humans and then resides in certain organs and bone surfaces for a long period of time. Once residing in the body, alpha radiation (from 238-Pu) kill or damaged a fraction of the nearby cells. A small fraction of the damaged cell would mutate and produce significant detrimental effects such as cancer or genetic abnormalities[3]. Once PuO_2 has entered the blood, it circulates and is deposited primarily in the lungs and the skeletal system (up to 45% each) and approximately 90% of the PuO_2 deposited in the lungs will eventually be transferred to the blood (ICRP 1986). Human plasma[30], largest component of blood, contains Fe, Zn, Cu, Mo, Cr, V, Mn and Ni which are transition metal elements and thus interaction between them and the plutonium dioxide needs to be studied.

Plutonium oxide storage

The stored plutonium oxides can be "pure" dioxides (91-97% PuO_2) with approximately 3-8% impurities or dioxides with larger impurities. The pure dioxide exhibit fairly stable behavior however when the oxides have impurities larger than 8% which include chloride salt (NaCl, KCl, $CaCl_2$ and $MgCl_2$) and other impurities such as oxides and compounds of Ca, Mg, Fe and Ni, then the storage concerns are increased as the behavior is less understood[2].

According to DOE-STD-3013-2012 standard, to store plutonium oxides, the moisture content to be packaged must be less than 0.5 wt% at the time of the packaging. The container it is stored in shall consist of two individually sealed, nested containers to isolate the material from the environment. This material must be fabricated of 304L or 316 L series stainless steel or equivalent. 304 L stainless steel is synthesized from Iron with atleast 10% Cr and mined as $FeCr_2O_4$ while 316L stainless steel has the addition of Molybdenum[3]. These transition metal elements can come in contact with the stored plutonium oxides.

All of the above scenarios include plutonium dioxide in possible contact with transition metals, from Ti-22, V-23, Cr-24, Mn-25, Fe-26, Ni-28, Cu-29, Zn-30, Zr-40, Mo-42, Rh-45, Ag-47, Ir-77, to Pt-78,

which are all possible contaminants to the plutonium dioxide. They have far-reaching concerns and require further studies to determine the effect of these impurities on plutonium oxides, especially PuO_2, the highest stoichiometric stable form of these oxides.

Transition Metals Background

Transition metals are elements whose atoms have a partially filled d-orbital and are included in the 'd-block of the periodic table. These elements make cations with an incomplete d sub-shell.

Magnesium (Mg) with atomic number 12 is not a transition metal but a paramagnetic, alkaline earth metal with a hexagonal close-packed (hcp) crystal structure and a +2 oxidation state. It is the fourth most abundant element on earth and is highly flammable.

Chromium, Z=24, is used most extensively to produce stainless steel via the use of ferrochromium. Chromium(IV) oxide (CrO2) is a magnetic compound and chromates can prevent corrosion of steel under wet conditions.

Manganese, Z=25, combines with other elements such as iron and is used to prevent corrosion on steel. It oxidizes easily and while all oxidation states have been observed from -3 to +7, most stable form is of +2.

Iron, Z=26, an essential element in all forms of life is also the most abundant metal refined currently. Iron is used to manufacture steel, with stainless steel having 10.5% chromium and other metal alloys such as nickel, molybdenum and copper to enhance strength, workability and corrosion resistance.

Nickel, Z=28, is magnetic at or near room temperature like iron. The nickel atom has two electron configurations, [Ar] 3d8 4s2 and [Ar] 3d9 4s1with disagreement as to which is more stable[31].

Zirconium, Z=40, in small amounts is used as alloying agents to prevent corrosion. Previously, small concentrations of zirconium in plutonium have been determined for a single measurement[32].

Molybdenum, Z=42, oxidizes in minerals and has one of the lowest coefficients of thermal expansion among commercially used metals and used as an alloy in high-grade stainless steel

Transition metals in plutonium dioxide

In the processes described above, the plutonium comes in contact with other materials such as a Zr- alloy cladding, the MgO crucible, the Fe from the reactions, impurities within the feed which include a few transition metal elements including but not limited to Cr, Mn, Fe, Ni, and Mo. Plutonium is reactive

and each sample has its own characteristic and impurities. When in an environment with oxygen, a metal may lose electrons to the oxygen and become oxidized. Note that oxides of metals with higher oxidation states are more covalent and tend to be acidic. Conversely oxides of metals in lower oxidation states that of less than or equal to +3 have a significant ionic character and tend to be basic. Pluotonium, with its five oxidation states is a complex metal that is highly reactive, and when exposed to air, it oxidizes into a powder. Thus these purified dioxides inherently include some impurities. The plutonium dioxide material can be destined for further processing depending on its constituents and the destination of the sample. Plutonium dioxide can either sent for long-term storage or utilized in other capacity[33–35]. The stored plutonium oxides are considered to be "pure" dioxides (91-97% PuO_2) if they have approximately 3-8% impurities[4].

Each of the above scenarios include plutonium dioxide in possible contact with transition metals, which are all possible contaminants, characterized as major, minor or trace impurities[36], to the plutonium dioxide. They have far-reaching concerns and require further studies to determine the effect of these impurities on plutonium oxides, especially PuO_2, the highest stoichiometric stable form of these oxides. While zirconium and plutonium solubility has been shown to exist[32] and there have been other studies of transition metals with plutonium[37,38], and plutonium dioxide[39] there has been no systematic study of transition metal impurity within plutonium dioxide. Studying the interaction between transition metals and plutonium dioxide is critical for better, more efficient storage plans as well as gaining insights to provide a better response to potential threats of exposure to the environment. In this study, we focused on six of these transition metals listed in

Table 1 as well as the alkaline earth metal magnesium because these are the elements that most likely to come in contact with the plutonium dioxide powder that is stored in storing facilities around the nation.

Table 1: Element Properties[40] unless otherwise noted.

El(Z)	O(8)	Mg(12)	Cr(24)	Mn(25)	Fe(26)	Ni(28)	Zr(40)	Mo(42)	Pu(94)
Oxi-state	**-2,** -1, +1,+2	**+2**, +1	−1, −2, −4, +1-+5, **+6**	-3 to +7, **+2**	−4, −2, −1, +1, **+2**, **+3**, +4, +5, +6	-2, -1, 1, +**2**, 3, +**4**	-2, +1, +2, +3, +**4**	-1, -2, -4, 1-3, **+4**, +5, **+6**.	1-8, **+4**
Atomic r(A):	cubic	1.60	1.28	1.27	1.26	1.24	1.60	1.39	1.59
C. Atomic r[Å][41]	0.48	1.45	1.66	1.61	1.56	1.49	2.06	1.90	1.75
Ionic Radii [Å]	0.60	1.50	1.40	1.40	1.40	1.35	1.55	1.45	1.75
Covalent Radii [Å]	0.73	1.30	1.27	1.39	1.25	1.21	1.48	1.45	1.87[42]
Van-der-Waals Radii [Å]	1.52	1.73	2.00[43]	2.2[43]	2.0[43]	1.63	2.2[43]	2.1[43]	2.37[44]
Crystal Radii [Å]	1.21	0.86	1.76	0.81	0.69	0.70	0.86	0.79	1.00
Sp. Gr (no)	C12/m1 (12)	P63/ mmc (194)	Im-3m (229)	I-43m (217)	Im-3m (229)	Fm3m (225)	P63/mm c (194)	Im-3m (229)	P21/m (11)
Struct	Mono	hcp	Bcc	bcc	bcc	fcc	hcp	Bcc	mono
Mag.	para	Para	AFM	para	FM	FM	Para	Para	para
A	5.403	3.2094	2.91	8.9125	2.8665	3.524	3.232	3.147	6.18
B	3.429	3.2094	2.91	8.9125	2.8665	3.524	3.232	3.147	4.822
C	5.086	5.2108	2.91	8.9125	2.8665	3.524	5.147	3.147	10.963
α	90.00°	90.00°	90.00°	90.00°	90.00°	90.00°	90.00°	90.00°	90.00°
β	132.53°	90.00°	90.000°	90.00°	90.00°	90.00°	90.00°	90.00°	101.79°
Γ	90.00	120.00°	90.000°	90.00°	90.00°	90.00°	120.00°	90.00°	90.00°

Chapter 2

Computational Methodologies

Plutonium dioxide is material that is difficult to study experimentally and therefore, theoretical studies can supplement the experimental efforts. Atomic and molecular scale modeling can be used to gain insights into interactions and properties of the material and how they behave with the environment.

According to quantum mechanics, the solution to the Schrödinger's equation, the quantum mechanical wave function contains, in principle, all the information about a given system.

$$H\Psi(x_1, x_2, ..., x_N; R_1, ..., R_N,) = E\Psi(x_1, x_2, ..., x_N; R_1, ..., R_N,) \quad \text{2-1}$$

For an N-body system,

$$\hat{H} = -\sum_{i=1}^{N}\frac{1}{2}\nabla_i^2 - \sum_{A=1}^{M}\frac{1}{2M_A}\nabla_A^2 - \sum_{i=1}^{N}\sum_{A=1}^{M}\frac{Z_A}{r_{iA}} + \sum_{i=1}^{N}\sum_{j>1}^{N}\frac{1}{r_{ij}} + \sum_{A=1}^{M}\sum_{B>A}^{M}\frac{Z_A Z_B}{R_{AB}} \quad \text{2-2}$$

where *A* and *B* run over *M* nuclei while *i* and *j* denote the *N* electrons in the system. We can simplify this Hamiltonian by utilizing the Born-Oppenheimer Approximation. This approximation states that nuclei are 10^3-10^5 more massive than electrons and due to this disparity in masses there will be very little momentum transfer between electrons and nuclei and because their momenta is similar, the nuclei will appear to be standing still in comparison to the fast-moving electrons. This will reduce the Hamiltonian to:

$$\hat{H} = -\sum_{i=1}^{N}\frac{1}{2}\nabla_i^2 - \sum_{i=1}^{N}\sum_{A=1}^{M}\frac{Z_A}{r_{iA}} + \sum_{i=1}^{N}\sum_{j>1}^{N}\frac{1}{r_{ij}} = \hat{T}_{ee} + \hat{V}_{ne} + \hat{V}_{ee} \quad \text{2-3}$$

where these three terms are the electron kinetics, the nuclei-electron attractions and the electron-electron repulsions. While the second term can be straightforward, the electron-electron interaction is can be difficult to compute. The e-e interaction must account for the electronic exchange and correlation, where exchange is refers to the Pauli exclusion force which satisfies the Pauli Exclusion Principle thereby insuring that no two electrons with the same spin can exist in the same orbital. Electron correlation refers to all affects that electrons have to each other that are missed if electrons are treated as independent entities versus particles that interact with each other.

Hatree-Fock method describes the electron-electron interaction by replacing the many-electron wave function by a set of many one-electron function thus having the wave function take on a separable solution form which can be approximated by a single slater determinant[45,46]. This inherently takes into account the Pauli exclusion principle with antisymmetric wavefunction. Thus, Hartree-Fock gives the exact exchange energy but does not account for any correlation. This interaction is too strong to be ignored or treated as perturbation. In fact, correlation energy is defined to the

$$E_{CORR} = E - E_{HF} \qquad 2\text{-}4$$

Therefore a system that takes into account both exchange and correlation energies is necessary. Furthermore it is not possible except for trivially simple cases, to solve the many-body equation exactly. This is because one mole of solid has 10^{28} electrons and the wavefunction has 3N degree of freedom (DOF). Density functional theory is a method of obtaining an approximate solution to the Shrodinger equation using charge density instead of wavefunction thereby reducing the DOF from 3N to 3 variables and a spin component.

Density Functional Theory

Density functional theory (DFT) is a computational modelling method for a many-body system. DFT is based on the principle that ground state properties can be determined by a unique ground state electron density *ρ(r)* and thereby avoids trying to solve the many-electron wave function by exploiting the properties of the electron density distribution, ρ(r).

Thomas Fermi Model represents the first effort to define a density based theory. Thomas Fermi equations together with an assumed variational principle, formulates in terms of electronic density alone. It assumes that the total energy of the electrons, sum of their kinetic and potential energies, comes from the interaction of electrons with one another and via an external potential. External potential is the attraction of the electrons to the nuclei. Furthermore these energies can be determined by *N* and *v(r)*, where *N* is the number of electrons and *v(r)* is the nuclear potential. Although this is the general idea, it leads to inaccuracies due to the limitation from the kinetic energy term as Thomas–Fermi equation does not account for the exchange energy of an atom due to Pauli principle. Thus, it ignores the energetic effects associated with correlation and exchange. A major problem with this theory is that it breaks down when it comes to molecules and fails to predict molecular binding[47].

Hohenberg-Kohn

While many improvements upon the Thomas Fermi model were made, in 1964 Hohenberg-Kohn (H-K) established an exact theory where TF model was an approximation. H-K first theorem states that electron density *p(r)* determines the external potential *v(r)* within a trivial additive constant, thus the ground-state density uniquely determines the external potential. H–K second theorem defines the energy functional for the system and proves that the correct ground state electron density minimizes this energy functional. Thus the ground state energy of the system can be obtained variationally with respect to the density. This can be proven via contradiction or *reductio ad absurdum.* Suppose if *v(r)* and *v'(r)* each giving same electron density ρ(r) for its ground state. Then *H* and *H'* from same ground state density with different normalized Ψ and Ψ'. Taking Ψ' as a trial function for the *H* and applying the variational principle, we get:

$$E_o < \langle \Psi' | H | \Psi' \rangle = \langle \Psi' | H' | \Psi' \rangle + \langle \Psi | H - H' | \Psi' \rangle = E'_o + \int \rho(\mathbf{r}) (v(\mathbf{r}) - v'(\mathbf{r})) d\mathbf{r} \qquad 2\text{-}5$$

Where E_0 and E_0' are ground-state energies for *H* and *H*'. Similarly, we can take the Ψ as a trial function for the *H*' Hamiltonian, to obtain:

$$E'_o < \langle \Psi | H' | \Psi \rangle = \langle \Psi | H | \Psi \rangle + \langle \Psi | H' - H | \Psi \rangle = E_o + \int \rho(\mathbf{r}) (v(\mathbf{r}) - v'(\mathbf{r})) d\mathbf{r} \qquad 2\text{-}6$$

When we add the above two equations, we then obtain the contradiction:

$$E'_o + E_o < E_o + E'_o \qquad 2\text{-}7$$

Since the above is a contraction, it is clear that there exists a unique map between the external potential and the ground state density as *ρ* determines *N* and *v(r)* hence all properties of ground state. This implies that all the energies, including the total energy, is a *functional* of the density. We write this as *E = E[ρ].* The density determines the Hamiltonian, and thereby, the wavefunction. The defined energy functional is

$$E_v[\rho] = T[\rho] + V_{ne}[\rho] + V_{ee}[\rho] = \int \rho(\mathbf{r}) v(\mathbf{r})\, d\mathbf{r} + F_{HK}[\rho] \qquad 2\text{-}8$$

Where, *T[ρ]* is the kinetic energy functional, V_{ne} *[ρ]* is the potential due to the nucleus-electron interaction while V_{ee}*[ρ]* includes the classical electron-electron repulsion term and the non-classical term that is a very elusive quantity and will be addressed shortly.

$$F_{HK}[\rho] = T[\rho] + V_{ee}[\rho] \qquad 2\text{-}9$$

is called the universal function which if known exactly would provide an exact equation for the ground state electron density as it is independent of the external potential, *v(r)*. The challenge is that $F_{HK}[\rho]$ is not known exactly and thus approximations must be taken.

Kohn-Sham

In 1965, Kohn and Sham[48] established an inventive approach to kinetic energy functional T[ρ], which instead of dealing with a set of interacting electrons reduces the problem to a set of non-interacting electrons N_e moving in an effective potential V_{KS}. Thus, it is possible to choose this potential such that the ground state density of the non-interacting system is the same as that of an interacting system subject to a particular external potential V_{ext}. This effective V_{KS} includes the external potential, V_{ext} and the effects of the exchange and correlation interactions.

$$V_{KS}(\vec{r}) = V_{ext}(\vec{r}) + \int \frac{\rho(r')}{|r - r'|} dr' + \frac{\delta E_{\mathrm{xc}}[\rho]}{\delta \rho(r)} \qquad 2\text{-}10$$

And thus the energy functional can now be represented as,

$$E[\rho] = T_s[\rho] + V_{\mathrm{ext}}[\rho] + E_H[\rho] + E_{xc}[\rho] \qquad 2\text{-}11$$

Where the $T_s[\rho]$ is the kinetic energy of the K-S non-interacting system, $V_{ext}[\rho]$ is the external potential due to the nuclei, $E_H[\rho]$ is the Hartree energy and the $E_{xc}[\rho]$ is the exchange-correlation term. Hartree potential describes the Coulomb repulsion between one electron and the total electron density. Here the self-interaction contribution arises, as the one electron being considered is also part of the total electron density, thus this invokes a Coulomb interaction between the electron and itself. Because this self-interaction is unphysical, the correction for it is lumped into third term. To solve Kohn-Sham equations, $E_{xc}[\rho]$ must be specified.

$$E_{xc}[\rho] = T[\rho] - T_s[\rho] + E_{\mathrm{ee}}[\rho] - E_H[\rho] \qquad 2\text{-}12$$

Modeling the $E_{xc}[\rho]$ becomes difficult within KS DFT and thus must be approximated because the exchange-correlation accounts for the difference between the exact ground-state energy and the

energy calculated above. The Kohn-Sham formulation thus succeeds in transforming the N-body problem into N single-body problems, each coupled via the Kohn-Sham effective potential. Note that any DFT algorithm will only calculate the ground state and no excited states.

The simplest approximation is the local-density approximation (LDA), which approximates the function $T[\rho]$ and $E_{xc}[\rho]$ by corresponding energies of a uniform electron gas. While LDA works for simple elements, it falls short when it comes to molecules because these systems have rapidly varying electron densities. Applying the gradient operator to the LDA gives the gradient generalized approximation or GGA of which one flavor is the PBE functional. This functional is used for DFT level of theory throughout this work. For strong coulomb interactions of localized electrons (such as 3d, 5f), LDA or even GGA cannot correctly describe the electronic behavior. To treat these strongly correlated electrons, an additional Hubbard-like term is added as parameters of U for on-site Coulomb and J for on-site exchange. These are usually obtained semi-empirically but can be obtained from ab-initio calculations. A single effective U_{eff} = U-J parameter accounts for Coulomb interaction thereby neglecting any higher order terms[49].

Another way to account for the highly localized electrons is to introduce a portion of Hartree-Fock in the exchange functional which gives rise to hybrid functional. PBE0 is the hybrid functional utilized in this work[50].

DFT computational codes are utilized to investigate the structural, magnetic and electronic properties of molecules, materials and defects. Two different codes were used in this work, WIEN2K and VASP which are described directly below.

WIEN2K

WIEN2K is an all-electron code based on the full-potential linearized augmented plane wave plus local orbitals basis (FP-L/APW+lo). Within the FP-L/APW+lo method, the unit cell is divided into non-overlapping muffin tin spheres and an interstitial region. Inside the muffin tin sphere, the wave functions are expanded using radial functions (solutions to the radial Schrödinger equation) times the spherical harmonics and in the interstitial region, the wave functions are expanded using plane waves. APW+lo basis is used to describe all s, p, d, and f (l=0,1,2,3) states. In this study, the muffin-tin radii have been chosen to be 1.22Å (2.3 Bohr) for plutonium and 0.85Å (1.6 bohr) for oxygen. The basis-set size

correspond to a $R_{MT}K_{MAX}$ =8.0, where R_{MT} is the smallest atomic sphere radius and K_{MAX} is the plane wave kinetic energy cut-off.

In the WIEN2k implementation of hybrid density functional theory can be applied to all electrons where a fraction, α, of the DFT-PBE[51] exchange interaction is replaced by Hartree-Fock (HF) exchange. This was scheme was implemented in a selected set of electrons, namely the correlated electrons, inside the atomic sphere[52]. Therefore, in the case of actinide oxides the hybrid-functional have been applied only to the 5f electrons. The hybrid exchange-correlation energy functional is described by,

$$E_{XC}^{PBE+\alpha HF} = \alpha E_X^{HF} + (1-\alpha)E_X^{PBE} + E_C^{PBE} \qquad 2\text{-}13$$

where E_X^{HF} is the Hartree-Fock exchange, E_X^{PBE} is the PBE exchange functional and E_C^{PBE} is the PBE correlation functional. The parameter *α* denotes the fraction of HF exchange replacing the PBE exchange. In this study we have use *α* = 0.25, which corresponds to the standard value in literature, known as PBE0, and have been shown to work well in different systems[53].

VASP – Vienna Ab-Initio Simulation Package

VASP is a DFT package used for ab-initio quantum-mechanical simulations by using pseudopotentials or the projector-augmented wave (PAW) method with a plane wave basis set. Algorithms are used in VASP to calculate the electronic ground state by optimizing the charge density and the wavefunctions. For the charge density mixing an efficient Broyden/Pulay mixing scheme is used. A self-consistent method is used for the Hamilton with the charge density and then the wavefunction is iteratively optimized. This optimized wavefunctions is then used to calculate a new charge density which is then mixed with the old initial charge density and the loop continues until the convergence criteria is met.

VASP computes an approximate solution to the many-body schrodinger's equation within the DFT theory. Current computations are performed with VASP and based on the DFT with PBE exchange-correlation functional. The common exchange-correlation functionals are local (spin) density approximation (L(S)DA) and generalized gradient approximation (GGA). LDA is defined as a homogeneous electron gas with a point-by-point mapping and GGA is the generalization of LDA by including the contributions from electron density gradient. To better describe correlation effects in some

strongly correlated systems such actinides (5f electrons) and some transition metals (3d electrons) several extensions to LDA and GGA such as L(S)DA(GGA)+U method have been done.

Linear augmented plane waves basis is used for all s,p,d and f states with additional spin-orbit coupling parameter in Pu 5f and 6s to account for strongly correlated system in plutonium and some 3d transition metals.

Computational details particular to each chapter in this work will be furthered described at the beginning of that chapter.

Chapter 3

Pristine PuO_2 Bulk to Surface

Considerable theoretical efforts have been made in the past few decades to studying and understanding the plutonium metal. Because plutonium readily oxides to plutonium dioxide, efforts for understanding this material have been made. Unfortunately, the material is radioactive in all known forms and experimental data is limited. A theoretical understanding is a good initial step in understanding the material. The generalized gradient approximation of the density functional theory implementation on the most common structures of plutonium dioxide builds a platform to further, more in depth studies.

One of the main motivation of this study is the desire to understand the surface corrosion of plutonium dioxide in presence of transition metals. While many papers are devoted to understanding environmental gasses on plutonium, few papers are present that study impact of transition metals on plutonium dioxide.

First we study the bulk of the stochiometric bulk of plutonium dioxide, then do analysis to find the optimal surface of the pristine plutonium dioxide. Once we have a good understanding of the pristine material we can dope the bulk and the surface with impurity as well as the effects of an oxygen vacancy to study the behavior of these doped systems.

Computational Details

Pristine bulk structure and the subsequent high symmetry surfaces were first calculated using the WIEN2K code[54]. Scalar relativistic, i.e. no spin-orbit (NSO) coupling, and spin-orbit (SO) inclusive hybrid density functional theory (hyb-DFT) calculations were performed using the WIEN2k code. WIEN2K is an all-electron code based on the full-potential linearized augmented plane wave plus local orbitals basis (FP-L/APW+lo). APW+lo basis is used to describe all s, p, d, and f (l=0,1,2,3) states. The muffin-tin radii have been specified as 1.22 Å (2.3) bohr for plutonium and 0.85 Å(1.6 bohr) for oxygen. The basis-set size correspond to a $R_{MT}K_{MAX}$ =8.0, where R_{MT} is the smallest atomic sphere radius and K_{MAX} is the plane wave kinetic energy cut-off. For implementation of hybrid density functional theory, a fraction $\alpha=0.25$, of the DFT-PBE[51] exchange interaction is replaced by Hartree-Fock (HF) exchange which is then applied to all 5f electrons as these are considered to be the strongly correlated electrons in the plutonium dioxide system. This fraction has been shown previously to work well in various systems and is known as PBE0.

Bulk System

Plutonium dioxide, PuO_2, is the most stable form of plutonium oxide. It has a powder-like consistency and is olive green at its most pure form. However, the color can vary from sample to sample dependent on the processes from which it was created.

The bulk PuO_2 is a face centered cubic (FCC) crystal with plutonium at cubic and oxygen at the tetrahedral sites. It has a fluorite crystal structure and belongs to space group Fm3m, number 225 with a lattice constant of 5.398Å.

The magnetic configuration of the system is controversial and therefore we test the three magnetic configuration, paramagnetic (NM), ferromagnetic (FM) and anti-ferromagnetic (AFM).

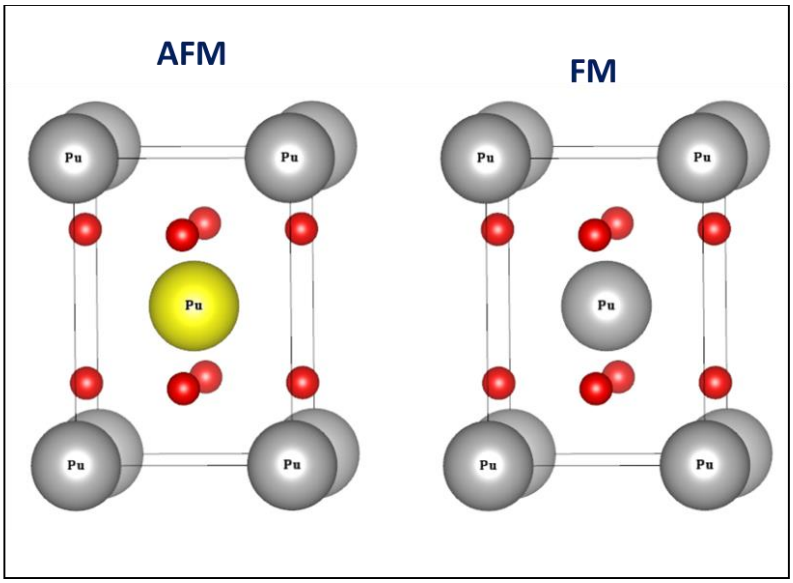

Figure 1: Bulk PuO_2; AFM and FM configurations, where grey plutonium atoms have spin parallel to each other and yellow plutonium atoms have the opposing spin. Red atoms are oxygen atoms with no spin added.

For the bulk, without spin-orbit coupling, the FM was the ground state however with inclusion of spin-orbit coupling, AFM was the ground state. However the differences between the AFM and FM were minute, see Table 2 so a magnetic configuration analysis for the surface is conducted as well.

Table 2: Energy difference relative to the ground state ΔE(eV/unit cell) for bulk PuO_2. AFM with spin-orbit coupling (SO) had the lowest energy.

Magnetic Config.	AFM (SO)	FM (SO)	AFM	FM
Energy Diff (ev)	0.00	0.003	1.215	1.222

High symmetry PuO_2 surfaces can be configured by cleaving bulk PuO_2 along [111], [110] and [001] orientations. Past studies have indicated that the order of surface increasing stability was (001) < (110) < (111).

Surface testing

We have observed that using hybrid DFT, the (111) surface is energetically more stable by 1.4 eV than the (110) surface, where the surfaces were modelled by 5 layers of PuO_2, see Figure 2.

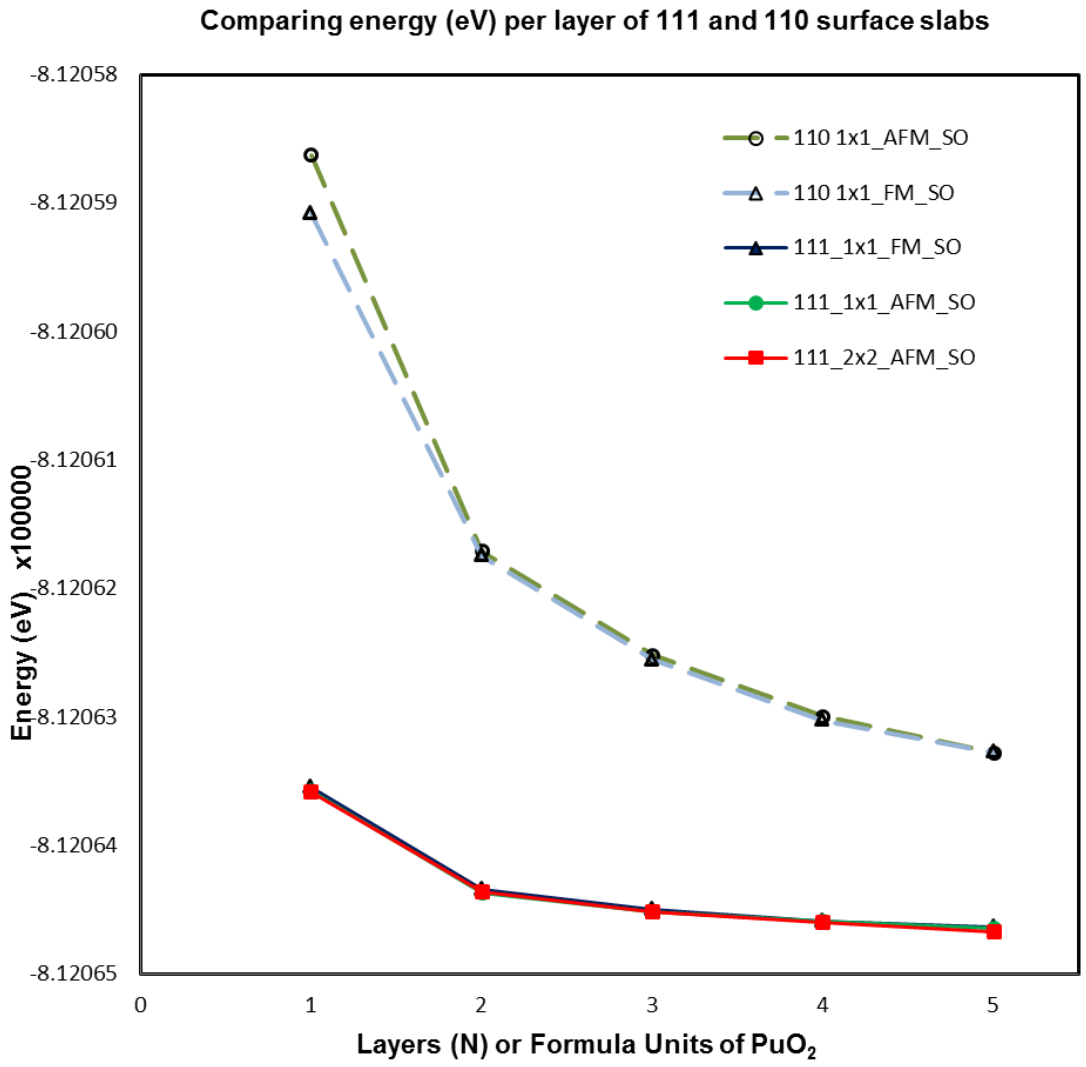

Figure 2: Energy (eV) of (111) and (110) surface slabs at each layer N per formula unit. Each (111) slab layer N is build with three sub-layers of O-Pu-O stacking which generates one stoichiometric PuO_2 per layer N. Note in 2x2 AFM each layer (N) has four stoichiometric PuO_2 per layer N. Note in 2x2 AFM each layer (N) has four stoichiometric PuO_2 and thus the energy at each layer has been scaled by ¼. The (111) surface (solid lines) are lower in energy than the (110) surface (dashed lines).

111 Surface

Thus in this study, only the (111) surface was considered. The surface modeled by periodic slabs of *N* stacked formula units (*N* = 1–6) with a 1×1 and 2×2 (see Figure 3) surface unit cells. It should be noted that for (111) surface, each formula unit comprises of three layers in an O-Pu-O stacking sequence and that the [111] plane of a face-centered cubic system is a hexagonal grid.

The large vacuum region of at least 15 Å was added to avoid any interaction between the periodic faces of the slab. The bulk lattice constants used to construct these AFM and FM slabs were taken from a previous study which employed the same computational parameters as this work[55]. The lattice constants were 5.432Å (AFM SO), 5.427 Å (AFM NSO), 5.440 Å (FM SO) and 5.407 Å (FM NSO), which are less than 1% higher than the experimental lattice parameter of 5.398 Å[8]. The stacking chosen ensured that the slab faces are terminated (with O layer) to yield a zero net dipole along the surface as Tasker [56] has shown that the surface energy will diverge if the dipole moment is non-zero. The 7x7x1 k-point mesh is used for both 1x1 and 2x2 surface slab. The k-point mesh densities were checked against the convergence of total energies of the surfaces. The energy and charge convergence criteria used in the computations are 0.00001eV and 0.0001*e*, respectively. The calculations involved total energy computations; no atomic relaxations were included as Rak et al. have shown that relaxation effects in the PuO_2 (111) slab are quite small[24]. To confirm that relaxation effects were indeed minor, the two layer 2x2 slab was relaxed and found to be in good agreement with the unrelaxed slab. Spin-orbit (SO) coupling interactions were included via a second variation procedure using the scalar relativistic eigenstates with energies below 68 eV (5.0 Ry) as basis.

As mentioned earlier, we only considered the AFM spin arrangement for the 2x2 slab as the 1x1 slab calculation demonstrated that the AFM configuration is very slightly favored over the FM configuration. Note that the monolayer of the 1x1 slab has only one plutonium atom and thus cannot be a true AFM layer however the 2x2 surface monolayer is of a true AFM arrangement with two spin-up plutonium atoms and two spin-down plutonium atoms. For the 1x1 slab, there is only one plutonium for each layer therefore the even layered (2, 4 and 6) slabs have no net magnetic moment with equal majority and minority spins however the odd layered (3 and 5) slabs do include net magnetic moment for one unmatched majority spin. For the AFM arrangement in the 2x2 slab we tested the AFM arrangements in two ways for the tri-layer and found no significant difference in their converged energies. In one configuration, the two up spin were next to each other, whereas in the other configuration they are at opposite corners of the layer. To utilize spatial inversion symmetry the layers were configured in the latter manner for the remaining slab layers.

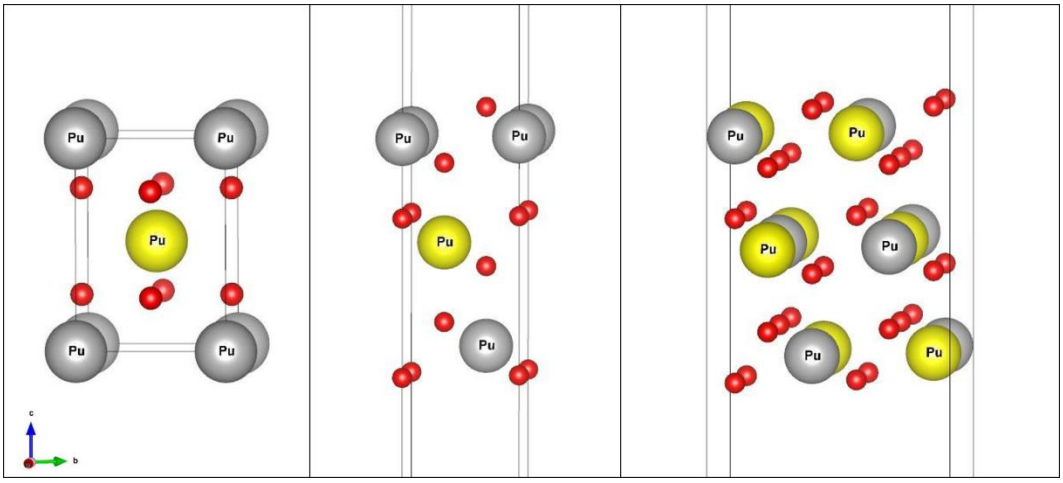

Figure 3: (Left) Unit cell of bulk PuO_2. (Middle) 1x1 three-layer slab of PuO_2 (111) in AFM arrangement. Each slab layer has 3 layers with 1 Pu atom sandwiched between 1 O atom above and 1 O atom below the Pu atom. (Right) 2x2 three-layer slab of PuO_2 (111). Each slab layer has 4 Pu atoms and 4 O atoms above and 4 O atoms below the Pu layer. The gray and yellow spheres represent plutonium atoms with opposing spins and red spheres represent O atoms.

Magnetic ordering of the 111 surface of the PuO_2

With the application of hybrid DFT with spin-orbit coupling to study the properties of PuO_2 (111) surface with FM and AFM plutonium spin configurations. Specifically, we studied the evolution of surface properties such as work function, surface energy, and band gaps with respective to the layer thickness. The behavior of the Pu 5f electron states was also studied via the electronic density of states. Also, different surface periodicities, namely 1x1 and 2x2, were considered to allow different AFM configurations. For the PuO_2 (111) surface, we considered both anti-ferromagnetic (AFM) and ferromagnetic (FM) surfaces for the 1x1 slab. However for the 2x2 slab, we only considered the AFM spin alignments as the spin-orbit calculations from the 1x1 slab showed that the AFM configuration is energetically more favorable over the FM configuration. We find that spin-orbit interactions are necessary to accurately determine the ground state spin structure. In this regard, the AFM configurations were lower in energy than the FM configurations. Like in bulk, Mott insulator type behavior was also found in the PuO_2 slabs. We also observed that the surface energy and work function converge reasonably for slabs within five atomic layer thickness or higher. It can thus be inferred that a PuO_2 (111) with five atomic layers is sufficient to model surface properties.

Energy Convergence

Pertinent computed surface properties, namely the incremental slab energies ΔE, surface energy γ, work function Φ, and the electronic band gap $\Delta_{gap}(N)$ have been tabulated. To determine the convergence of energy with respect to number of layers in slab we have calculated the slab incremental energy defined by,

$$\Delta E(N) = E_{tot}(N) - E_{tot}(N-1) \qquad 3\text{-}1$$

where $E_{tot}(N)$ is the total energy of an *N*-layer slab per formula unit of PuO_2. The incremental energy measure the change in the total energy as more "bulk" is added and in the limit $N \to \infty$, $E_{tot}(N)$ should converge to the bulk total energy while $\Delta E(N)$ should converge to 0. A plot of $\Delta E(N)$ versus *N* in Figure 4 indicates that the incremental energy is well converged by *N*=6 for each configuration. Therefore, in principle, a slab of thickness equal to 5 layers, with ΔE < 0.1 eV, should be sufficient to model ultrathin film (UTF) of PuO_2 surface.

To understand the role of magnetism in PuO_2, we did a layer by layer comparison of the energy difference between the 1x1 AFM and FM surface slabs and bulk. The bulk calculations show that the AFM is the true ground state for both cases of NSO and SO, see Table 3. This is in agreement with previously published theoretical works [13,57–59]. Our layer calculations in Table 4 show that while some NSO slabs, namely slabs with 2 and 4 formula units, favor FM ground state, all of the SO slabs prefer an AFM ground state. Note that all the numbers are scaled per formula unit.

Table 3: Incremental energy, ΔEN (eV), at each slab thickness (N) per formula unit of PuO_2.

ΔE(eV) Layer Thickness	2x2 AFM SO	1x1 AFM SO	1x1 FM SO	2x2 AFM NSO	1x1 AFM NSO	1x1 FM NSO
1						
2	-0.78	-0.80	-0.79	-0.76	-0.76	-0.73
3	-0.16	-0.15	-0.16	-0.20	-0.20	-0.17
4	-0.08	-0.07	-0.09	-0.10	-0.10	-0.11
5	-0.07	-0.05	-0.04	-0.07	-0.06	-0.06
6	-0.03	-0.02	-0.02	-0.03	-0.04	-0.03

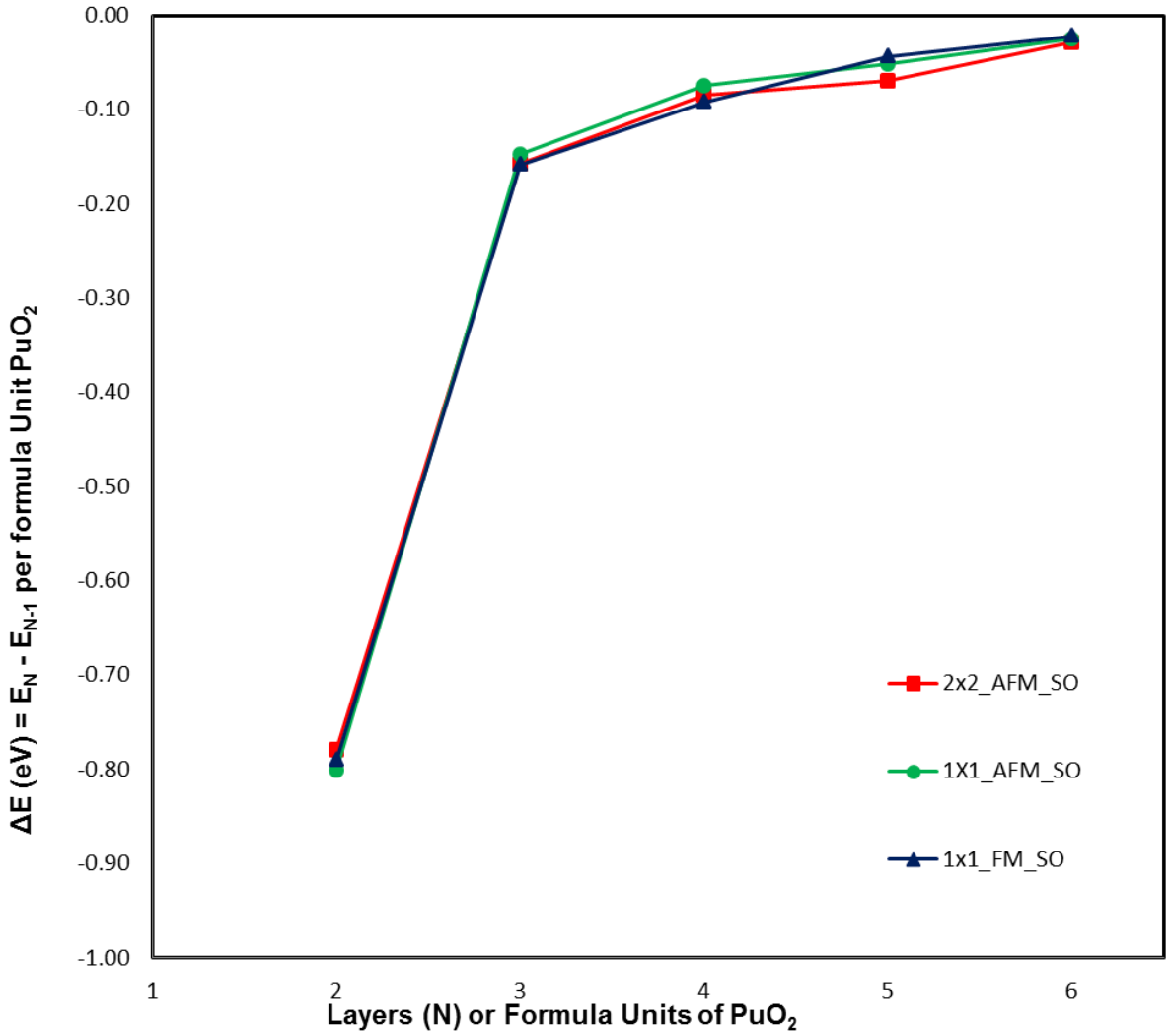

Figure 4: . Incremental energy per formula unit of PuO_2 at each layer (N). Note in 2x2 AFM each layer (N) has four stoichiometric PuO_2 and thus energy at each layer has been scaled by ¼.

Table 4: Energy difference (eV) between AFM and FM arrangements of the 1x1 PuO_2 slabs, with and without spin-orbit coupling, at each slab thickness (N) and bulk per formula unit of PuO_2. Note the (-) indicates AFM state has lower energy.

ΔE(meV)	$\Delta E_{AFM} - \Delta E_{FM}$	$\Delta E_{AFM} - \Delta E_{FM}$
Layer	SO	NSO
2	-30.76	21.38
3	-19.53	-3.14
4	-2.31	0.16
5	-9.72	-0.31
6	-12.19	-12.59
Bulk	-24.05	-48.18

Plutonium spin magnetic moments are of particular importance. In the ideal ionic limit, each Pu atom will have a spin magnetic moment of 4μB (bohr magnetons) since Pu4+ has a 5f4 valence state. For Bulk PuO_2, previous studies[7] reported that for the AFM configuration with spin orbit coupling included, the PuO_2 bulk spin magnetic moments using LDA+U and GGA+U methods are 3.72 and 3.75 respectively. Our surface slab magnetic moments, based on the 2.3 RMT, are slightly lower than these values. The magnetic moments for the 6 layer slab at the AFM SO level are reported in Table 5 (note that the values are magnitudes per plutonium atom and other slabs had similar trends) and the magnitude of the spin magnetic moment is quite close to that at 3.7μB (NSO) and 3.6 μB (SO) indicating that the 5f electron states are fairly localized at the atomic sites. Therefore the 5f electron density of states is expected to be confined within a narrow energy range in the vicinity (just below) of the Fermi level. For a fully ionic behavior, we expect the spin moment of 4μB for each of the plutonium atoms; as the spin moment is around 3.6 in the SO configuration, we can theorize that there is mostly ionic bonding with some covalent bonding for PuO_2.

Table 5: Averaged spin moments (μ_B) of Pu atoms in the arrangements below. The average was taken as the sum of the absolute value of the Pu moments in the particular arrangement divided by the number of Pu atoms present.

μ_B	Bulk	1x1 N=6	Bulk	1x1 N=6	2x2 N=6	outer	sub-surf	bulk-like
Layer	FM	FM	AFM	AFM	AFM	AFM	AFM	AFM
NSO	3.75	3.75	3.71	3.73	3.73	3.74	3.72	3.73
SO	3.60	3.59	3.57	3.58	3.58	3.57	3.59	3.59

Surface Energy

The surface energy (γ) is another important quantity for characterizing the stability of a surface. γ is defined as the work done to cleave a surface of area A along a given orientation and it is computed as[60]

$$\gamma = \frac{1}{2A}\left[E_{tot}(N) - NE_B\right] \qquad 3\text{-}2$$

Here N is the number of layers, E_B is the total energy per formula unit of the bulk crystal and $E_{tot}(N)$ is the total energy of an N-layer slab. The way E_B is computed can ultimately affect the convergence or

divergence of γ[61]. The standard approach is to determine E_B from a separate bulk calculation. However, this can result in inconsistencies between the bulk and slab energies, e.g., different k-point densities and number of plane wave basis functions. Hence E_B is more reliably calculated if we first re-write the above equation in the form

$$E_{tot}(N) = NE_B + \kappa \qquad 3\text{-}3$$

followed by a least square linear fit of $E_{tot}(N)$ versus N (where N is sufficiently large). This fit yields slope E_B and intercept $\kappa = 2A\gamma$. This fitted value of E_B is internally consistent with slab calculations as opposed to using a value of E_B obtained from a separate bulk calculation. Once E_B is obtained from the linear fit, γ is computed via the above equation for each N- layer thick slab. We must mention that the value of γ obtained from the intercept of fitted line, that is, $\gamma = \kappa / 2A$, is the surface energy of the slab with semi-infinite thickness. The surface energies computed with the prescribed method are reported in Table 6.

Table 6: Surface Energies γ (J/m^2) of PuO_2 slab of thickness (N) at each configuration

γ *(J/m^2)* Layer Thickness	2x2 AFM SO	1x1 AFM SO	1x1 FM SO	2x2 AFM NSO	1x1 AFM NSO	1x1 FM NSO
1	0.83	0.82	0.82	0.87	0.87	0.83
2	0.69	0.63	0.66	0.79	0.78	0.73
3	0.74	0.66	0.69	0.8	0.8	0.77
4	0.77	0.7	0.69	0.81	0.81	0.76
5	0.75	0.71	0.72	0.8	0.84	0.77
6	0.79	0.76	0.78	0.86	0.84	0.81
Semi-Inf	0.76	0.71	0.73	0.82	0.82	0.78

We begin by examining the surface energies at the scalar relativistic (i.e NSO) level. The relative fluctuations with increasing slab size are quite small and therefore the surface energies for each system seem to converge to their respective semi-infinite values. From Figure 5 it thus appear that the 2x2 NSO surface energies are almost similar to the AFM-NSO values of 1x1 surface and slightly higher than the FM-NSO values. Rak et al [24] considered the FM arrangement of the PuO_2 slab and reported the surface

energy of 0.78 J/m^2 which is in agreement with our FM NSO semi-infinite surface energy while our AFM NSO of both 1x1 and 2x2 slab were slightly higher at 0.82 J/m^2.

When spin-orbit coupling was considered, surface energies were generally lower than their NSO counterparts. In fact, that is true for every slab and every magnetic configuration. Therefore, this key result highlights the importance of including spin-orbit coupling in Pu-based calculations. Figure 5 indicate that the SO surface energies remains oscillatory up to the maximum layer considered, N=6. Again the 2x2 surface energies at the SO level are higher than the 1x1 SO surface energies. Comparing the 1x1 surface energies for AFM and FM spin structures, we see clearly from Table 6 that the AFM surface energies are lower at SO level, which is not surprising as the AFM slabs are energetically more stable than the FM slabs (c.f. Figure 2). However, at NSO level the FM structure has lower surface energies; in fact, the surface energies are quite close at the SO level. Although the AFM SO arrangement did have the lowest energy, the difference in energies is slight enough that the FM arrangement cannot be completely ruled out from the thin films configurations.

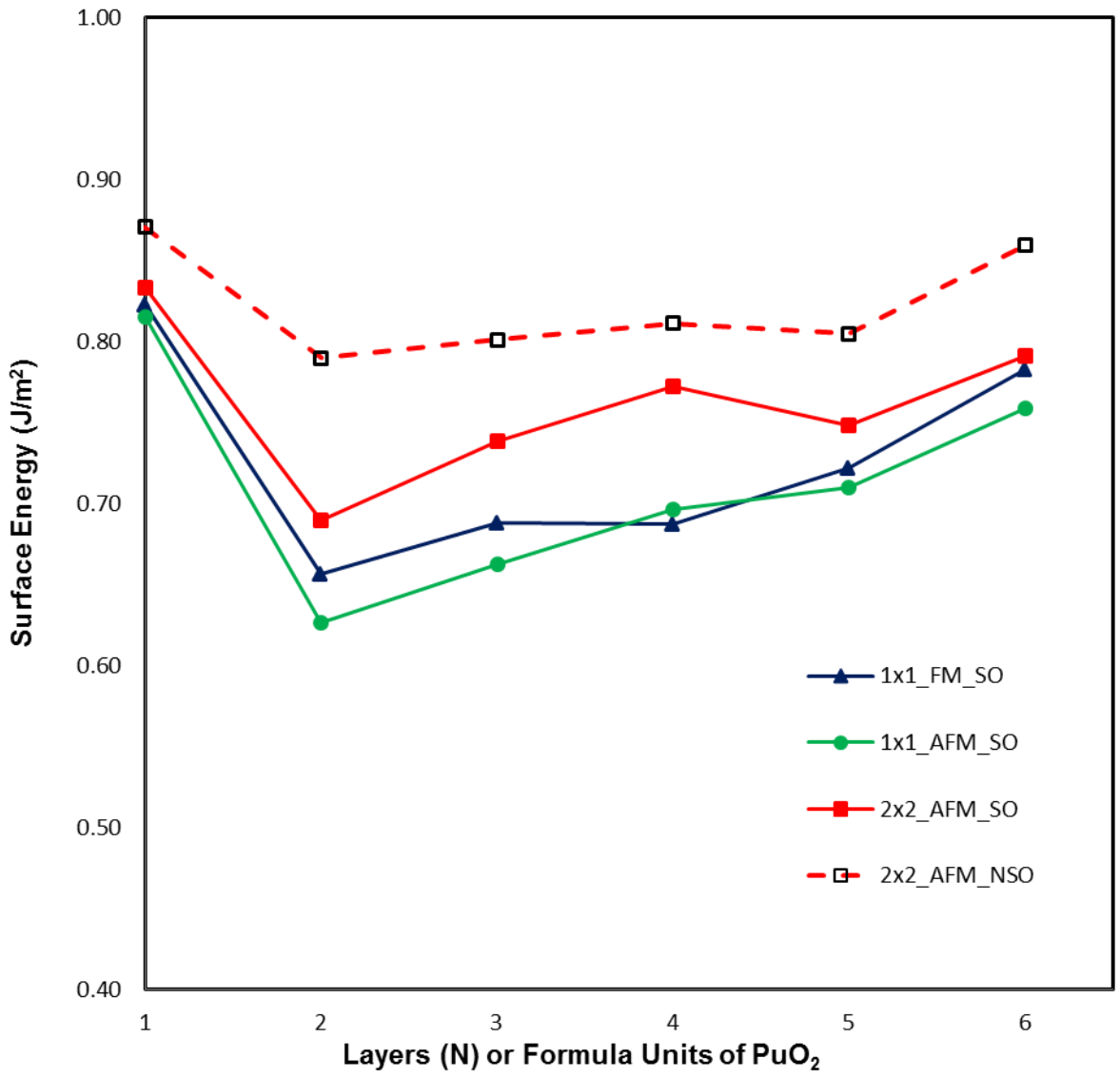

Figure 5: Surface energies (J/m2) of 2x2 AFM SO, 2x2 AFM NSO, 1x1 AFM SO and 1x1 FM SO configurations per layer N. Note the values are per formula unit (PuO_2) and thus the 2x2 values have been scaled by ¼.

Overall, the semi-infinite surface energy in each configuration (1x1 FM, 1x1 AFM, and 2x2 AFM) at NSO level of calculation was consistently higher than that of SO by up to 8%. In particular, the AFM SO configuration in the 1x1 slab has the lowest surface energy when compared with others thereby making it the most stable of the surfaces modeled. Our surface energies are in the range of 0.7 – 0.8 eV, with AFM SO semi-infinite energy of 0.73 J/m^2 for the 1x1 slab which is comparable to the value reported by Sun et

al[22] GGA+U calculation of 0.72 J/m^2 for the (111) AFM surface of PuO_2. Again, comparing the surface energies of semi-infinite AFM (2x2) and FM (1x1) slabs, both SO and NSO FM configurations have lower surface energies, by 0.04 J/m^2 and 0.03 J/m^2 respectively. This implies that PuO_2 surface may exhibit FM behaviors. However, as the energy difference between the AFM and FM configurations is not large, both AFM and FM magnetic behavior can be found in such surface.

Work function

In addition to surface energy, we also computed the work function of (111) surface. The work function is the smallest energy required to remove an electron from inside the bulk crystal through the surface and far away from the surface on the atomic scale but close to the macroscopic scale. Therefore a higher work function corresponds to a more stable, less reactive surface. The work function is computed as

$$\Phi = V_{\text{vacuum}} - E_F \qquad 3\text{-}4$$

where V_{vacuum} is the Coulomb electrostatic potential energy in the middle of vacuum layer in the unit cell and E_F is the Fermi Energy. The work functions are relatively high for the (111) surface, averaging about 5.3 eV for the 1x1 AFM SO slab and 5.5 eV for the 2x2 AFM SO slab. Comparing the PuO_2 surface's work function to that of the pure plutonium (111) surface (3.2 eV) and β-Pu_2O_3 (2.52eV), the oxide layer thought to form as the dioxide (PuO_2)-metal (Pu) interlayer [62], indicates that the electrons in the PuO_2 (111) slab will find it harder to escape the bulk. The higher work function of the PuO_2 suggests that this stoichiometry is more stable than the Pu_2O_3 and not as reactive as Pu or Pu_2O_3 as expected. Previous works have calculated the work function to be 6.1eV from LDA+U and GGA+U calculations [22] which is slightly higher than our calculated results using hybrid DFT. Our average work function was 5.2-5.3eV for all magnetic configurations of our 1x1 slabs but had higher average Φ for our 2x2 AFM slabs with 5.56eV and 5.49 eV for NSO and SO respectively (See Table 7). Although both AFM and FM of the 1x1 configurations' work functions almost plateau out by the fourth layer, that is not the case in our 2x2 configuration as shown in Figure 6. There is a dip in the work function in layers 3 and 4, indicating it is easier for the electron to be removed at this surface thickness. This is supported by corresponding reduction of the band gap at the same thickness level as seen in Figure 7.

Table 7: Work Function Φ (eV) of PuO_2 slab of thickness (N) at each configuration

Φ(eV) Layer Thickness	2x2 AFM SO	1x1 AFM SO	1x1 FM SO	2x2 AFM NSO	1x1 AFM NSO	1x1 FM NSO
1	5.56	4.93	4.95	5.75	5.72	5.68
2	5.66	5.26	5.28	5.84	5.89	5.75
3	5.29	5.26	5.28	5.25	5.23	5.34
4	5.34	5.31	5.12	5.4	5.23	5.02
5	5.59	5.28	5.24	5.74	5.16	5.01
6	5.59	5.31	5.1	5.48	5.24	4.94
Average	5.49	5.28	5.2	5.56	5.35	5.21

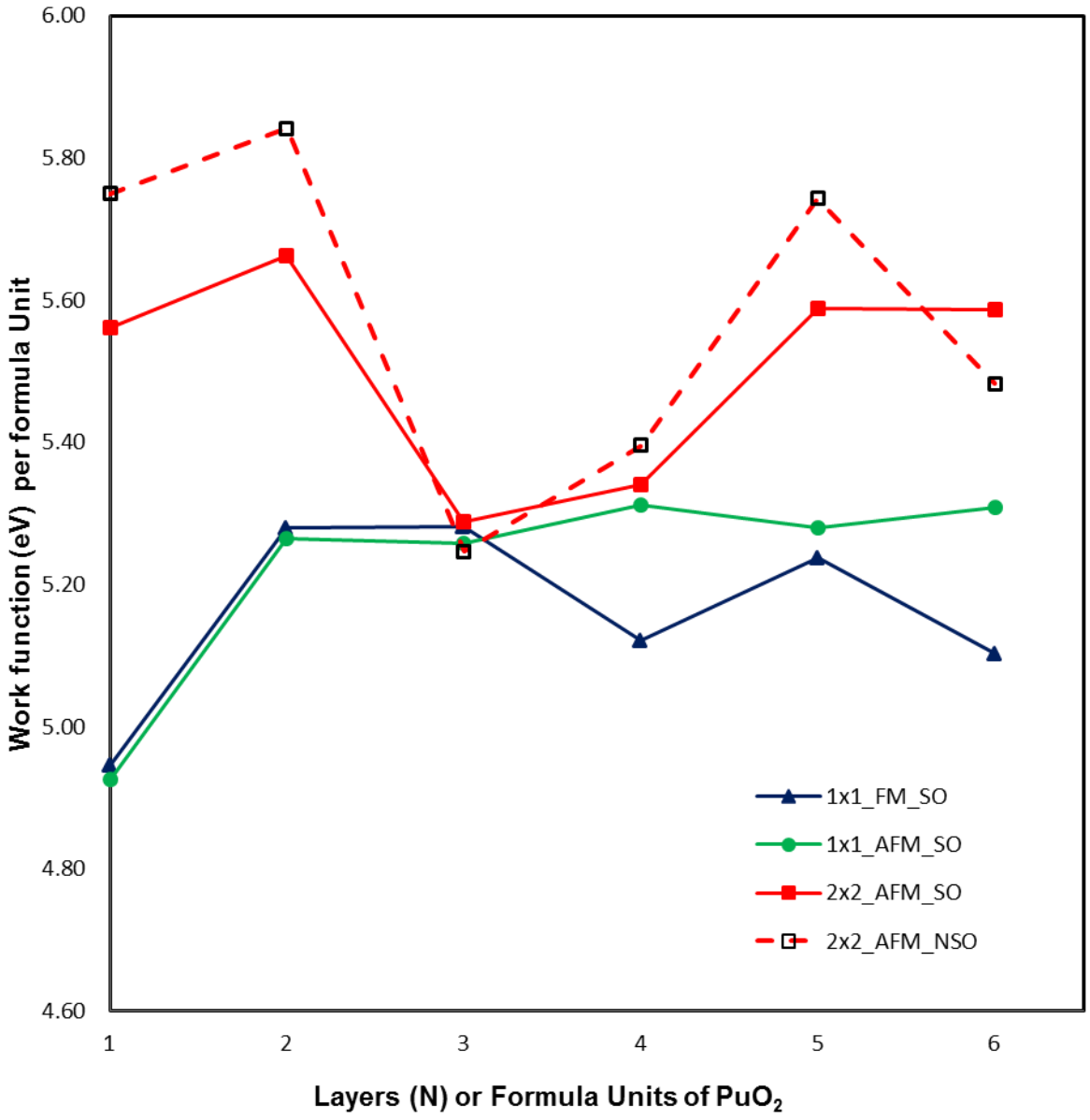

Figure 6: Work function (eV) for 2x2 AFM SO, 2x2 AFM NSO, 1x1 AFM SO and 1x1 FM SO at layer N. Note the values are per formula unit (PuO_2) and thus the 2x2 values have been scaled by ¼.

Band Gap

For band gap calculations, our k-mesh is 7x7x1 for all slabs and includes the Γ-point. The experimental band gap of bulk PuO_2 has been widely accepted as 1.8eV[63] however recent experiments by McCleskey et al. yielded a gap of 2.80 eV[64]. Prodan recently predicted the band gap of 2.7 eV using the HSE hybrid density functional [65] but did not include SO coupling. Our band gaps of multiple configurations are all within the reasonable range as shown in Table 8, as this theory does tends to overestimate the band gap[50]. For our AFM SO bulk we got the band gap of 1.88eV, which is the closest to experimental band gap of 1.8eV. When comparing the band gaps of the surface to the calculated bulk, we note that the gap in the 2x2 slab for $N = 6$ is closer to the bulk gap. When working with the surface slabs, the band gap oscillates slightly but stays within the range of 0.3 eV for the AFM SO and 0.75 for FM NSO with the rest of configurations within this range. Note that for each of the layer configurations, inclusion of SO narrows the gap. There is a dip in the band gap for layer thickness 3 and 4 of the AFM SO and NSO configurations in the 2x2 cells, which have a corresponding work function dip as discussed above. The upward shift of the valence band is responsible for the reduction of band gaps for these two slab configurations.

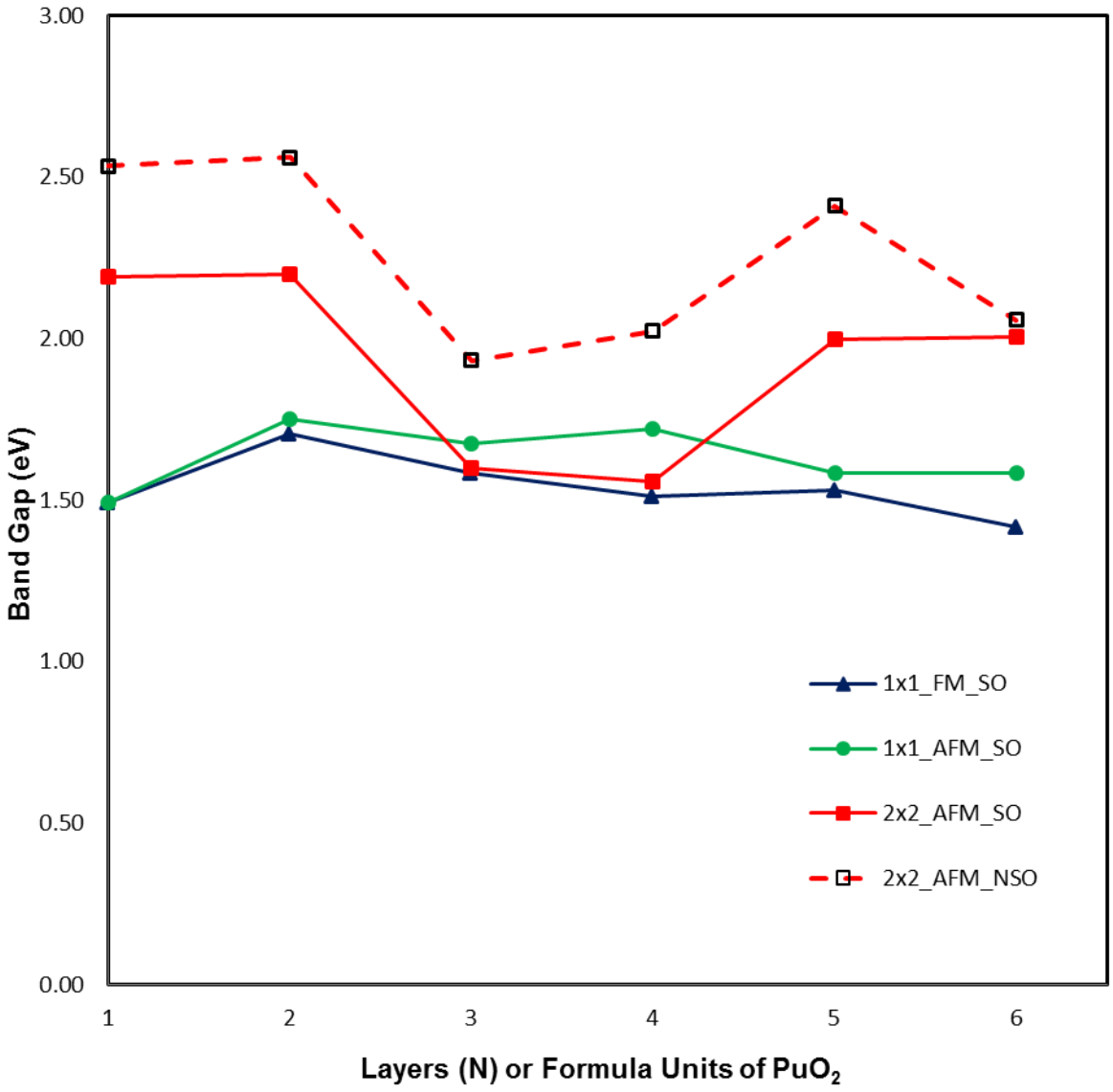

Figure 7: Band gap (eV) as calculated in WIEN2K for 2x2 AFM SO, 2x2 AFM NSO, 1x1 AFM SO, 1x1 FM SO at each layer N. Note the values are per formula unit (PuO_2) and thus the 2x2 values have been scaled by ¼.

Density of states

The density of states (DOS) plot of the bulk PuO_2 (see Figure 8c) shows that the f-orbitals exist both at the valence band maximum and at the conduction band minimum, indicating that the PuO_2 is a Mott-insulator[66]. As shown in Figure 8a,b, the DOS plots for the AFM SO surface slabs, 1x1 and 2x2 slabs of layer thickness N=6, reveal that the surfaces retain this insulating characteristic. The surface is

clearly more localized than the bulk as evidenced by the steeper rising and sharper peaks of the Puf state on the pDOS plot of the surfaces as compared to the bulk of PuO_2. The DOS plot of the 1x1 surface slab shows that there is significant hybridization in between the valence Pu 5f electrons and O 2p electrons. This suggests that there may be some covalent bonding feature in PuO_2. The 2x2 slab is an extension of the 1x1 slab yet there are slight variances in the valence band when compared with each other, such as the 2x2 slab shows a slightly higher degree of hybridization of the oxygen's p orbital with the plutonium's f-orbital state. This difference can be simply due to the difference in the AFM arrangements in 1x1 and 2x2 slabs. From both Figure 8a and b, surface states are clearly distinguishable just below the Fermi level (0-0.5eV). At the SO-level, the 6-layer surfaces first peaks at about 0.2 eV below the Fermi level whereas the bulk PuO_2 peaks at about 0.5 below Fermi. When comparing the Op contribution in ratio with the plutonium f state contribution at the top of the valence band, the ratios are almost similar between the 1x1 surface slab and the 2x2 surface slab at 0.32 and 0.35 respectively. This is also similar to the 0.34 ratio in the bulk PuO_2. The 6d states are relatively inactive, and were found to have some presence below -4eV and have significant contribution at higher energy into the conduction band above 4eV.

The 2x2 6 Layer thick surface has 6 total layers, each layer with four Pu atoms in the same plane with 4 O atoms in a plane above and 4 O atoms in a plane below. When we look at the distinct layers within the 6-layer 2x2 slab, we can distinguish them as the outer-layers (the two layers in contact with the vacuum), sub-surface-layers (the layers just below the outer layers) and the bulk-like layers (the layer that is farthest from the vacuum). While Figure 8 shows the entire pDOS plot of the systems under discussion, Figure 9 is the enlargement of Figure 8c,d,e,f near the Fermi level and highlights the Puf and Op contributions. Please note that when presenting the layer by layer p-DOS, the total DOS is only for that layer. The DOS plots indicate that the Pu 6d and 7s states are not prominent in the valance band, while there is a strong hybridization between the Pu 5f and O 2p states.

The pDOS plot shows that the outer layer is more of a charge-transfer type of insulator as the characteristic Op curve clearly contributes more near the top of the valance on this layer than the sub-surface, bulk-like or the actual bulk of PuO_2 (see Figure 9). This is further validated when we compare the ratios of the Op/Puf characteristics present in the first peak at the top of the valance band of the outer

layer to the inner and bulk layers. The outer layer ratio is 0.64, much higher than the subsurface layers, bulk-like layers and bulk of PuO_2 which are respectively 0.22, 0.42 and 0.34. Thus the outer layer shows more of a charge transfer characteristic with electron hopping between the Pu and O atoms. Note that both the inner layer and the bulk-like layer pDOS have the Puf and Op states hybridizing and are present on top of the valance band as well as on the bottom of the conduction band signifying the Mott-insulating behavior that is also present in the bulk PuO_2.

Table 8: Band Gap (eV) as calculated of PuO_2 slab of thickness (N) at each configuration

*Gap (*eV) Layer Thickness	2x2 AFM SO	1x1 AFM SO	1x1 FM SO	2x2 AFM NSO	1x1 AFM NSO	1x1 FM NSO
1	2.19	1.49	1.49	2.54	2.47	2.48
2	2.20	1.75	1.71	2.56	2.61	2.43
3	1.60	1.68	1.59	1.93	1.93	2.01
4	1.56	1.72	1.51	2.02	1.87	1.69
5	2.00	1.59	1.53	2.41	1.81	1.69
6	2.01	1.58	1.42	2.06	1.85	1.52
Bulk	1.88	1.88	1.14	2.18	1.88	1.41

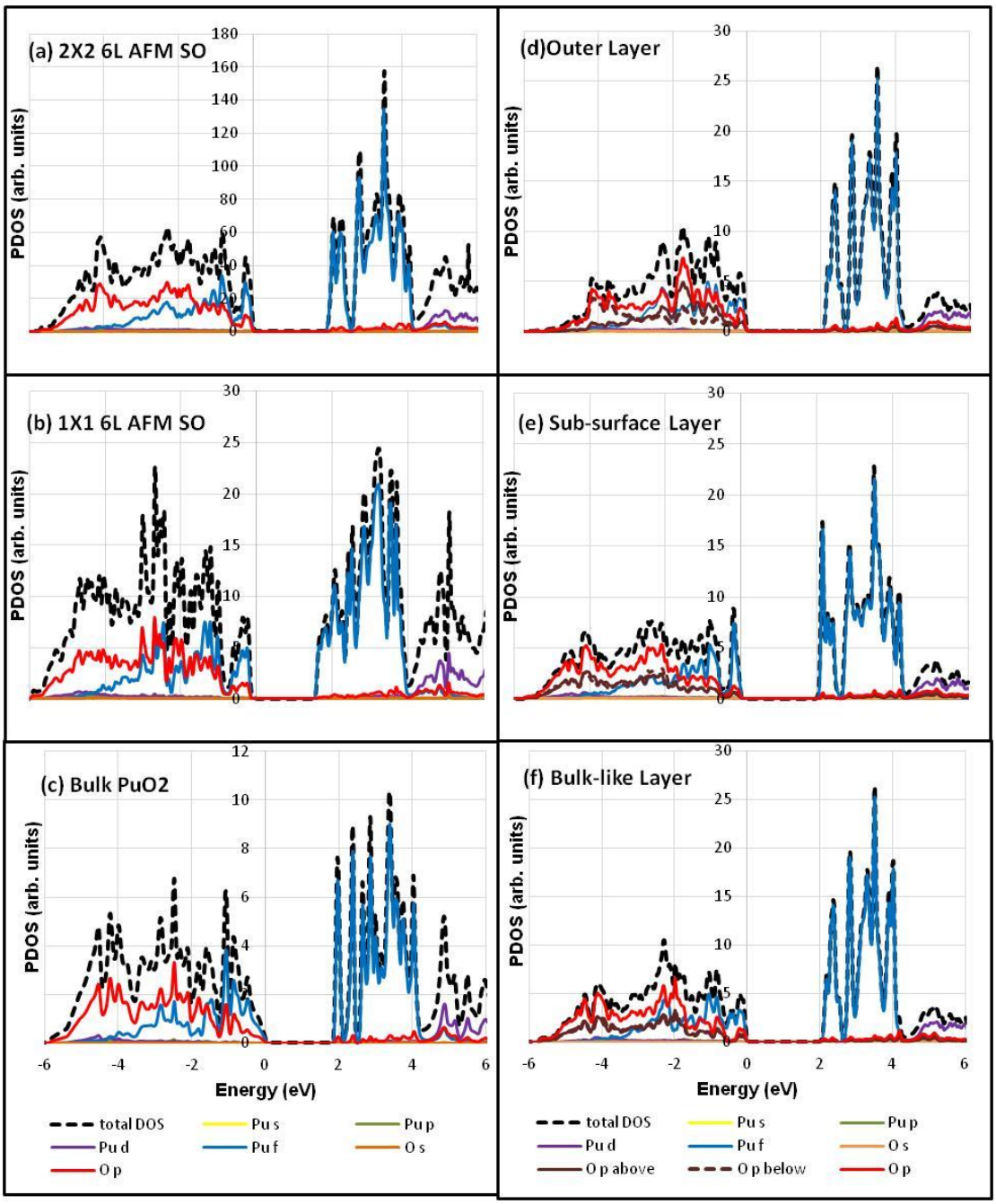

Figure 8: . pDOS plots of PuO_2 with AFM arrangement including spin-orbit coupling (a) 2x2 6-layer thick slab of PuO_2 (b) 1x1 6-layer thick slab of PuO_2 (c) bulk PuO_2 (d) outermost layer of the 2x2 6-layer slab of PuO_2 (e) sub-surface layer of the 2x2 6-layer slab of PuO_2 (f) inner or most 'bulk-like' layer of the 2x2 6-layer slab.

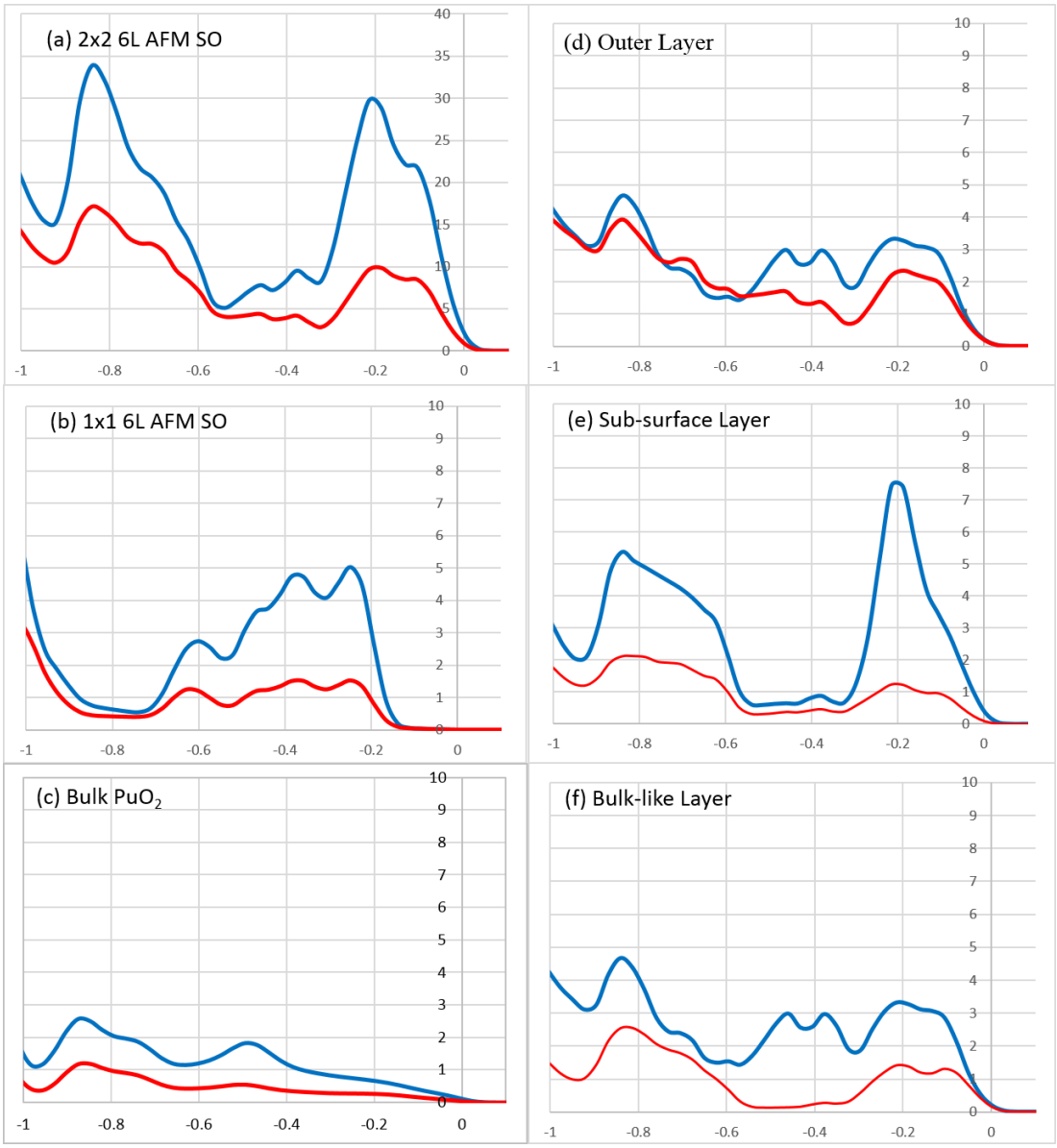

Figure 9: Enlargement of (Fig. 7) pDOS plots of PuO_2 bulk and (111) 6-layer surface slabs with AFM arrangement with spin-orbit coupling. (a) 2x2 6-layer thick surface slab of PuO_2 (b) 1x1 6-layer surface slab of PuO_2. (c) bulk PuO_2 (d) outermost layer of the 2x2 6-layer slab of PuO_2 (e) sub-surface layer of the 2x2 6-layer slab of PuO_2 (f) inner or most 'bulk-like' layer of the 2x2 6-layer slab. Outer layer of the 2x2 6-layer slab of PuO_2 shows a charge transfer type character while sub-surface layer of the 2x2 6-layer slab of PuO_2 and 'bulk-like' Layer of the 2x2 6-layer slab retain the Mott-insulator type character of the bulk of PuO_2.

Conclusion

The anti-ferromagnetic configuration is the ground state for the surface of plutonium dioxide. For surface calculations, 5 layer slab should be sufficient to model the system. The top or the outer layer of the slab is most reactive with a charge transfer type of insulating behavior while the sub-surface and bulk-like layer act more like a mott-insulator.

Chapter 4

PuO_2 bulk with metal Impurities

Introduction

Plutonium oxides, especially PuO_2, is of widespread significance due to its applications as nuclear fuels and most importantly as the primary storage form of plutonium from spent fuel and nuclear weapons in long-termed storage. Plutonium is an extremely reactive metal and exposure to impurities that occurs before and during storage of the plutonium in form of plutonium oxides will be retained in long-term storage. The most common form of this oxide is plutonium dioxide, with the stoichiometric PuO_2 being the most stable[4]. The stored plutonium oxides are considered to be "pure" dioxides (91-97% PuO_2) if they have approximately 3-8% impurities[4].

In the stoichiometric PuO_2 compound, Pu occurs in the Pu(IV) oxidation state, corresponding to a localized f4 shell. Oxygen vacancies cause Pu(III)-5f state to form by taking up electrons released by oxygen. While the PuO_2 compound is stable with respect to free oxygen at 0K, the delicate energy balance suggests the possible deterioration of the material at higher temperatures in long-term storage [67].

During various process (a few out-lined in chapter 1) plutonium metal or the plutonium dioxide can be in possible contact with transition metals, which are all possible contaminants, characterized as major, minor or trace impurities[36], to the plutonium dioxide. They have far-reaching concerns and require further studies to determine the effect of these impurities on plutonium oxides, especially PuO_2. While zirconium and plutonium solubility has been shown to exist[32] and there have been other studies of transition metals with plutonium[37,38], and plutonium dioxide[39] there has been no systematic study of transition metal impurity within plutonium dioxide. Studying the interaction between transition metals and plutonium dioxide is critical for better, more efficient storage plans as well as gaining insights to provide a better response to potential threats of exposure to the environment. In this chapter, the focus is on six of these transition metals listed in Table 9 as well as the alkaline earth metal magnesium because these are the elements that most likely to come in contact with the plutonium dioxide powder that is stored in storing facilities around the nation.

Our results reveal interesting volume contraction of PuO_2 when one plutonium atom is substituted with one of the transition metals as well as further reduction of volume if an oxygen vacancy exists in

conjunction with the impurity in the system. This reduction of volume of the stored plutonium oxides can have practical consequences in determining storing facility. To ensure existence of oxygen vacancies, the plutonium and/or plutonium should be formed within O-poor conditions. Then the impurities should be exposed to the sample during or after processing to further contract the volume thus affecting during long-term storage. Studying the interaction between transition metals and plutonium dioxide is critical for better, more efficient storage plans as well as gaining insights to provide a better response to potential threats of exposure to the environment.

Computation Details

Density functional theory (DFT) is often referred to as principle or ab initio method as it determines many properties of the system with just some basic structural inputs and provides a theoretical basis for experimental work. Here the calculations were performed within DFT and with the VASP code, in which we used the projector-augmented wave (PAW) method for the core electrons. PuO_2 forms a fluorite structure with space group Fm3m with plutonium forming the face centered cubic structure and O atoms at octahedral sites with experimental lattice constant of 5.398A. The $6s^2 7s^2 6p^6 6d^2 5f^4$ electrons for Pu atoms and $2s^2 2p^4$ electrons for O atoms are respectively treated as valence electrons. For the metallic impurity, *2p3s* electrons for Mg, *3d4s* electrons for Cr, Mg, Fe and Ni atoms, while a *4d5s* electrons for Zr and Mo atoms are taken to be the valance electrons. The exchange and correlation interactions are described by the spin-polarized generalized gradient approximation (GGA) in the PBE functional [68]. The plane-wave cut-off energy was set at 400 eV with a 3x3x3 Monkhorst-Pack k-point mesh[69] for cubic lattice lengths near 10.7 Å for the 2x2x2 PuO_2 supercell. The plutonium atoms were arranged in anti-ferromagnetic arrangement as in the previous chapter[70]. Energy convergence criteria was set at $1x10^{-6}$ eV and Hellmann-Feynman forces on each ion to be less than 0.01 eV/Å.

DFT cannot accurately describe localized electron systems due to the inherent self-interaction for electrons and thereby to reduce error due to self-interaction of electrons, DFT+U, the Dudarev formulism in the Hubbard model is used to treat strong on-site Coulomb interaction[59]. However, structure optimizations of all atoms (96 atoms or 95 atoms due to oxygen vacancy) in the 2x2x2 supercell were allowed to relax without symmetry in the framework of DFT, based on the GGA and the PAW method. This allowed the positions of the atoms as well as the lattice parameters of the unit cells to be relaxed.

This relaxation scheme gave us total energies of the configurations slightly lower (about 0.05 eV) than those relaxed with symmetry constraints. Relaxations at the DFT level are agreeable as Sun et. al [20] found that while DFT underestimates the lattice parameter by ~2% and GGA+U with U_{eff}=4 overestimates by~1.3% for stoichiometric PuO_2. Ma et. al [55] found inclusion of spin-orbit coupling has little impact (less than 0.7 percent difference) on the lattice parameter for anti-ferromagnetic plutonium dioxide. Furthermore previous literature also suggests that the spin orbit interaction is of the second order to the Hubbard term and thus can be ignored in regards to the geometry of the structure [21,24,71] if not the chemistry. GGA+U with spin-orbit coupling calculations were then performed on these relaxed structures to account for the strong on-site coulomb repulsion in the 4d and 5f electrons for transition metals and plutonium atoms respectively. An effective U ($U_{eff} = U - J$) value of 4 eV was selected for Pu 5f electrons. U_{eff} incorporates both the coulomb U and the exchange J parameters. This value has been to be reasonable in previous literature for reproducing the experimental lattice parameter, bulk modulus, band gap, and reaction energy of PuO_2 [67,71,72]. Similiarly, the U_{eff} was chosen for the metal impurities within this paper that were employed previously in literature and are dependent on their local environment [73]; these values are listed inTable 9, row 2. Mg, Zr and Mo were assigned the U_{eff} =0 due to their position on the periodic table.

Table 9: Row 1: Element and their Z number. Row 2:Effective U values of ElementsRow 2: the oxi-state in the local environment. Row3: Ionic Radii of the element. Row4: lattice parameter a0 of the relaxed system with metal impurity (this work). Row 5: lattice parameter a0 (this work)

Element (Z)	**O(8)**	**Mg(12)**	**Cr(24)**	**Mn(25)**	**Fe(26)**	**Ni(28)**	**Zr(40)**	**Mo(42)**	**Pu(94)**
U_{eff}	0	0	3.24	3.19	4.09	4.4/6.07	0	0	4
Oxi-state	**2-**	**2+**	**4+**	4+	3+	2+/ 4+	4+	4+	4+
Ionic Radii[Å]	0.6	1.5	1.4	1.4	1.4	1.35	1.55	1.45	1.75
a_0 M:PuO_2 (Å)		5.34	5.34	5.36	5.34	5.336	5.36	5.35	5.45
a_0 M-O_v:PuO_2(Å)		5.33	5.33	5.34	5.335	5.33	5.34	5.34	5.36

First an impurity is added via direct substitution of one metallic atom (M) in place of one Pu atom in the FCC lattice site. The system is relaxed within DFT with a Gamma point. Thereafter, a single point

calculation with a larger k-mesh of 3x3x3 and a dos calculation with an even larger k-mesh of 5x5x5 for further accuracy are completed.

The fully relaxed 2x2x2 supercell of the pristine, stoichiometric PuO_2 has a lattice constant of 5.45 Å with the FCC lattice minimally distorted. The largest distortion occurred with lattice *a* at 0.29% distortion while lattice *b* and *c* had less than 0.15% distortion from the lattice constant. With an added defect of one oxygen vacancy (near the center of the cell), we find that the volume contracts by 5.16% giving the lattice constant of 5.35Å with individual lattice contraction of *a* by 1.8% and *b* and *c* by 1.7% within the supercell. Furthermore, the volumetric distortion of the FCC lattice is less than 0.21% due to the oxygen vacancy. Comparing the lattice constant of pristine PuO_2 to the lattice constant of the system with one oxygen vacancy, or $Pu_{32}O_{61}$, we note that the experimental lattice constant of 5.398Å is between the two numbers, which may imply that the oxygen vacancies may be inherent to the system.

In the pristine supercell, nearest Pu-Pu distances averaged between 3.85-3.86 Å while the Pu-O bond lengths are within 2.36-2.37Å. With an oxygen vacancy, the nearest neighbor plutonium atoms formed a closer bond with the surrounding oxygen at 2.27-2.28 Å. In this arrangement, the Pu-O bond length further away from the vacancy are also reduced to 2.31-2.32 Å. Pu-Pu distances were between 3.71 – 3.79 Å with largest nearest plutonium distance at 3.81 Å near the vacancy, see Figure 10. Overall, formation of a single oxygen vacancy reduced the distances between the atoms in the whole super cell, hence an overall reduction of volume. It has been shown that Frenkel defects for oxygen can lead to an expanded lattice[74,75], Kato et. al. [76] calculated that the expansion will be no higher than 3% at 2500K and much less in lower temperatures.

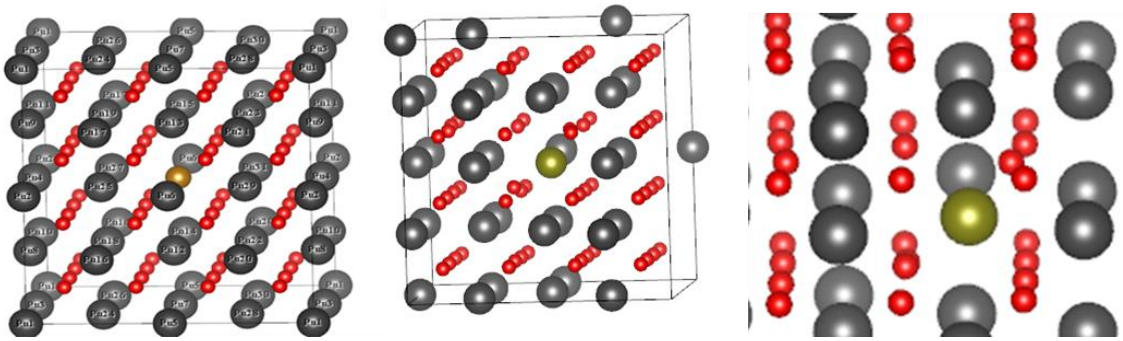

Figure 10 (L). 96 atom supercell PuO_2 with a metal (gold) impurity $Pu_{31}O_{64}M_1$. (M). 95 atom supercell with PuO_2 with a metal (gold) impurity and an oxygen vacancy - $Pu_{31}O_{63}M_1$. (R). Highlights metal atom bonding with 7 nearest oxygen atoms instead of 8 due to the vacancy.

Impurities considered within this study, focus mainly on the transition metals which are characterized by partially filled *d* orbitals with one exception of magnesium (Mg) which is an alkali earth metal. Impurities were only considered for the Pu substitutional site. Hernandez et. al. [39] found these were the only energetically favored site among other high-symmetry sites including interstitial and O-substitution sites within PuO_2 supercell. When a metal atom is substituted for one plutonium atom in the 2x2x2 PuO_2 system here after referred to as M:PuO_2, it creates a 3.22% impurity within the system. For the system with an oxygen vacancy and a metal impurity substitution, referred to as (M-O_v):PuO_2, the defective bulk system has 1.6% of oxygen vacancies or effectively M:$PuO_{2.03}$.

Formation Energies

Formation energies of a defect or impurity are the energies needed for these defects/impurities being formed within the plutonium dioxide bulk. Defects such the oxygen vacancy are intrinsic defects that can be found in fluorite structures and doping with selected impurities can also create vacancies in a crystal. To explore these variances, we doped the fluorite structure with a metallic impurity and considered the formation energies of the system with and without an additional oxygen vacancy. Formation energies for the substituted impurity within PuO_2 was calculated by

$$E_f[\mathrm{M:PuO_2}] = \mathrm{E[M:PuO_2]} - \mathrm{E[PuO_2]} - \frac{1}{\mathrm{n}}\mathrm{E[M]} + \mu[\mathrm{Pu}] \qquad 4\text{-}1$$

Where $E_f[M{:}PuO_2]$ is the energy of the system with the defect/impurity, $E[PuO_2]$ is the energy of the pristine system, $E[M]$ is the energy of the bulk metal system, n is the number of atoms in the bulk metal system and $\mu[Pu]$ is the energy of the plutonium atom from bulk which is added as one of the

plutonium atom was removed. Since the formation of impurity depends on the growth environment, we considered plutonium rich, plutonium poor conditions. Chemical potential of the pristine system must satisfy $\Delta H_f = \Delta\mu[Pu] + 2\Delta\,\mu[O]$), where ΔH_f is the formation enthalpy of PuO_2. With these the formation energy can be defined as

$$E_f[\mathrm{M:PuO_2}] = \mathrm{E[M:PuO_2]} - \mathrm{E[PuO_2]} - \frac{1}{\mathrm{n}}\mathrm{E[M]} + \mu[\mathrm{Pu}] + \Delta\mu[\mathrm{Pu}] \qquad \text{4-2}$$

where $\Delta\mu[Pu] = 0$ for Pu-rich conditions and $\Delta\mu[Pu] = -\Delta H_f$ for Pu-poor conditions.

Oxygen vacancies readily form with the formation energy of -2.18 eV in plutonium rich/O-poor conditions. Impurities may also form in plutonium poor conditions. Considering first impurities within the system without the vacancies, our calculations show that the most likely impurities doping in the plutonium oxide will occur in plutonium poor conditions. Doping with magnesium and zirconium have lowest formation energies while chromium, nickel, iron and molybdenum impurities are also likely to occur. Manganese impurity is relatively unlikely to form within the system as it has the highest formation energy of the those studied here at 0.55 eV. In presence of an oxygen vacancy, the formation energy is determined by

$$E_f[\mathrm{M-O_v:PuO_2}] = \mathrm{E[M-O_v:PuO_2]} - \mathrm{E[PuO_2]} - \frac{1}{\mathrm{n}}\mathrm{E[M]} + \mu[\mathrm{Pu}] + \mu[\mathrm{O}] + \Delta\mu[\mathrm{Pu}] + \Delta\mu[\mathrm{O}] \qquad \text{4-3}$$

where μ[O] is the energy of the oxygen atom taken from the oxygen molecule calculation. We find that systems with zirconium, magnesium impurities are still most likely to form followed by molybdenum and chromium, see Figure 11. However nickel, iron and manganese have positive formation energies therefore not as likely to co-exist in system with oxygen vacancies.

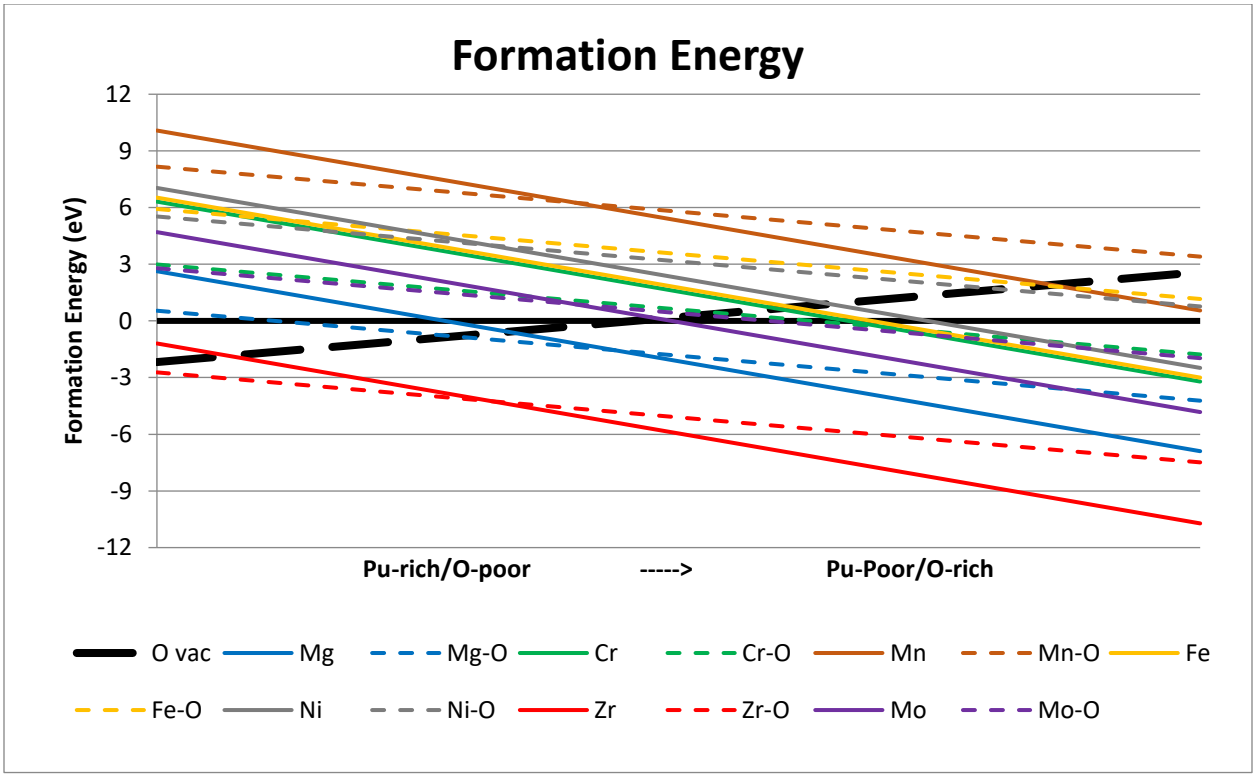

Figure 11: Formation Energies of PuO_2 system with metal impurity in a plutonium poor environment (solid : impurity substitution; dashed: impurity substitution and oxygen vacancy).

Oxidation states and ionic radii

To oxidize, metals lose electrons to oxygen thereby acquiring a positive charge with oxygen atoms forming an oxide ion (2-). Oxides of metal in lower oxidation states (less than 3+) have significant ionic character while those in higher oxidation states tend to have more covalent characteristics. Plutonium has multiple oxidation states with the most stable being the 4+ state. It forms a very stable stoichiometric plutonium dioxide. Other metals considered in this paper have multiple oxidations states as well with the most common states listed in Table 9. The 4+ oxidation state compared to 2+ or 3+ oxidation state would create a hole-state and almost a p-type semiconductor. But the PuO_2 is a Mott-insulator with a band gap of 1.8 eV [77]. In pure DFT calculations there are bands around the fermi energy indicating it as metal, see Figure 12a. However with the inclusion of spin-orbit coupling and U_{eff} = 4 on plutonium atoms 5f bands, the gap opens up to 1.65 eV which is very close to the experimental band gap of 1.8eV, see Figure 12b.

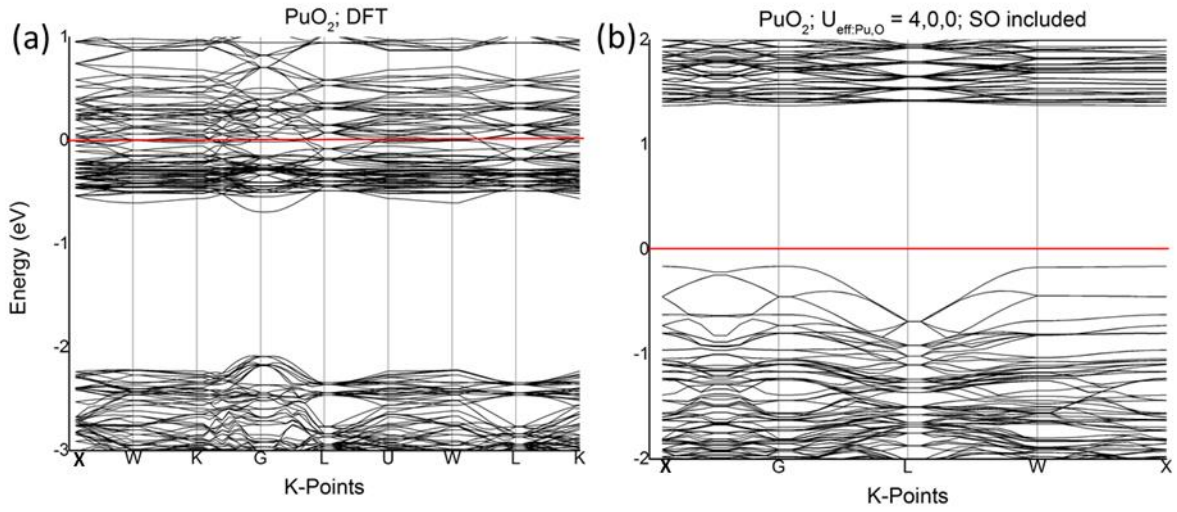

Figure 12: a: Pristine bulk PuO_2 DFT band structure with AFM configuration; b: Pristine bulk PuO_2 band structure with Ueff =4 and spin orbit coupling.

To a first approximation, atoms with an outer radius may be defined by the outer electron orbitals. Generally the atomic radii increases from left to light and top to bottom in s-d block elements such as the metals studied here, and the ionic radii slightly decreases across a row of periodic table, see Figure 13[78]. Note that even for atoms of the same type, the atomic radii can vary due to the oxidation state as well as, the type of bonding and especially the local coordination environment. Cations (M=Mg, Cr, Mn, Ni, Fe, Zr, Mo) become smaller than their respective neutral atom as the coulomb repulsion is decreased and the nucleus pulls the electrons closer thereby creating a smaller ionic radii as compared to the neutral atomic radii, see Table 9. Within the plutonium dioxide system, the local coordination environment is four oxygen atoms nearest to the cation. When we substitute one transition metal impurity in the system, there is a greater pull toward the nucleus of a transition metal atom than a plutonium atom because the ionic radius increases with increasing coordination number hence dependent on the metal. To this end, we compare the ionic radii of the metallic impurity to the plutonium atom and can plainly deduce that the smaller radii of the TM cation compared to the Pu atom leads to the decreased volume of the unit cell.

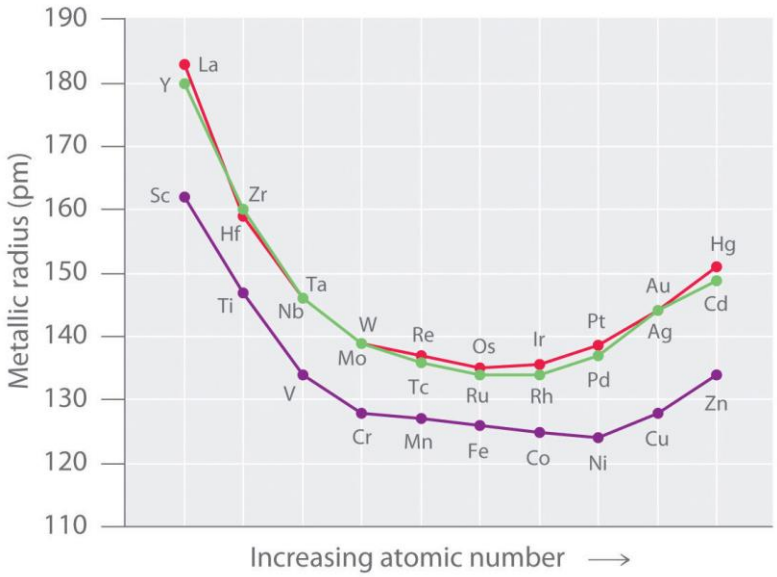

Figure 13: The metallic radii of the first, second and third row of transition metals[78]. The radii of the atoms may vary depending on the oxidation state and the local environment.

Bond Lengths

While the ionic radius of one cation change may reduce the volume, it by itself is not responsible for the reduced volume. We discern that in the pristine system, the Pu-Pu distance is about 3.85 Å and Pu-O bond length is about 2.36 Å. Pu-Pu distance is reduced with addition of an oxygen vacancy to 3.76-3.78Å. Substituting one metal impurity instead of a plutonium atom decreases the distance between the metal and the nearby plutonium even further, see Figure 14. Adding an impurity reduces the Pu-O bond lengths in the unit cell to around 2.3Å. Comparing the bond lengths of nearest neighbor Pu-O bonds with the Pu-O bond length farthest from the impurity, we find that these bond lengths do not deviate significantly from each other. However, the metal-oxygen bond length is consistently shorter than the average Pu-O distance within the M:PuO_2 and (M-O_v):PuO_2 systems. With an oxygen vacancy, the magnesium impurity cell also has a smaller M-O bond length as compared with the Pu-O bond lengths within that structure. The largest contraction of bond length occurs with impurities, Fe-O and Ni-O at lengths of 1.85 and 1.86 respectively, see Table 10.

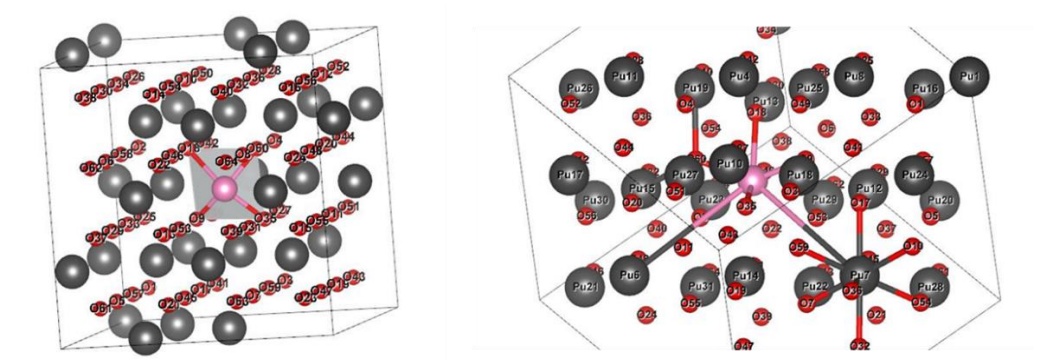

Figure 14: (L)The impurity bond length with the closest oxygens. (R) The farthest plutonium and oxygen atoms from impurity.

The Pu-O average bond length is calculated to be about 2.3 Å in the relaxed system with an oxygen vacancy defect. Within the M-O_v:PuO_2, an O vacancy and a substituted metal impurity, the average bond length of Pu-O nearest to the metal impurity decreased in the case of Mg, Cr, Mn and grew longer with Ni as compared with the Pu-O bond length further away from impurity. Metal impurity of Fe, Zr and Mo did not have a significant effect on the Pu-O bond length due to the distance from the said impurity.

With the oxygen vacancy, all impurities showed a shorter bond length distance with oxygen than the M-O bond lengths within the vacancy free cell. The plutonium - oxygen bond lengths did not deviate significantly (2% or less) even near the impurity within the defective cell. The lone exception was in the Mg-O_v:PuO_2 system where the shortest bond length of nearby plutonium and oxygen atom was 2.18 or about 6% shorter than the Pu-O bond lengths far from the impurity.

The above indicates that while the introduction of impurities reduces the Pu-O bond lengths by about 2-4% from the pristine cell, it has an even greater effect of reducing M-O bond length even further by as much as 21% difference with Ni and Fe.

Table 10: Bond lengths: Rows 1 and 2: Pu-Pu average length in system. Rows 3 and 4: Pu-O shortest bond length of the plutonium close to impurtiy and the closest oxygen atom. Rows 5-6. Shortest Pu-O bond length of the plutonium farthest from the impurity. Rows 7-8: Shortest M-O bond length. Rows 9-10: shortest M-Pu bond length. All length are in Å.

Bond type:	Exper.	No impurities	Mg	Cr	Mn	Fe	Ni	Zr	Mo
Pu-Pu (Å)	3.815	3.850	3.770		3.780	3.770	3.770	3.770	3.760
Pu-Pu (-O:PuO_2)		3.320		3.700	3.770	3.760	3.760	3.77	3.770
Pu-O near M;	2.34	2.360	2.300	2.300	2.282	2.300	2.300	2.310	2.350
Pu-O near M (-O:PuO_2)		2.310	2.180	2.260	2.270	2.290	2.300	2.30	2.300
Pu-O far from M		2.360	2.300	2.300	2.310	2.310	2.280	2.300	2.310
Pu-O far from M (-O:PuO_2)		2.320	2.280	2.270	2.309	2.290	2.28	2.30	2.300
M-O shortest distance			2.317	1.950	2.310	1.850	1.860	2.210	2.130
M-O shortest distance (-O:PuO_2)			2.150	2.030	2.169	2.050	2.100	2.11	1.997
M-Pu shortest distance			3.719	3.350	3.724	3.190	3.080	3.740	3.710
M-Pu shortest distance (-O:PuO_2)			3.570	3.680	3.594	3.494	3.697	3.62	3.617

Volume

Oxygen vacancy is most likely defect to form in PuO_2[22] . We found that having only one O vacancy in a 96 atom supercell decreased the volume of the unit cell by a factor of 5% which is a significant decrease of volume in a confined space. However with an added impurity, a substitution of one transition metal element for one out of 32 plutonium atoms in our supercell reduces the volume of the pristine supercell in all seven impurities we calculated. The volume contraction due to an impurity is larger than the volume contraction due to the single oxygen vacancy, see Table 11, row 5. When these impurities were added in addition to the to the O vacancy in the supercell, every supercell contracted further from 0.% for Zr impurity to as much as 1. 5% contraction for Ni impurity, see Table 11, row 6. This indicates that deliberately adding these impurities to the sample of plutonium dioxide storage

Table 11. Volume percent difference: Row 2 has the volume in (A^3) of the between pristine 2x2x2 PuO_2 and of the 2x2x2 cell of PuO_2 with one Pu atom substituted for one metal impurity atom. Row 3 indicates the volume % difference of pristine PuO_2 with the defect of metal substation. Note the negative sign shows contraction of volume. Row 4 is the volume of the unit cell with two defects; one oxygen vacancy at 1st nearest neighbor to the metal substitution. Note that the R4, C2 is only one defect of an oxygen vacancy which is an enlarged volume by 0.91% from the pristine cell. Row 5 is volume difference of the metal impurity defect only with the volume of the singly defective - oxygen vacancy unit cell. Row 6 is volume difference of the doubly defective system with a singular defective - oxygen vacancy in the plutonium dioxide supercell (32 Pu, 63 Oxygen).

PuO_2 **(in 2x2x2 cell)**	**No impurities**	**Mg (12)**	**Cr(24)**	**Mn(25)**	**Fe(26)**	**Ni(28)**	**Zr(40)**	**Mo(42)**
Volume (M:PuO_2)	1,297.68	1,217.03	1,216.75	1,228.48	1,217.43	1,215.39	1,229.22	1,225.98
% difference from PuO_2	0.00	-6.21	-6.24	-5.33	-6.18	-6.34	-5.28	-5.53
Volume ((M-O_v):PuO_2)	1,230.72	1,212.97	1,212.90	1,218.15	1,214.61	1,212.29	1,220.76	1,217.69
% difference of ((M-O_v):PuO_2) from PuO_2	-5.16	-6.53	-6.53	-6.13	-6.40	-6.58	-5.93	-6.16
% difference of (M:PuO_2) from (-O_v:PuO_2)		-1.11	-1.14	-0.18	-1.08	-1.25	-0.12	-0.39
% difference of ((M-O_v):PuO_2) from (-Ov:PuO_2)		-1.44	-1.45	-1.02	-1.31	-1.50	-0.81	-1.06

Spin-Orbit Coupling

We recognize that the spin-orbit coupling is necessary to ensure better chemical properties of these materials which were not considered for relaxation purpose. Inclusion of spin-orbit (SO) coupling to the system to calculate band structures reveals the charge-transfer type insulating behavior of the plutonium dioxide is retained even with the addition of impurities. In pristine bulk of 2x2x2 PuO_2, adding the spin-orbit coupling and U_{eff} = 4 opened up the gap as expected. There is a dip at the L-point (½ ½ ½) that is present in the spin orbit coupling's band structure with other impurity systems as well, see Figure 12 and Figure 15. This band has p and f orbital contributions primarily. This may indicate the hybridizing behavior of plutonium with oxygen. Checking the most significant impurities with SO, we note that the gaps are revealed in these cases. Adding SO on a system that has an impurity of one Mo atom within the bulk reduced the gap to 0.77 eV. However, the system's bands are fairly dispersionless in the conduction band indicating that the electrons will have less mobility.

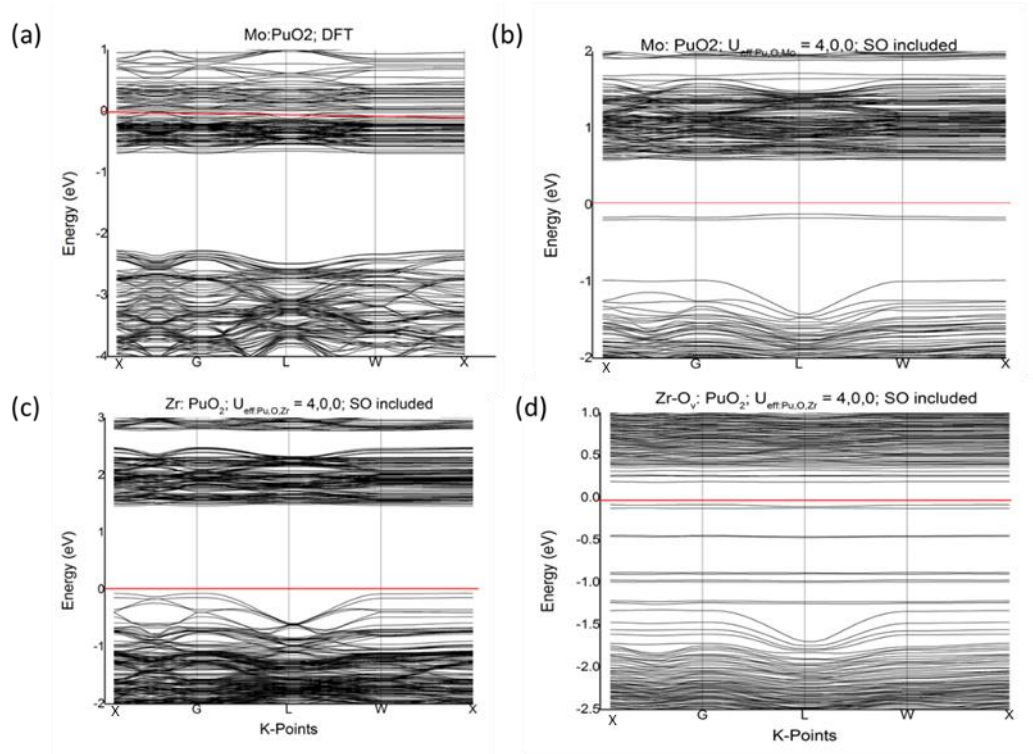

Figure 15: (a) DFT band structure of Mo: PuO_2. b) SO band structure of Mo: PuO_2. It reveals a band gap of 0.77 eV. (c) Zr: PuO_2 with spin-orbit coupling - Band structure reveals a band gap of 1.2 eV. (d) Zr -O: PuO_2 with spin-orbit coupling - Band structure reveals a band gap of 1.08 eV with 3 occupied impurity bands.

Adding SO also opens up the band gap with Zr impurity, however with a higher band gap of about 1.2 eV. Here the dip in the L-point is also present but there are no bands above the fermi level. This behavior changes with the presence of an oxygen vacancy, see Figure 15d.

Adding an Oxygen vacancy shortens the gap and creates occupied bands near the fermi energy. Two bands within 0.1 eV of the fermi energy and another band 0.45 eV below the fermi energy has mostly f-and p orbital occupancy indicating it is due to the plutonium atoms.

Conclusion

This chapter focuses on single metal impurities with and without a single oxygen vacancy as the nearest neighbor to the metal atom and does not regard any other defects formed. The least likely impurity to form within the crystal of PuO_2 is of manganese as it has

relatively large positive formation energies. In an oxygen rich environment, oxygen vacancy are not likely to form but they will co-exist or even form with certain impurities within the system. In plutonium poor conditions, Cr, Fe, Ni and Mo impurities may form as well. Please note that zirconium impurities within the plutonium dioxide structure will form regardless of the existence of oxygen vacancy and in both plutonium rich and plutonium poor conditions. These impurities contract the volume of the sample by as much as 6.2% in presence of oxygen vacancy. With an oxygen vacancy in the supercell, a Ni impurity causes the largest contraction at 6.58% but is less likely to form while Zr impurity still has the impressive contraction at 5.93% and the highest likelihood of formation among the impurities tested herein. The best incorporation of a M:PuO_2 system would be of zirconium, magnesium and molybdenum as their formation energies are quite low and they produce a significant contraction of the volume of the supercell as well. the existence of an additional O vacancy. While chromium is also likely to exist with and without oxygen vacancy and result in a contraction of the cell volume, it is less likely than the above three. In a more likely environment of oxygen vacancies, the volume contraction of supercell is larger than the corresponding supercell without an oxygen vacancy for every impurity studied herein. This reduction of volume of the stored plutonium oxides can have practical consequences in for long-term storage as alpha decay from the sample is responsible for the increase in lattice parameter over time [4]. The material to be stored prepared within O-poor conditions can ensure existence of oxygen vacancies. Furthermore, impurities with low formation energies can be added during or after processing to further contract the volume thus positively affecting the long-term storage.

Chapter 5

Surface with and without impurity

Introduction

Surfaces and its properties provides important information as they largely determine how a material interacts with each other and with their environment. As plutonium dioxide is radioactive and reactive to the environment, it is imperative that surface properties of these materials are explored.

To explore surface interaction, only the 111 surface was explored with five formulaic layers. From previous study (chapter 3), it is evident that a 5-layer surface will be sufficient for modelling defects. Here a 2x2 5-formulaic layer slab was constructed, each formulaic layer having 4 plutonium atoms with 2 oxygen layers, one above and one below the plutonium layers, see Figure 16, for a total of 15 atomic layers. Only anti-ferromagnetic configuration was considered with spin stacking chosen to ensure zero net dipole along each of the layers.

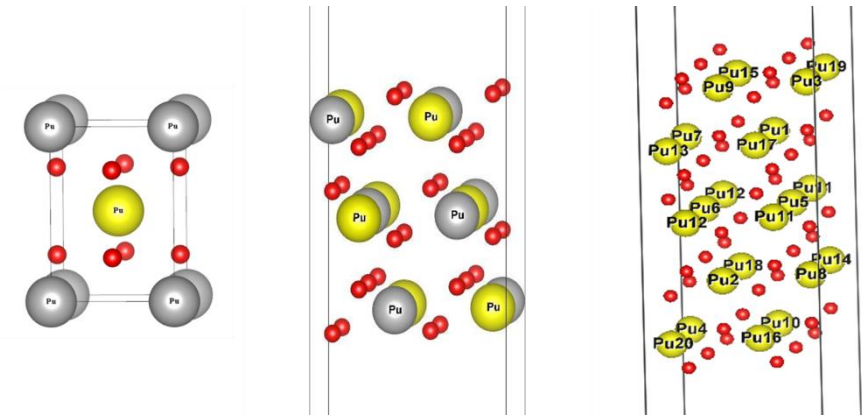

Figure 16: (L) AFM-bulk to (R) AFM 5 layer plutonium dioxide for 111 surface. (M) shows the spin arrangement for a 3 layer slab. This arrangement is similar in the 5-layer slab on the right.

Computational Details

Calculations were performed within the scope of density functional theory (DFT) using the VASP code, which uses the projector-augmented wave (PAW) method for the core electrons. PuO_2 forms a fluorite structure with an experimental lattice constant of 5.398Å and previously calculated lattice constant of 5.450Å, the latter of which was used to cleave the surface in the 111 direction. Once again, the $6s^2 7s^2 6p^6 6d^2 5f^4$ electrons $2s^2 2p^4$ electrons were considered as valence electrons for Pu and O atoms respectively. For the metallic impurity of Zr, *4d5s* electrons are taken to be the valance electrons. The exchange and correlation interactions are described by the spin-polarized generalized gradient approximation (GGA) in the PBE functional [68]. The plane-wave cut-off energy was set at 400 eV with a 3x3x1 Monkhorst-Pack k-point mesh[69] for a,b lattice constant near 7.6 Å and c near 30 Å for the 2x2 PuO_2 5 layer slab. When relaxed, the slabs were relaxed within the DFT theory and with a 3x3x1 k-point mesh. The single point calculations were performed with the inclusion of spin orbit coupling and U_{eff} =4eV for plutonium atoms. The plutonium atoms were arranged in anti-ferromagnetic arrangement as in the chapter 3[70]. The five layer slab has 20 plutonium atoms and 40 oxygen atoms, thus the anti-ferromagnetic arrangement was configured such that each layer started as magnetically neutral with two spin up Pu-atoms and two spin down Pu-atoms to ensure zero net magnetic dipole moment along the surface. Energy convergence criteria was set at $1x10^{-5}$ eV and Hellmann-Feynman forces on each ion to be less than 0.01 eV/Å.

Pristine Plutonium dioxide slab

The relaxation of the AFM pristine slab was done within the density functional theory. As mentioned previously, different levels of theory have very little impact on the lattice constant of the plutonium dioxide[55]. Similar to Rak[24], there was insignificant relaxation of the ions within the slab. Table 12 lists the most significant of the contractions of the pristine slab and this confirms that PuO_2 surface is fairly stable and relaxation of slabs will not yield significantly

variant behavior. The largest bond contraction between a plutonium and oxygen atom is of 0.16Å as noted at the outer layer exposed to the vacuum and least amount of contraction is in the bulk-like layer. The sub-surface layer contraction is similar to bulk behavior.

Table 12: Slab relaxation of the pristine PuO_2. Only the largest bond contractions between two atoms in the specific layer are listed. Distances, d are in Å.

	Atom	Atom	Initial d Å	Relaxed d Å	Δ Å
Outer layer	Pu3	O25	2.35	2.19	0.16
Outer layer	Pu3	Pu13	3.84	3.76	0.08
Sub-layer	Pu1	O23	2.35	2.30	0.05
Sub-layer	Pu13	Pu3	3.84	3.76	0.08
Bulk layer	Pu5	O5	2.35	2.31	0.04
Bulk layer	Pu5	Pu1	3.84	3.77	0.07

The 0.16 Å for the top-layer plutonium-oxygen distance is about a 6.8% difference while the plutonium-plutonium distance is less significant at 2.1% contraction.

Within DFT level of theory, the slab had no net magnetic moment. However with the addition of spin-orbit coupling and U_{eff} term, the pristine slab has a net magnetic moment of 6.309 μ_B with most of moment coming from the f-orbital. The pDOS of the relaxed pristine slab is

O-vacancy

Oxygen vacancies occur naturally in the material. To explore this phenomenon, one oxygen atom was removed from the slab in two extrema cases. In the first case, one oxygen vacancy is present in the most bulk-like, i.e the center layer of the 5 layer slab, henceforth known as the bulk-vacancy or B-O_{vac}. The second case studied is the outer-layer oxygen vacancy where an oxygen atom was removed from the outer-most layer of the slab which interacts with the environment and is suspected to be most reactive, see Figure 17. Note that is removal of one oxygen atom out of 40 in the pristine slab.

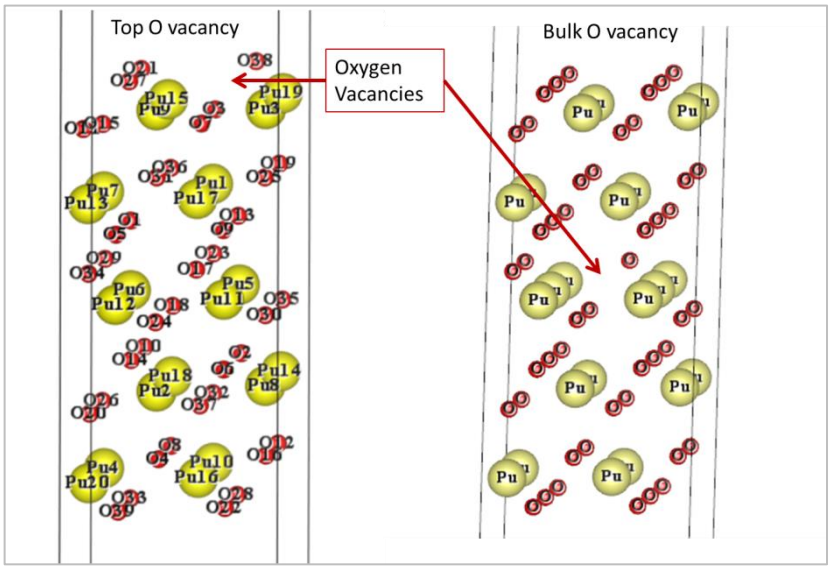

Figure 17: (L) Oxygen vacancy in the top layer of the surface of PuO_2. (R) Oxygen vacancy in the bulk-like layer of the surface of PuO_2.

The system with the oxygen vacancy at the outer layer (O-O_{vac}) is relaxed within the DFT level of theory and exhibits a slight contracting movement of the system, with the largest contraction between the two nearest plutonium atoms closest to the vacancy at 0.21 A, and largest contraction of first nearest neighbor plutonium which moved closer to another oxygen by 0.17 Å. These contractions are by 5.5% and 7.2% respectively.

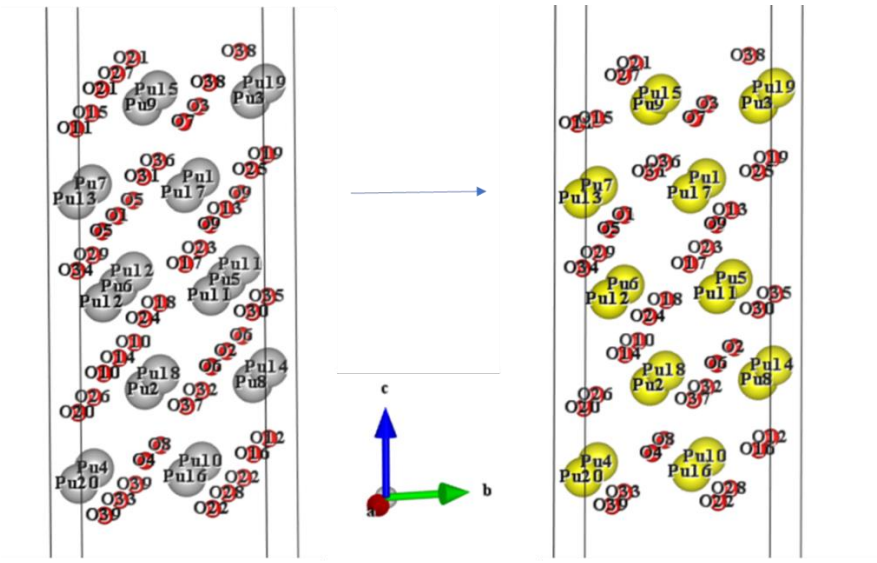

Figure 18: O-vacancy in the outer most layer (at the top). (L) Unrelaxed surface with O vacancy. (R) Fully-relaxed surface with O vacancy.

Oxygen vacancy close to the middle of the surface slab illustrates most bulk-like oxygen vacancy (B-O_{vac}) for the slab system. The formation energies, see

Figure 19 suggest oxygen vacancies will form at the top layer and at the bulk layer easily in oxygen-poor conditions and vacancies at the bulk are slightly more favored than at the outer layer.

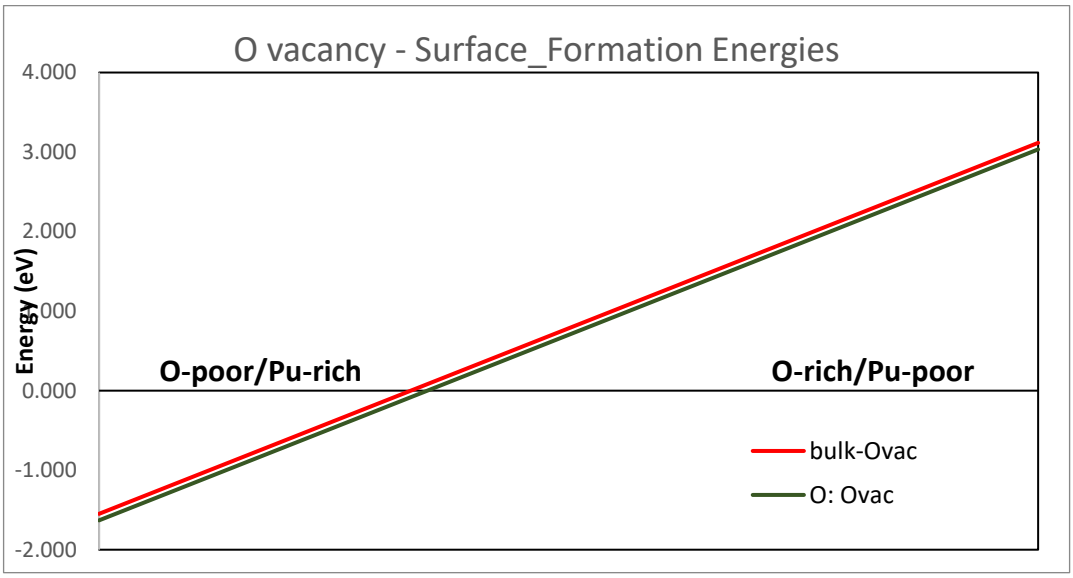

Figure 19: Formation Energies of oxygen vacancy on PuO_2 (111) Surface

Table 13: Comparison of the difference of the shortest bond length between two plutonium atoms on each layer and the closest plutonium atom and oxygen atom. Comparison from fully relaxed pristine slab with fully relaxed surfaces with oxygen vacancy at the outer layer and at the bulk layer. Only the difference of the distances (all of which are contractions with respect to the initially cleaved surface) are listed here in Å.

	Pristine		Outer O_{vac}		Bulk O_{vac}	
Layer	Pu-Pu	Pu-O	Pu-Pu	Pu-O	Pu-Pu	Pu-O
O: Pu1	0.08	0.16	0.21	0.17	0.12	0.07
O: Pu2	0.07	0.16	0.21	0.15	0.17	0.07
O: Pu3	0.07	0.14	0.19	0.17	0.12	0.07
O: Pu4	0.07	0.15	0.03	0.14	0.06	0.06
S: Pu1	0.07	0.05	0.13	0.12	0.10	0.08
S: Pu2	0.07	0.04	0.09	0.06	0.06	0.06
S: Pu3	0.08	0.04	0.08	0.06	0.10	0.08
S: Pu4	0.07	0.05	0.08	0.03	0.17	0.10
B: Pu1	0.07	0.03	0.13	0.07	0.13	0.09
B: Pu2	0.07	0.04	0.13	0.07	0.14	0.10
B: Pu3	0.07	0.03	0.09	0.08	0.14	0.10
B: Pu4	0.07	0.04	0.07	0.07	0.10	0.09

A single vacancy can affect the surrounding bonds. In the outer layer, when a vacancy is present, the contraction between closest plutonium atoms and their respective bond lengths between other plutonium atoms and closest oxygen atoms is significantly increased.

Compare the Pu-Pu contracted distance by 0.21 Å in the outer layer with an oxygen vacancy to the pristine slabs largest contracted distance of only 0.08Å. Interestingly, Pu-O distances are not as affected by an oxygen vacancy as compared with pristine slab, a difference of only 0.01Å.

Having a bulk layer oxygen vacancy (B-O_{vac}), contracted the Pu-Pu distances slightly less than O-O_{vac} (0.14 Å versus 0.21 Å within the same layer as the vacancy) contracted the distances in the outermost layers. Bulk-layer oxygen vacancy also contracted the Pu-O distances throughout the slab. These contractions are greater than in pristine slab and in the bulk and sub-surface layer of O-O_{vac} slab. Only the outer layer's Pu-O distances are shorter than the Pu-O distances of Bulk O vacancy slab.

However, overall the atoms in the slab with a vacancy relaxed closer to each other than a slab without a vacancy.

The total dos show that there may be a small gap in the system with oxygen vacancy, and there are defect bands at the bottom of the conduction band for the outer layer O_{vac}. However, the bulk O_{vac} the defects bands are almost in the middle of the gap. The B-O_{vac} shows a greater band gap than O-O_{vac}.

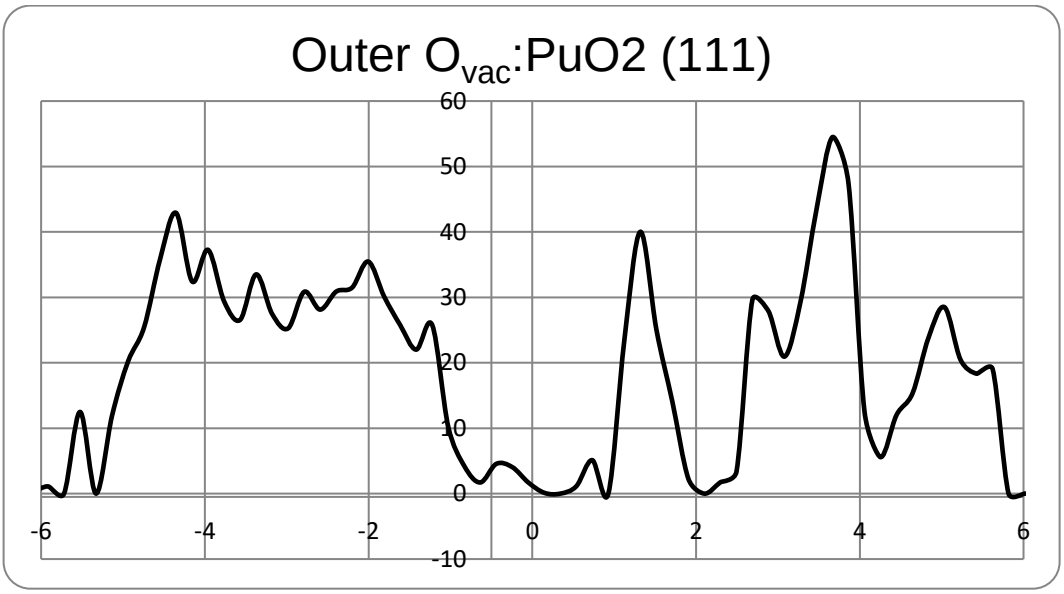

Figure 20: Total DOS of outer O_{vac}:PuO_2 (111) slab at DFT+U with spin-orbit coupling.

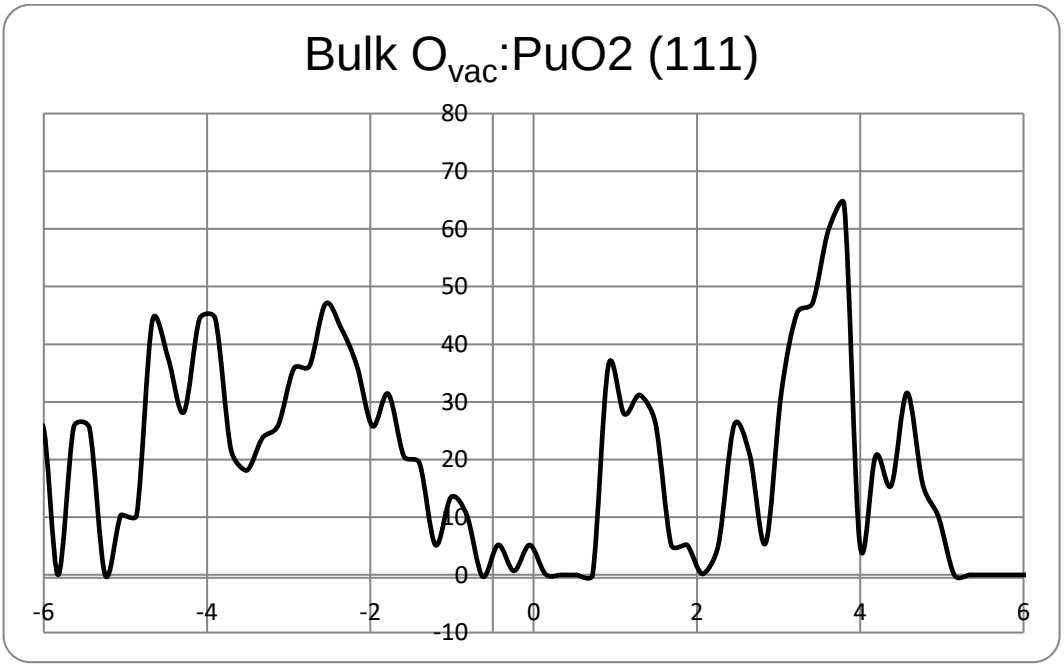

Figure 21: Total DOS of Bulk O_{vac}:PuO_2 (111) slab at DFT+U with spin-orbit coupling.

Zirconium impurity within the slab

Zirconium is the most promising dopant found in the previous section for contracting the volume as well as having a low formation energy when doped in bulk plutonium dioxide. To compare this transition metal impurity in the surface of PuO_2, a zirconium atom was substituted in place of a plutonium atom in a 2x2 five-formula unit slab PuO_2-111. There are three positions the zirconium atom was placed in. At the outer most plutonium layer, at the innermost plutonium layer (as pictured in Figure 22), and at the sub-surface layer between the two aforementioned layers. These position will henceforth be referred to as O-Zr:PuO_2, B-Zr:PuO_2, and S-Zr: PuO_2 respectively.

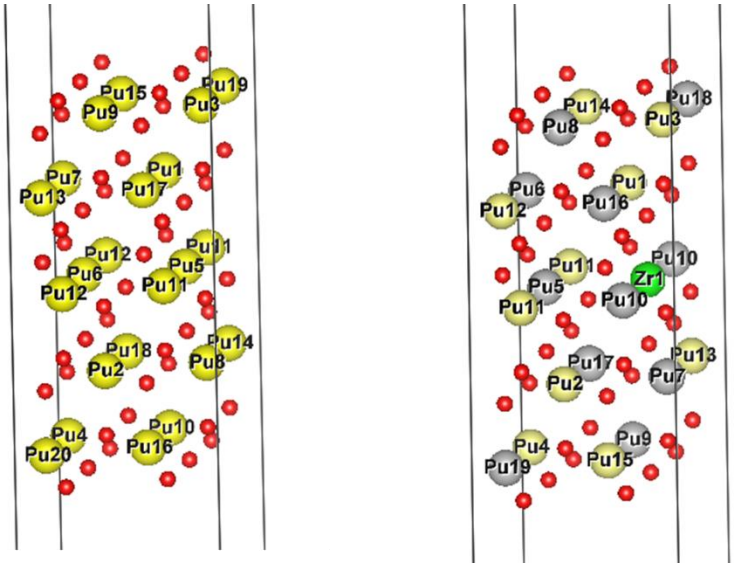

Figure 22: Zr substitution in the bulk-like layer.

Formation Energies

Formation energies determine the possibility of existence of these impurities in this position within the host slab. I either extrema, oxygen rich and oxygen-poor conditions show that the zirconium substituted in plutonium site is a system that is very likely to exist and or

form. The interesting factor is that the it is likely to exist in each type of layer, from top-most to most bulk-like layer, see Figure 23.

Although they formation energy is negative for Zr impurity at the surface, it is still favorable to be in the bulk than the surface. It also favors the bulk-like layer at the surface. Energetically as expected the pristine slab has the lowest energy followed by the doped slabs, see Table 15.

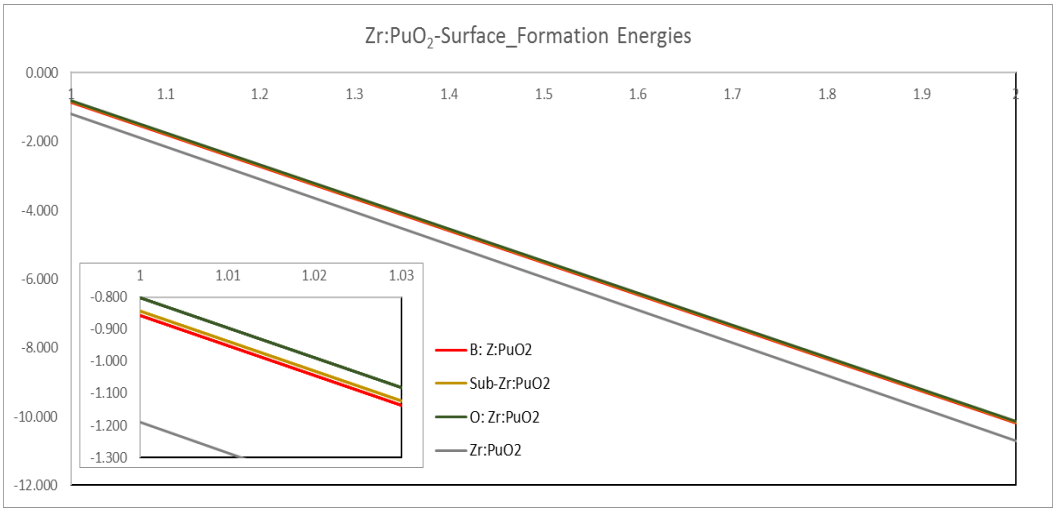

Figure 23: Formation Energies of Zr impurity on PuO_2 (111) surface. For comparison, Zr impurity in bulk (gray) is also shown.

Bond Length

The Zirconium dopant in the outer layer, the most reactive layer was fully relaxed. As compared with pristine system, the layer with zirconium has shorter Pu-Pu distances by 0.11Å as oppose to the almost consistent Pu-Pu contraction of the pristine slab of 0.08 Å. Only the Zr-O distance was the shortest with 0.23 Å contraction from 2.35 Å to 2.12 Å. The rest of the plutonium in that outer layer had Pu-O distances 2.25-2.27 Å for closest Pu-O distances. Interestingly, the sub-surface layer has larger Pu-O contraction suggesting zirconium impurity

has an effect at that layer. This exaggerated contractions are definitely not seen on the other side of the slab (or the far-outer and far sub-surface slabs) as seen in

Table 14, left two columns. The bulk is repeated and same on these columns as the middle two columns. Thus the zirconium impurity has definite effects on the bonding characteristics of the surrounding atoms in the surface slab.

Table 14: Difference of distances between atoms for pristine as comparted with slab with Zr in outer layer. Highlighted is actually Zr-Pu and Zr-O distance as that layer has one zirconium impurity. Far Outer Zr:PuO_2 is the outer layer on the other side of the slab. This layer has no zirconium impurity and thus models the pristine layer. This layer is also the furthest layer from zironium impurity. The Far sub-surface layer is the layer above the far outer layer and is one layer closer to the zirconium impurity.

	Pristine		Outer Zr: PuO_2		Far Outer Zr: PuO_2	
Layer	Pu-Pu	Pu-O	Pu-Pu	Pu-O	Pu-Pu	Pu-O
O: Pu1	0.08	0.16	0.09	0.08	0.07	0.05
O: Pu2	0.07	0.16	0.11	0.09	0.08	0.08
O: Pu3	0.07	0.14	0.11	0.1	0.07	0.04
O: Pu4	0.07	0.15	**0.11**	**0.23**	0.07	0.06
S: Pu1	0.07	0.05	0.09	0.05	0.07	0.07
S: Pu2	0.07	0.04	**0.11**	0.13	0.07	0.07
S: Pu3	0.08	0.04	0.10	0.10	0.10	0.06
S: Pu4	0.07	0.05	0.11	0.12	0.08	0.08
B: Pu1	0.07	0.03	0.08	0.07	0.08	0.07
B: Pu2	0.07	0.04	0.09	0.06	0.09	0.06
B: Pu3	0.07	0.03	0.08	0.05	0.08	0.05
B: Pu4	0.07	0.04	0.07	0.06	0.07	0.06

Magnetism

The surface was configured to be fully AFM and thus with an even number of plutonium should be close to neutral. However the layered AFM slab has an overall magnetic moment. Of the total moment in the cell, the largest amount of magnetism, within the same order is in the f-orbital as expected.

Table 15: Surface Energetics(eV) and Magnetism(μ_B) values. The lowest energies are for pristine slabs and the energies have been scaled with respect to this slab.

	DFT	DFT+U (SO)	DFT Mag.	Magnetism with DFT+U(SO)		
	Energy	Energy		Mag x	Mag y	Mag z
PuO_2 AFM	0.000	0.000	-0.0607	2.573	-1.576	5.541
B-Ovac	8.049	8.547	0.3890	-0.909	0.532	-0.3696
O-Ovac	7.967	7.873	0.0012	-0.905	0.638	-0.3514
B-Zr: PuO_2	5.076	3.058	-3.9745	-0.061	0.036	-3.644
S-Zr: PuO_2	5.091	3.061	-3.9093	-0.180	0.103	-3.658
O-Zr: PuO_2	5.134	3.367	3.8481	1.334	0.563	6.088

Zirconium dopant in the top or outer layer has significantly varied magnetic behavior then the Zr impurity in the bulk-like or the sub-surface layer in the c or z-direction. In the Outer layer with Zr:PuO_2 system, Zr is substituted for one of the plutonium atoms in one of the two outer-most layer of the slab. This layer is exposed to the vacuum and thereby not fully coordinated. The two closest plutonium atoms in the same layer lose most of their magnetic spin in the z-direction and have only about 10% of the spin as other plutonium in the slab. The third plutonium in the same top layer but farthest from the impurity loses it even more significantly. In the x-y direction, these same plutonium atoms have the greatest magnetic spin moments, ten times the moment of other plutonium atoms in the slab. This may indicate that Zr is acting like a charge trap. This behavior is singular in this layer, sub-surface and bulk–layer systems with zirconium impurity has similar total magnetic profile. In this layers, plutonium have net magnetic moment in the z-direction and very small net magnetic moment in x-y directions.

Band Gap

DOS plots confirm that for the DFT level of theory, the surface is depicted to be a metallic regardless of the impurity.

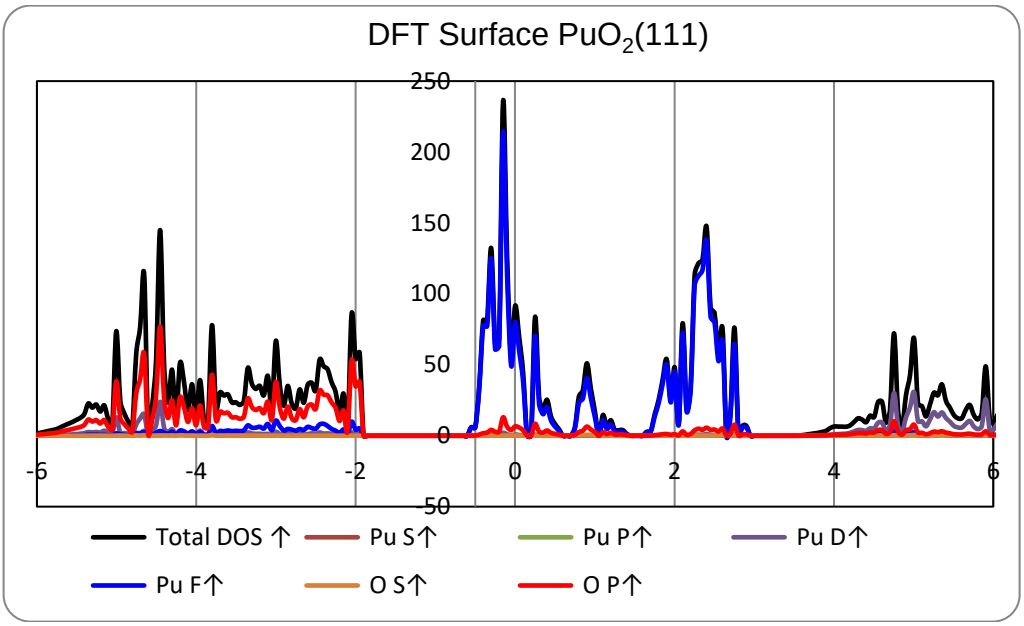

Figure 24: pDOS dft of 2x2 pristine PuO_2 (111) surface.

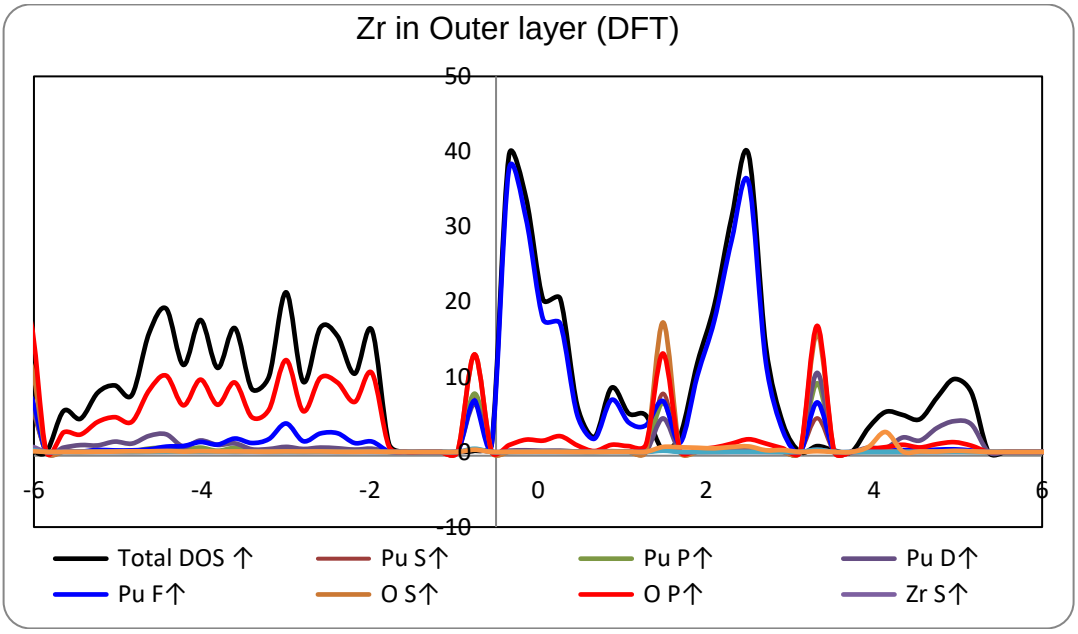

Figure 25: pDOS DFT of Outer Zr: PuO_2. Note the defect bands below the conduction band.

With DFT+U with spin-orbit coupling added reveals a gap of 1.77 eV which is agreement with the experimental band gap of 1.8eV.

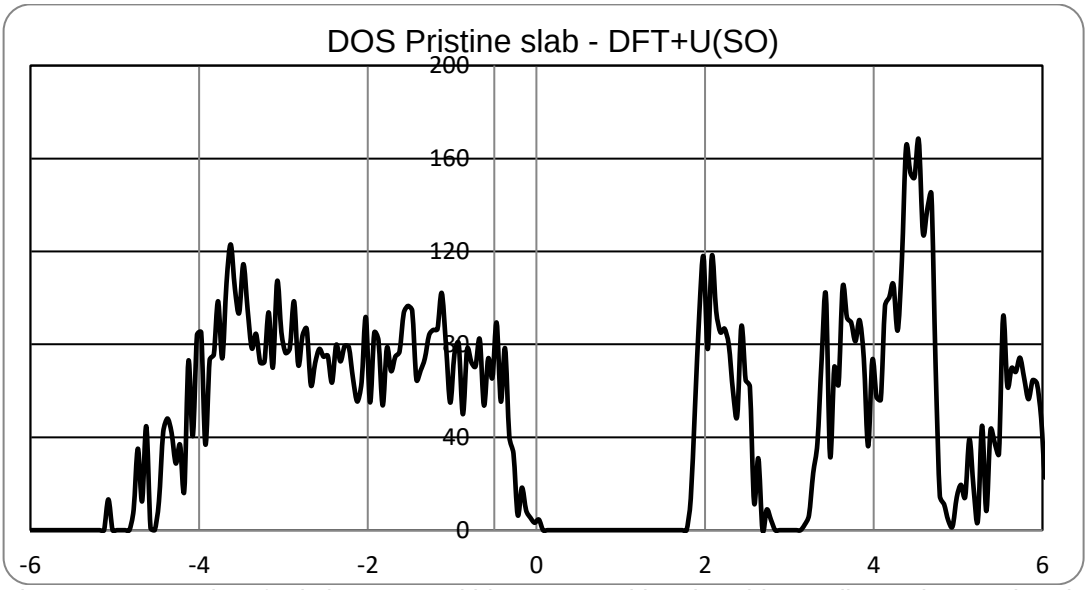

Figure 26: DOS plot of pristine PuO_2 within DFT+U with spin-orbit coupling. Shows a band gap of 1.77 eV

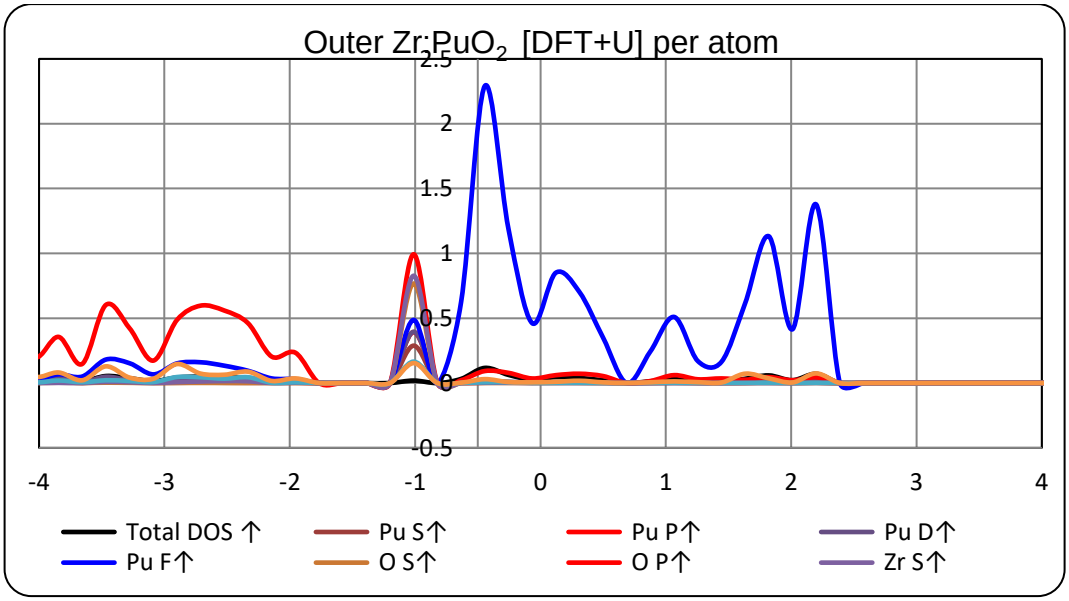

Figure 27: pDOS per formula Unit at DFT+U Outer Zr:PuO_2.

Our DOS plots indicate that to get a band gap or insulating behavior for the surface, spin-orbit coupling must be included. Without spin-orbit coupling, only DFT+U has some bands in the bleeding into the conduction band. With DFT, it was found that the bottom of the conduction band has electrons making it almost like a semi-conductor.

Adding spin-orbit coupling to a DFT+U level of theory, we were able to get a band gap with the zirconium impurity. The total dos was also calculated with spin-orbit coupling.

Whereas in the most bulk-like layer, as well as the sub-surface layer the dos plot shows similar bulk-like behavior. The surface band gaps of with Zr impurity at the three distinct layers are all larger than the band gap of 1.2 eV in the bulk with a zirconium impurity, see Figure 28-Figure 30.

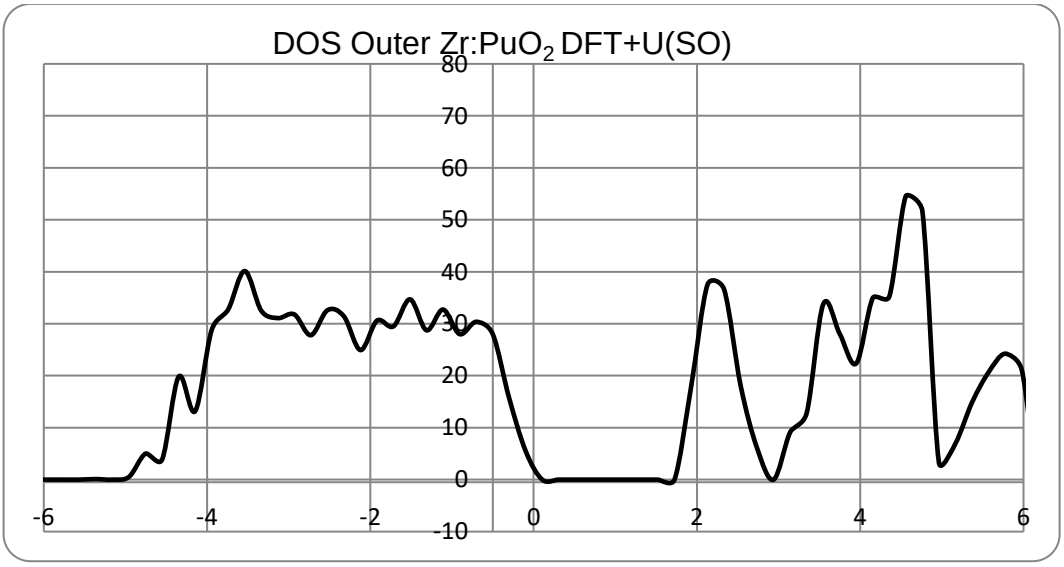

Figure 28: Total DOS DFT+U+SO of Outer Zr: PuO_2 . Shows a band gap of 1.7eV

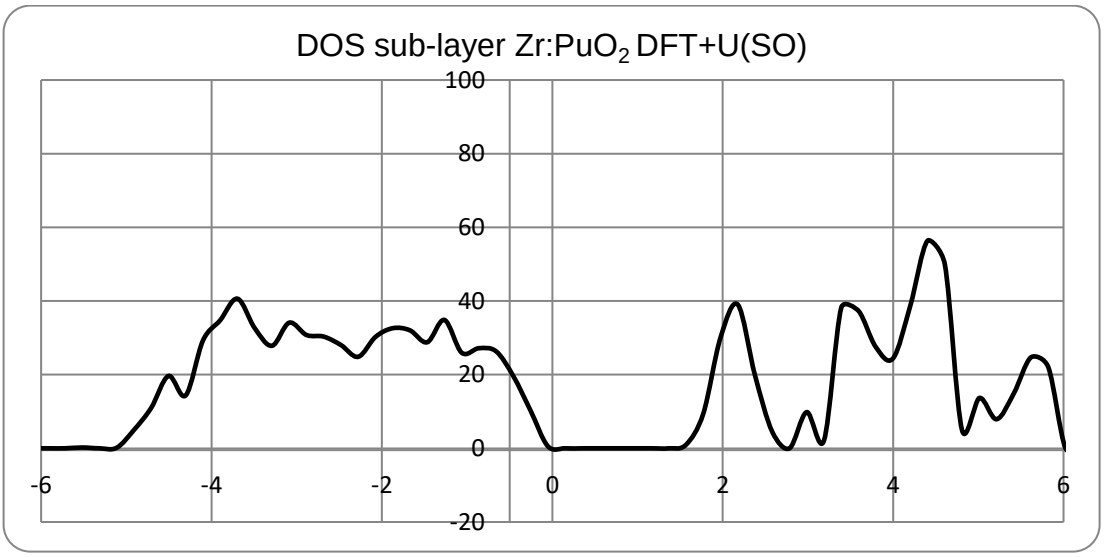

Figure 29: Zr in sub-surface layer. Total DOS indicats a band gap of 1.57 eV

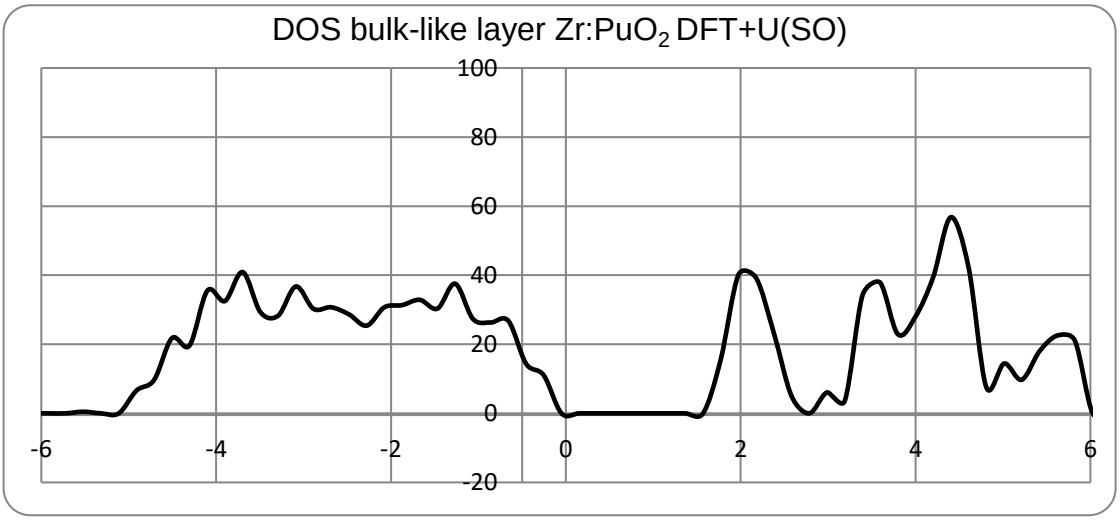

Figure 30: with spin-orbit coupling and DFT+U level of theory, Bulk Zr:PuO_2. has a band gap of 1.57 eV as compared to bulk behavior and band gap of 1.2 eV.for (Zr:PuO_2) and 1.7 eV for pristine slab.

Conclusion

For an impure surface of plutonium dioxide, only (111) in AFM arrangement was prepared. Defects such as one oxygen vacancy were added into the very outer oxygen layer of the slab. Another was an oxygen vacancy at the almost the center of the slab. Geometry did

not change much with the addition of an vacancy but did contract. Formation energy curves suggest that these systems may exist spontaneously in oxygen poor conditions. Adding a vacancy did reduce the gap when the vacancy was in the bulk layer and further removed the gap when the vacancy was in the outer layer as compared with the pristine slab.

Zirconium atom was also substituted in outer plutonium layer; it was also substituted for one plutonium in the sub-surface layer and one layer in the bulk-layer. The relaxation of the slabs with the substituted impurity showed contractions within the layer that suggested that zirconium plays an significant role in slab stability. While this needs to be explored further, the contractions may suggest that a zirconium in top layer of host slab affects the layer underneath it. Formation energy curves readily show that these systems may exist spontaneously in either oxygen rich or oxygen-poor conditions. The magnetic behavior with impurity on top was significantly different than the sub-surface layer and bulk layer substitution of zirconium. The DOS plot also show that the gap for top layer, sub-surface layer and bulk layer were very similar at 1.52 and 1.56eV.

Chapter 6

Conclusion

Plutonium dioxide, PuO_2, is the most stable form among the plutonium oxides. This is significant as plutonium oxides are of widespread importance with application in nuclear fuels, space missions, and long-termed storage of plutonium from spent fuel and nuclear weapons. The processes which refine and ready plutonium for either storage or to be utilized in other applications bring many other elements in contact with the plutonium metal and thus affecting the chemistry of the plutonium. Pure plutonium metal is reactive and readily corrodes to an oxide, most stable of which is stoichiometric PuO_2. Iimpurities and vacancies can form in the plutonium dioxide before, during and after either processes it undergoes or even during storage. So-called “Pure” plutonium dioxides have 3-8% impurities. As transition metals come in contact during the previously mentioned process including nuclear fuel cycle and storage condition, studying the interaction between transition metals and plutonium dioxide is critical for better, more efficient storage plans as well as gaining insights to provide a better response to potential threats of exposure to the environment.

Plutonium dioxide has an experimental lattice constant of 5.398Å and has a FCC (face-centered cubic) crystal system, with the oxygen atoms at the (¼, ¼, ¼) sites and the plutonium atoms at the (0,0,0) sites. It is in the space group FM3m, No. 225. Using density functional theory, first the bulk and then the PuO_2 (111) surface of the pristine system have been investigated. The bulk results show that magnetic configurations of PuO_2 are still debatable and need to be tested in surface slabs. The pristine periodic slab models of the surface, from one to six molecular layers, were examined to find surface properties and slab size effects. Both ferromagnetic (FM) and anti-ferromagnetic (AFM) configurations were considered with and without spin-orbit coupling for the 1x1 slab for both 110 and 111 cleaved surfaces. While the (111) surface with is more energetically favored, there was very minute difference between the energies of the two magnetic configurations. Hence, thermodynamically both magnetic states

are possible. However due to the calculated surface energy which favored the anti-ferromagnetic configuration slightly for majority of the layer calculations, the AFM configuration was taken as the ground-state magnetic order. Therefore, the effect of periodicity was explored between AFM configured 1×1 and 2×2 super cell. In the (111) surface slab, each molecular layer consist of a layer of plutonium atoms in between two layers of oxygen atoms. Each plutonium layer in the 2x2 supercell had 4 plutonium atoms and that layer was initially anti-ferromagnetically configured to give zero net magnetic moment, i.e two atoms with spin up and two atoms with spin down.

Analyzing their surface energies, work functions, band gaps and density of states indicated that 5-6 molecular layer is sufficient for surface modelling. Except for the outer layer, the surface in general retains the Mott-insulator property of the bulk. The outer layer shows more of a charge-transfer type of insulator.

Secondly the effects of impurity and defects in the bulk and then the PuO_2 (111) surface have been investigated. Selection of seven transition metals, magnesium, chromium, manganese, iron, nickel, zirconium, and molybdenum, which have a likelihood of being exposed to the plutonium or the plutonium oxide during various process or possible leaks to the environment was determined. We explored a system of substituted metal impurity in PuO_2 supercell one impurity at a time. We then repeated the calculations with an additional oxygen vacancy. These systems were fully relaxed and showed insignificant distortion in the FCC lattice. An impurity-defect band manifests itself at the bottom of the conduction band and affects the band gap of the unit cell. Of the seven impurities within the bulk PuO_2 tested, Zr and Mg are optimal dopants for the material. They are likely to form regardless of the oxygen-rich or poor conditions. Our results reveal interesting volume contraction of PuO_2 supercell when one plutonium atom is substituted with a metal atom. The Mott-insulating character of the PuO_2 was retained even with an added dopant.

Extending the impurity dopant to a five molecular layers of 2x2 PuO_2(111) surface slabs, three layers were highlighted. The outer layer, exposed to the vacuum, the bulk layer in the middle of the slab and the subsurface layer sandwiched between the bulk and the outer layer. Oxygen vacancy in the outer layer is less favorable than the bulk-layer and affects the Pu-Pu distances beyond the layer that it resides in. Zirconium impurity tested on each of these layers, has negative formation energy in either extreme conditions of oxygen-rich and oxygen-poor conditions and has minimal impact on the slab beyond its nearest neighbor atoms. The non-pristine slab contracts due to dopants and defects as well but retains the Mott-insulating character with an impurity within the PuO_2 (111) surface slab.

The highlights or the significant results of the works are following:

- Pristine PuO_2 (111) is more energetically stable than the 110 surface.
- 5-6 molecular layers was found to be sufficient for modeling the surface of PuO_2.
- While the outermost layer exhibited charge-transfer type of insulator, the sub-surface and bulk-like layer of the slab retained the mott-insulating property of the bulk.
- A substitution of a single metal impurities leads to significant contraction of volume with Zr as the most favorable.
- Addition of a nearby oxygen vacancy in the impurity system leads to further contraction of the volume with Zr dopant with an oxygen vacancy to be the most favorable system.
- While an Zr impurity within the bulk-like layer was favored over an impurity on the outermost layer, there was not a significant difference. The relaxed slabs also revealed bond contractions between the atoms but they did not affect the plutonium-plutonium distances beyond the nearest neighbors.
- The vacancy at the outer layer instigated larger contractions in that layer than the bulk-layer oxygen vacancy. Both types of vacancies caused defect bands at the bottom of the conduction band.

Appendix A

pDOS of M:PuO_2 and M-Ov:PuO_2 and extra information

Our system is spin polarized and initial magnetic structure is in the AFM configuration.

Our relaxed system lattice constant is 5.42 A as compared to the experimental lattice constant of 5.398A. Note our relaxed supercell volume is 1276.64 A^3 while the experimental supercell would be $(5.398x2)^3$=1258.3 A^3.

We added LDA+U parameter to 5f and 3d states of plutonium and metals respectively. The relaxation, single point and dos calculation with the U parameter were similarly done. U values for the metals was taken from literature to accommodate the local environment of being surrounded by 4 O^{2-} atoms. These U value were explored in (ref: 10.1103/PhysRevB.90.115105.). The values were used are in table below:

Metals	U=U-J	Comments:
Mg	0	Z=12; No U needed
Cr	3.24	Z =24; 4+ state
Mn	3.19	Z=25; 4+ state
Fe	4.09	Z=26, 3+state
Ni	4.40 and 6.07	Z=28; 2+ and 4+ states
Zr	0	Z=40; Ref
Mo	0	Z=42; Ref.

Our DFT relaxations of one metal impurity and of one metal impurity with an adjacent oxygen vacancy clearly shows a contraction of volume as comparted to the pristine, listed below.

Volume Changes M:PuO_2:

PuO_2	Cr	Fe(26)	Mn(25)	Mg(12)	Mo	Ni(28)	Zr
1219.62	1216.75	1217.43	1228.48	1217.03	1225.98	1215.39	1229.22
%diff	0.24	0.18	-0.73	0.21	-0.52	0.35	-0.79

Volume Changes with M-Ovac: PuO_2

PuO_2	Cr(24)	Fe(26)	Mn(25)	Mg(12)	Mo(42)	Ni(28)	Zr(40)
1230.72	1212.90	1214.61	1218.15	1212.97	1217.69	1212.29	1220.76
-0.91	1.45	1.3	1.02	1.44	1.05	1.44	0.81

If O vacancy is the most likely defect in PuO_2 then introducing transition metal impurities, such as of Cr, Ni and Mg may reduce overall volume of the stored PuO_2 which in turn would reduce the pressure in the storage containers.

O vacancy increases the volume but the addition of these impurities may reduce the volume back to the original volume or even lesser. It has been shown previously[79] that neutral oxygen vacancies lead to lattice expansion while charged vacancies lead to lattice contraction.

We found that presence of impurity reduces the volume, which is to be expected as Pu is a large atom while the metal is small in the bulk. The bonds between Pu and O also shrink.

DOS:

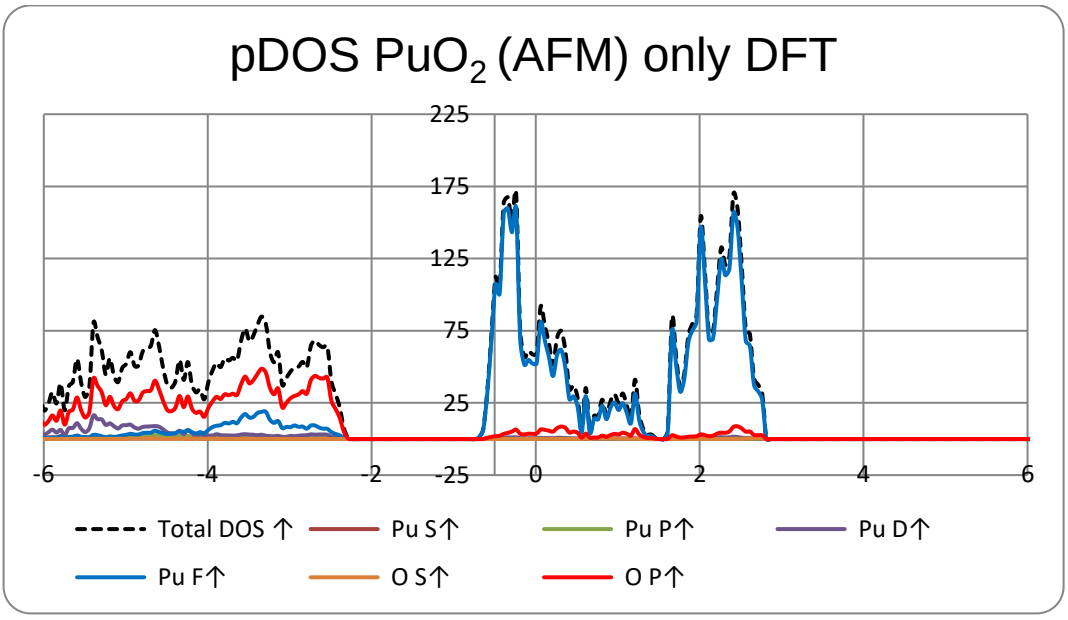

Figure 31: DFT PuO_2. Shows as a metal

With O vacancy,

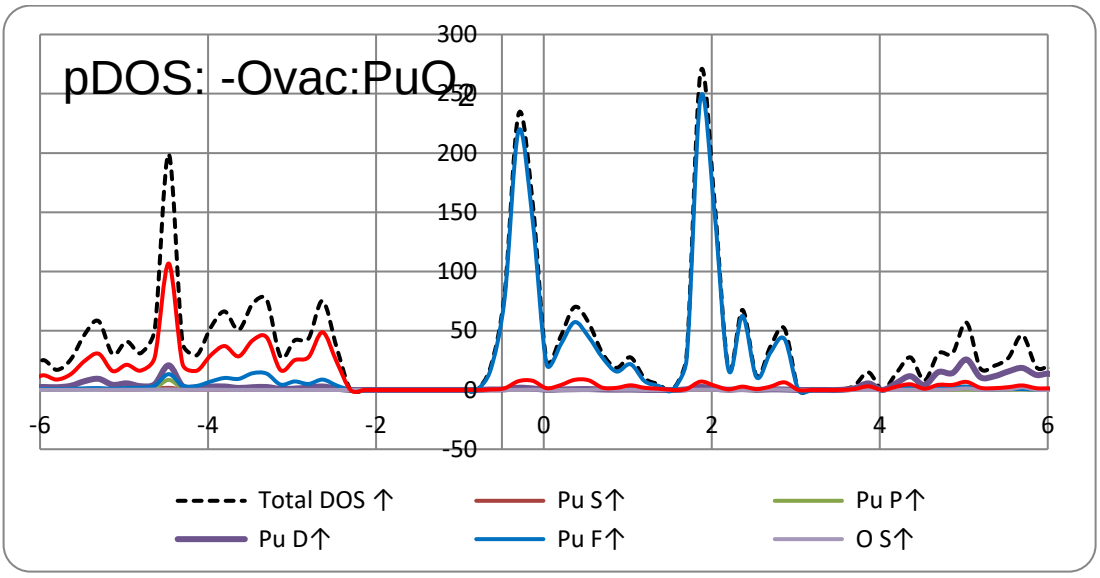

Figure 32: PuO_2 with oxygen vacancy or in ($-O_v$:PuO_2). Note: shows as a metal.

Comparing the pDOS of a close Pu-O to the oxygen vacancy with the farthest Pu-O bond, we find that the difference in their pDOS is insignificant.

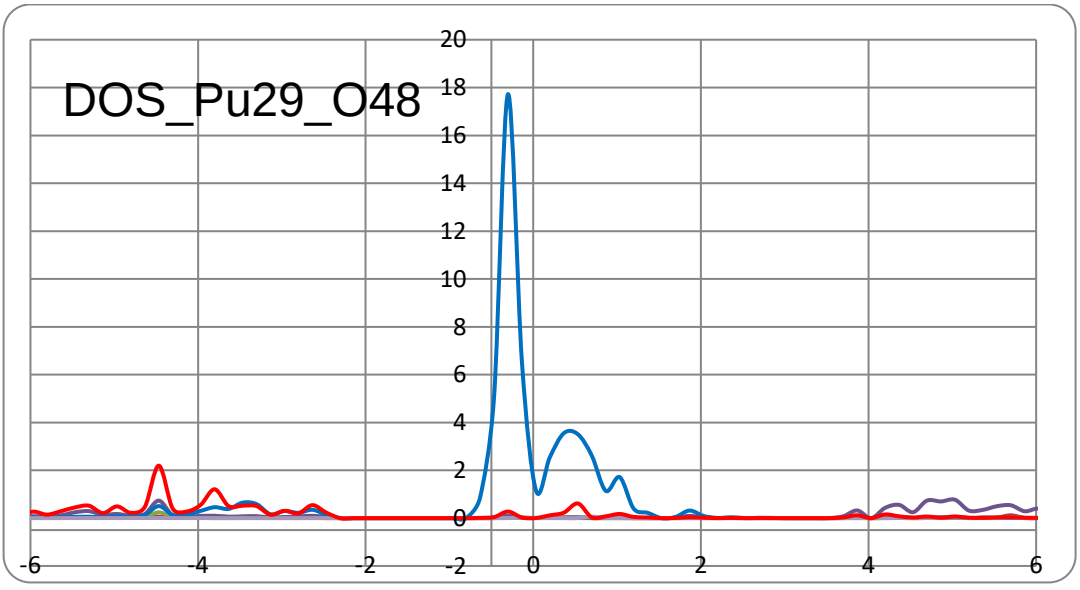

Figure 33: close Pu-O pDOS for PuO_2 cell with 1 O vacancy or in ($-O_v$:PuO_2)

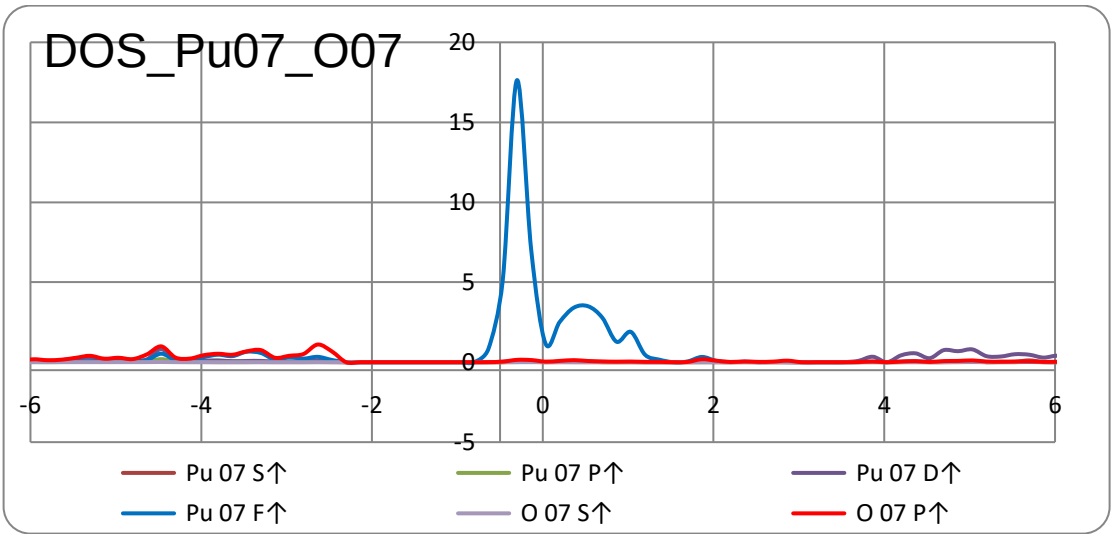

Figure 34: far Pu-O pDOS for PuO_2 cell with 1 O vacancy or in ($-O_v$:PuO_2)

Other metal impurities full DOS are as follows:

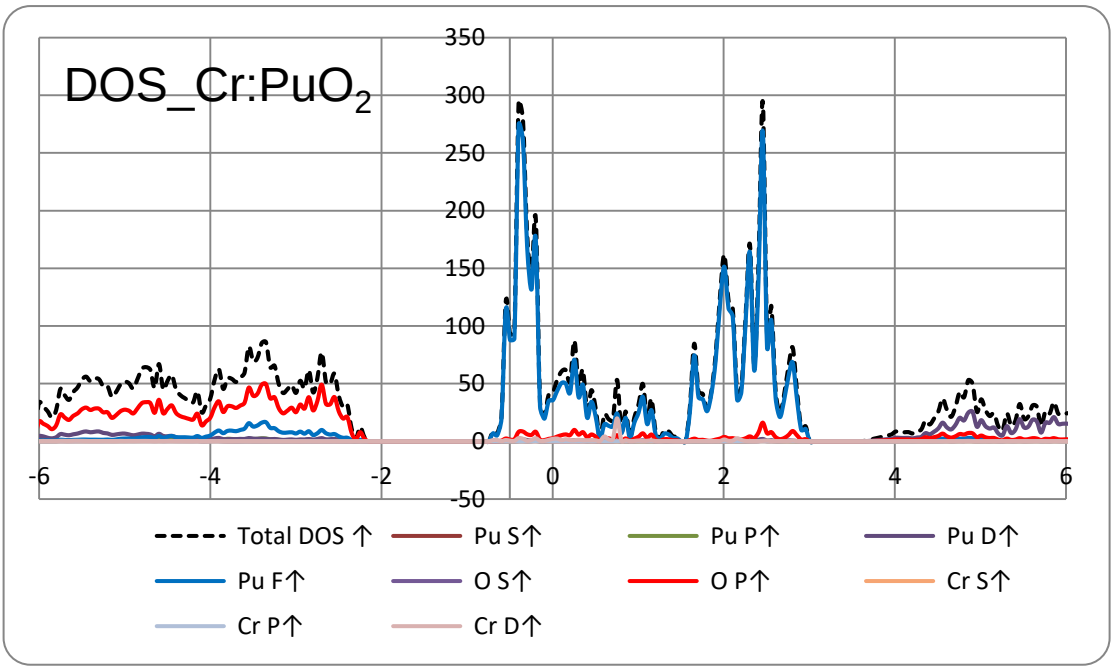

Figure 35: pDOS of Cr impurity in $Pu_{31}O_{64}$ bulk or Cr:PuO_2.

-

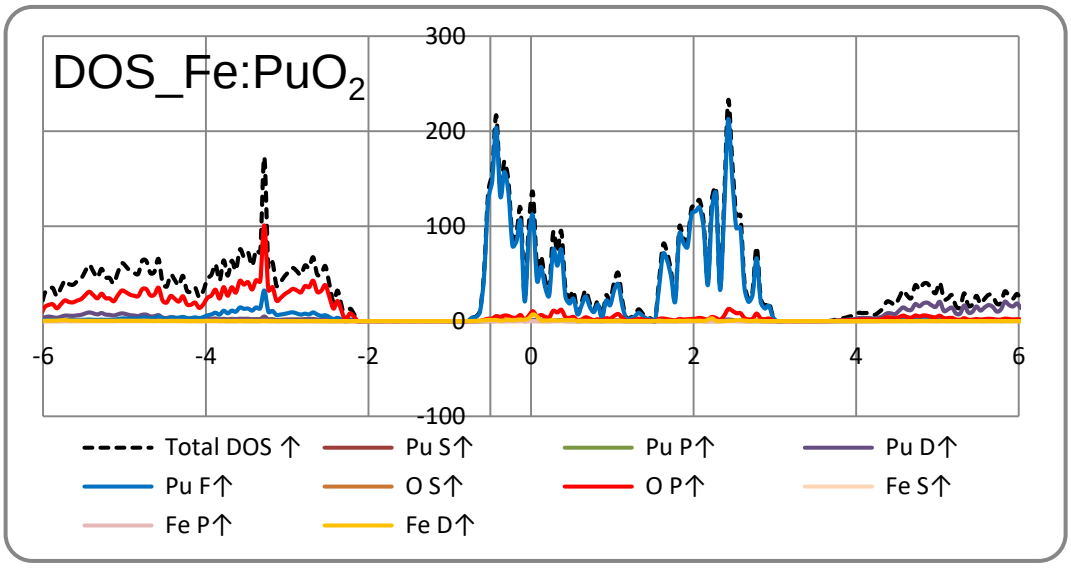

Figure 36: pDOS of Fe impurity in $Pu_{31}O_{64}$ bulk or $Fe:PuO_2$.

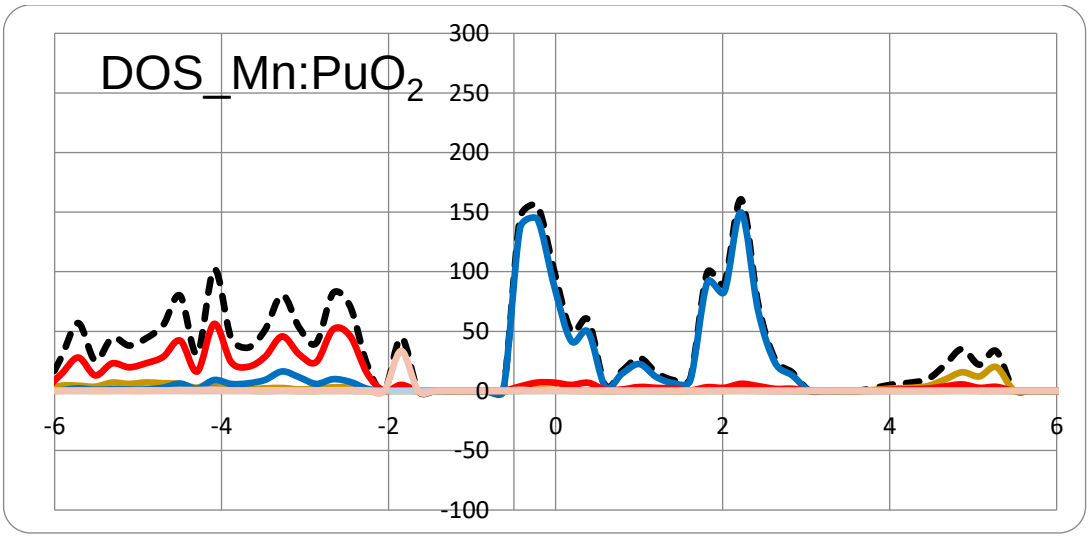

Figure 37: pDOS of Mn impurity in $Pu_{31}O_{64}$ bulk or $Mn:PuO_2$.

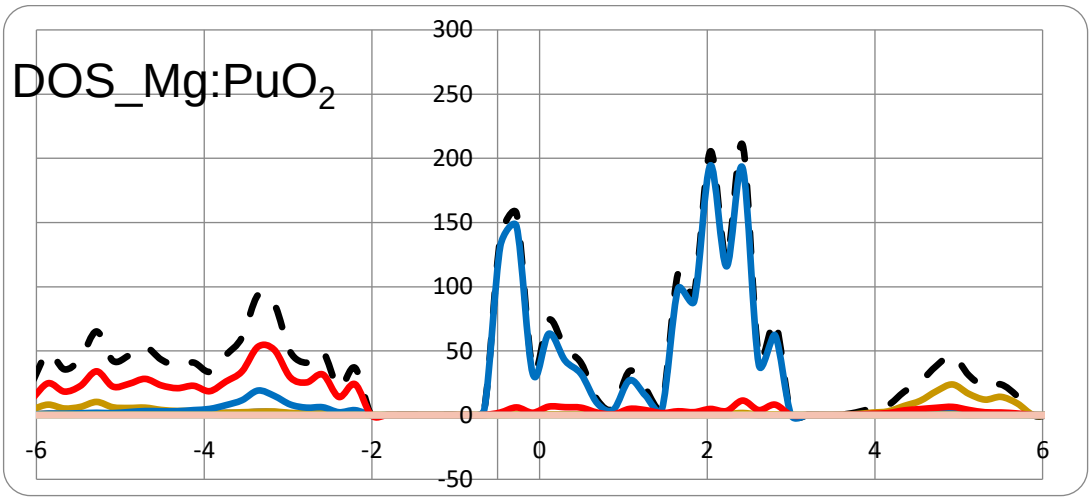

Figure 38: pDOS of Mg impurity in $Pu_{31}O_{64}$ bulk or $Mg:PuO_2$.

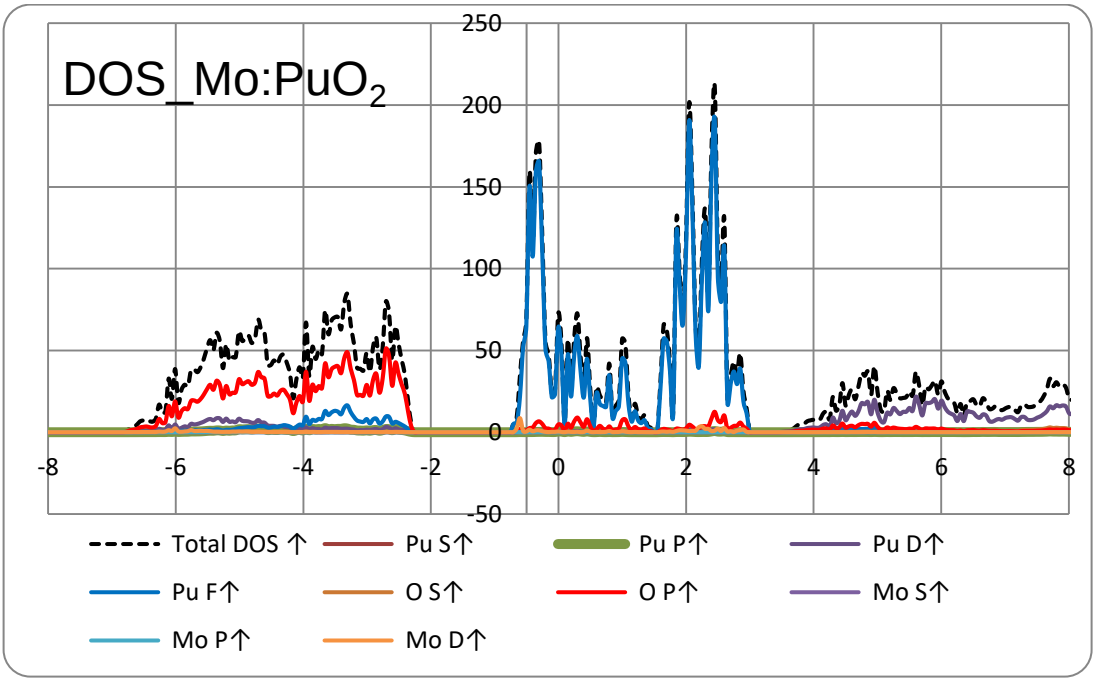

Figure 39: pDOS of Mo impurity in $Pu_{31}O_{64}$ bulk or $Mo:PuO_2$.

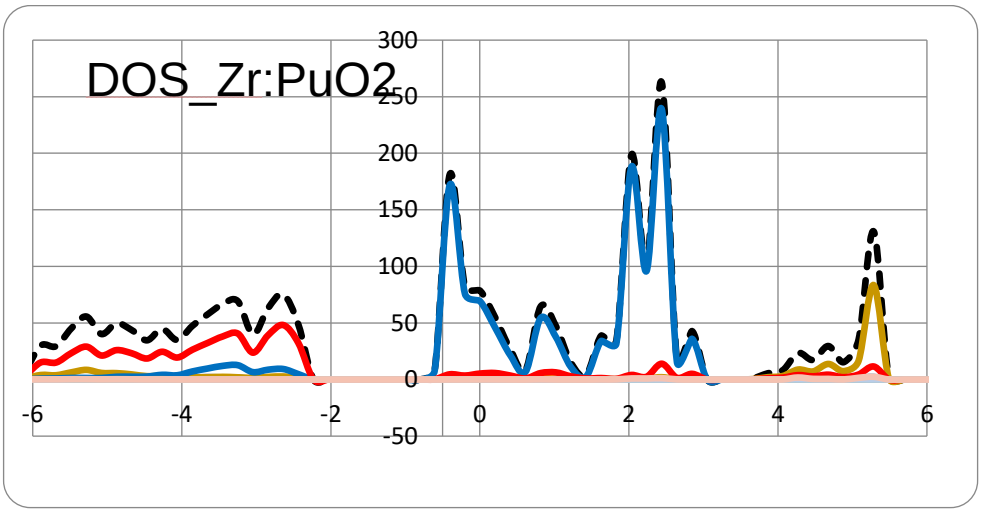

Figure 40: pDOS of Zr impurity in $Pu_{31}O_{64}$ bulk or $Zr:PuO_2$.

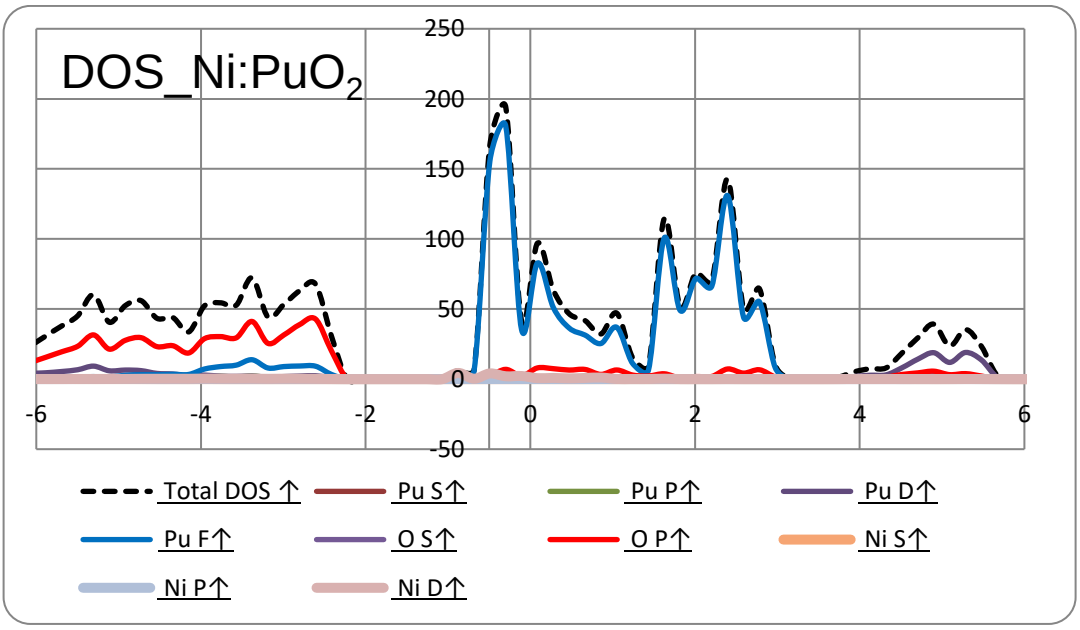

Figure 41: pDOS of Ni impurity in $Pu_{31}O_{64}$ bulk or $Ni:PuO_2$.

There are occupied f-orbit activity just below the fermi energy in the conduction band with the addition of the impurity. This may indicate that these have semi-conducting properties.

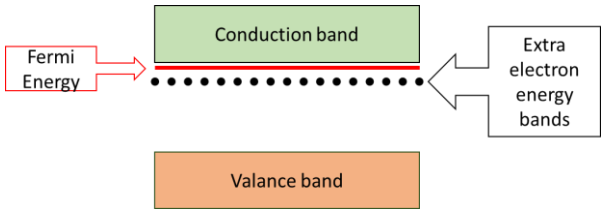

Figure 42. defect band for doped semiconductors.

Because the impurity's effort to take a lattice position of a Pu atom, there may be electrons that are essentially 'extras' and those electrons has pushed away to a higher energy-level and thus less strongly bounded to the location. These are therefore not in the valance band but also not fully in the conduction band.

The same impurity in an oxygen vacancy subtly yet significantly changes the dynamics.

Table 16: For each metal impurity with and without defects. Within DFT, bottom of conduction has bands.

System*	F (bottom)	Ratio $F_b/F_{valance}$	Ratio F_b/T_{val}	With 1 O vacancy	F (bottom)	Ratio $F_b/F_{valance}$	Ratio F_b/T_{val}
Pu	59.67	0.71	0.14	$PuO_2 - O$	77.93	0.76	0.18
Ni	57.25	0.73	0.14	Ni-O	66.67	0.77	0.16
Cr	73.89	0.78	0.18	Cr-O	61.42	0.76	0.15
Mo	53.59	0.73	0.13	Mo-O	45.71	0.70	0.11
Mn	79.47	0.78	0.14				
Mg	77.08	0.78	0.16				
Fe^{I}	69.90	0.77	0.16	Fe-O	59.31	0.74	0.14
Zr	58.93	0.75	0.13				

The amount at the bottom of the conduction level reduced with the exception of Ni with the addition of one oxygen vacancy. Addition of impurity of Ni did reduce the volume of the unit cell.

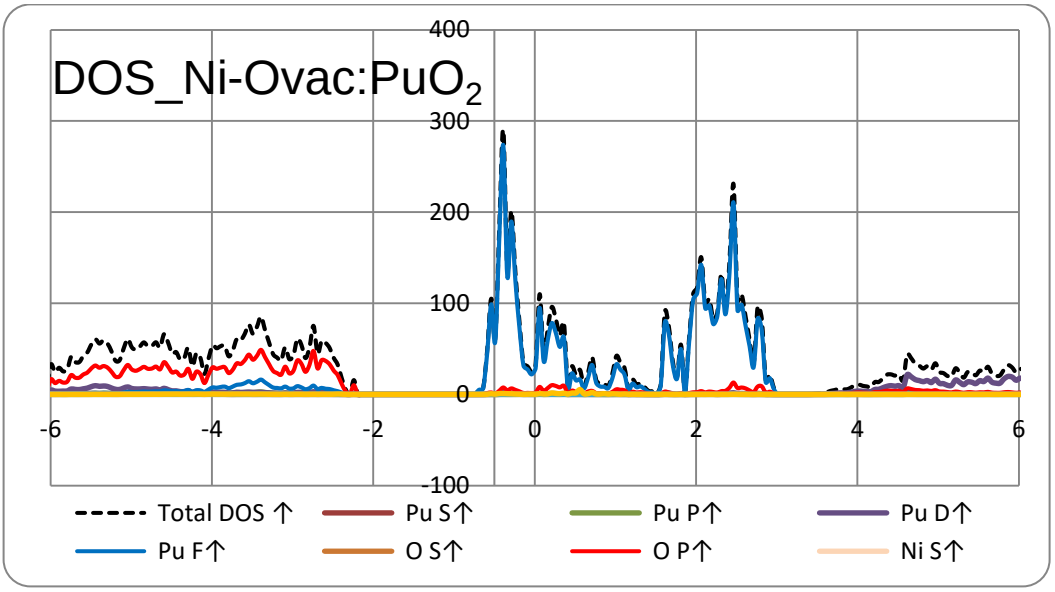

Figure 43: pDOS of Ni impurity and oxygen vacancy. Ni-O:PuO_2

Other transition metal impurities within a Unit cell of Pu-31, O-63 (this introduces a single O vacancy close to the impurity).

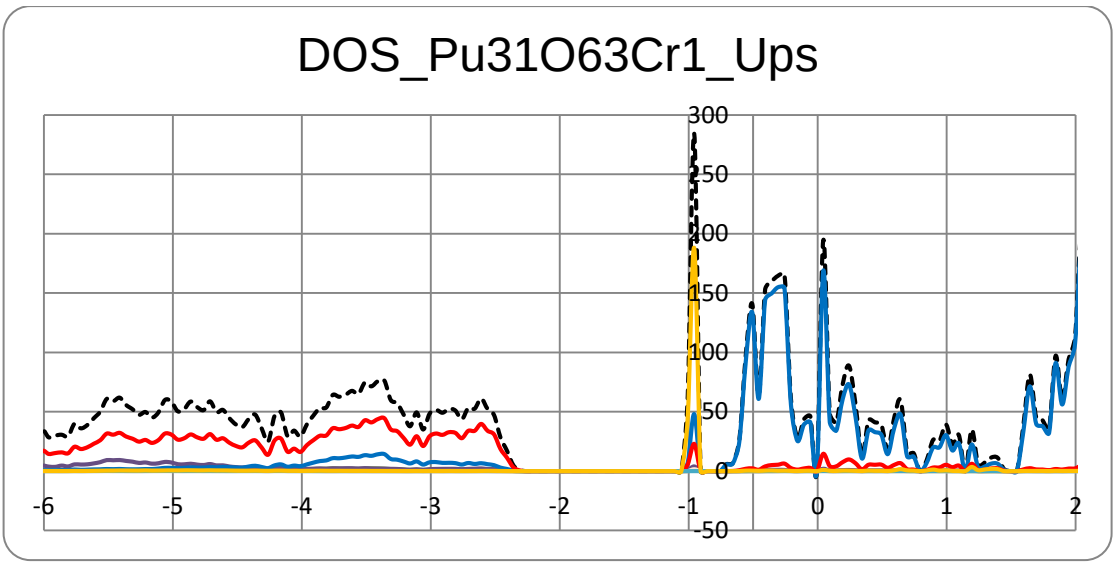

Figure 44: pDOS of Cr impurity and oxygen vacancy. Cr-O:PuO_2.

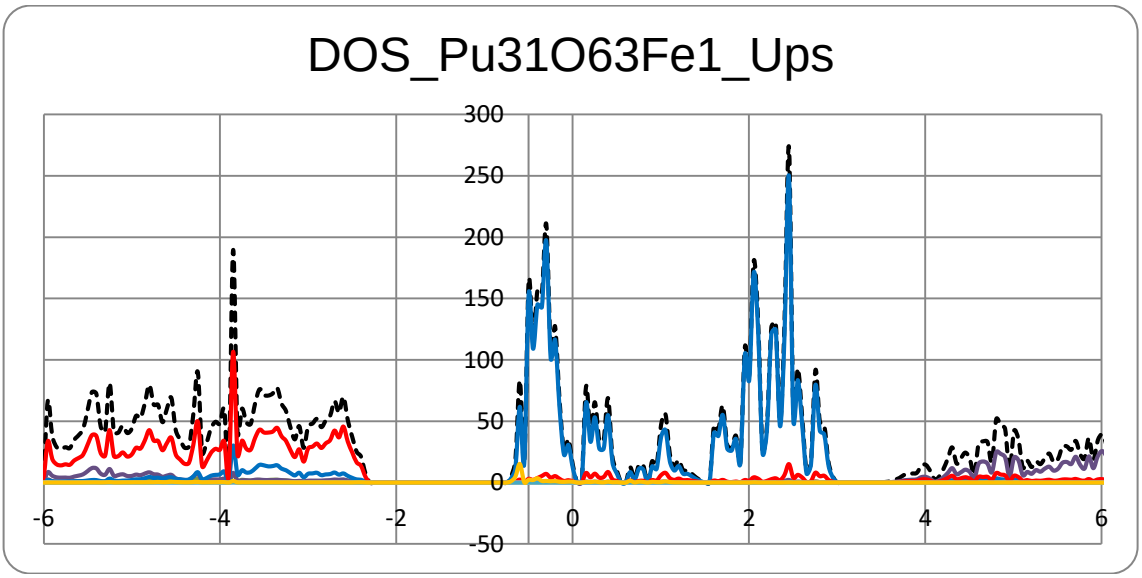

Figure 45: pDOS of Fe impurity and oxygen vacancy. Fe-O:PuO2

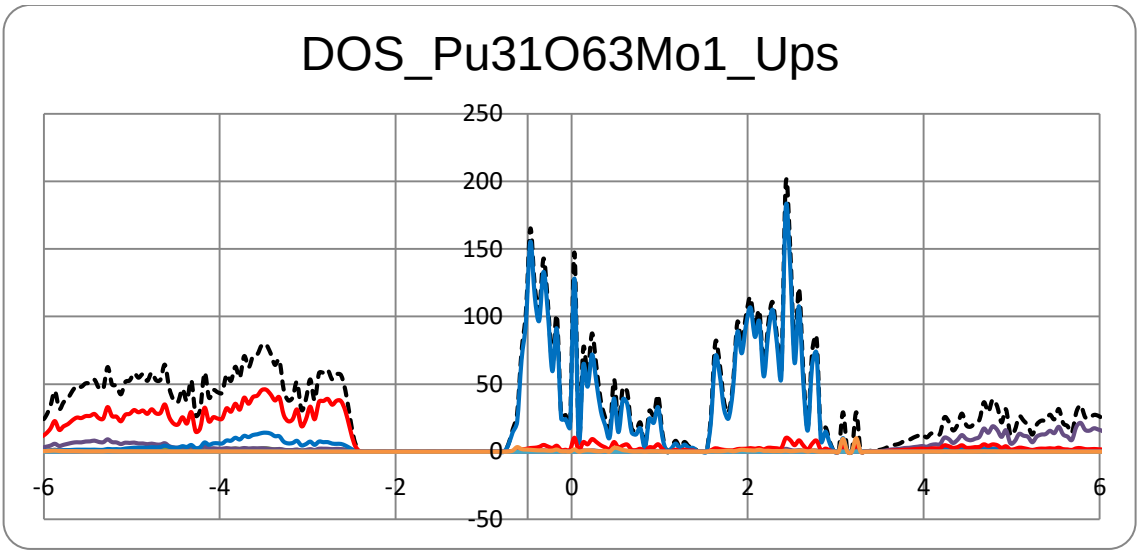

Figure 46: pDOS of Mo impurity and oxygen vacancy. Mo-O:PuO2

References

1. Mian Z, Glasser A. 2015 Fissile Materials Report: Nuclear Weapon and Fissile Material Stockpiles and Production. In: *Global Fissile Material REPORT 2015. Nuclear Weapon and Fissile Material Stockpiles and Production.* New York: NPT Reveiw conference; 2015.
2. Haschke JM, Allen TH, Stakebake JL. Reaction kinetics of plutonium with oxygen, water and humid air: moisture enhancement of the corrosion rate. *J Alloys Compd*. 1996;243:23-35. doi:10.1016/S0925-8388(96)02328-6.
3. Zakrajsek JF, Woerner DF, Cairns-Gallimore D, Johnson SG, Qualls L. NASA's Radioisotope Power Systems planning and potential future systems overview. In: *IEEE Aerospace Conference Proceedings*.Vol 2016-June.; 2016:1-10. doi:10.1109/AERO.2016.7500646.
4. J. Haschke and J. Stakebake. *The Chemistry of the Actinide and Transactinide Elements, Chapter 29: Handling, Storage, and Disposition of Plutonium and Uranium*. (Lester R. Morss, Norman M. Edelstein, Jean Fuger, eds.). Springer; 2006.
5. Plutonium. *World Nucl Assoc*. 2017. www.world-nuclear.org.
6. Santini P, Lémanski R, Erdős P. Magnetism of actinide compounds. *Adv Phys*. 1999;48(5):537-653. doi:10.1080/000187399243419.
7. Wang H, Konashi K. LDA+U study of Pu and PuO_2 on ground state with spin–orbital coupling. *J Alloys Compd*. 2012;533:53-57. doi:10.1016/j.jallcom.2012.03.117.
8. Haschke JM. Reaction of Plutonium Dioxide with Water: Formation and Properties of PuO_2+x. *Science* 2000;287(5451):285-287. doi:10.1126/science.287.5451.285.

9. Jomard G, Amadon B, Bottin F, Torrent M. Structural, thermodynamic, and electronic properties of plutonium oxides from first principles. *Phys Rev B*. 2008;78(7):75125. doi:10.1103/PhysRevB.78.075125.

10. Haschke JM, Fauske HK, Phillips AG. Pyrophoric potential of plutonium-containing salt residues. *J Nucl Mater*. 2000;279:127-138. doi:10.1016/S0022-3115(00)00027-1.

11. Haschke JM, Allen TH, Martz JC. Oxidation kinetics of plutonium in air: consequences for environmental dispersal. *J Alloys Compd*. 1998;271-273:211-215. doi:10.1016/S0925-8388(98)00056-5.

12. McNeilly CE. The electrical properties of plutonium oxides. *J Nucl Mater*. 1964;11:53-58. doi:10.1016/0022-3115(64)90120-5.

13. Prodan ID, Scuseria GE, Sordo J a., Kudin KN, Martin RL. Lattice defects and magnetic ordering in plutonium oxides: A hybrid density-functional-theory study of strongly correlated materials. *J Chem Phys*. 2005;123(2005):1-6. doi:10.1063/1.1953427.

14. Wu X, Ray AK. A density functional study of plutonium dioxide. *Eur Phys J B*. 2001;19:345-351. doi:10.1007/s100510170309.

15. Gouder T. Thin layers in actinide research. *J Alloys Compd*. 1998;271-273:841-845. doi:10.1016/S0925-8388(98)00230-8.

16. Boettger JC, Ray a. K. Fully relativistic density functional calculations on hydroxylated actinide oxide surfaces. *Int J Quantum Chem*. 2002;90(4-5):1470-1477. doi:10.1002/qua.10350.

17. Wen XD, Martin RL, Scuseria GE, Rudin SP, Batista ER. A screened hybrid DFT study of actinide oxides, nitrides, and carbides. *J Phys Chem C*. 2013;117(25):13122-13128. doi:10.1021/jp403141t.

18. Petit L, Svane a., Szotek Z, Temmerman WM, Stocks GM. Electronic structure and ionicity of actinide oxides from first principles. *Phys Rev B*. 2010;81(4):45108. doi:10.1103/PhysRevB.81.045108.

19. Martin P, Grandjean S, Ripert M, Freyss M, Blanc P, Petit T. Oxidation of plutonium dioxide: An X-ray absorption spectroscopy study. In: *Journal of Nuclear Materials*.Vol 320.; 2003:138-141. doi:10.1016/S0022-3115(03)00180-6.

20. Sun B, Zhang P, Zhao X-G. First-principles local density approximation + U and generalized gradient approximation + U study of plutonium oxides. *J Chem Phys*. 2008;128(8):84705. doi:10.1063/1.2833553.

21. Jomard G, Bottin F, Geneste G. Water adsorption and dissociation on the PuO_2 (110) surface. *J Nucl Mater*. 2014;451(1-3):28-34. doi:10.1016/j.jnucmat.2014.03.012.

22. Sun B, Liu H, Song H, et al. First-principles study of surface properties of PuO_2: Effects of thickness and O-vacancy on surface stability and chemical activity. *J Nucl Mater*. 2012;426:139-147. doi:10.1016/j.jnucmat.2012.02.029.

23. Jomard G, Bottin F. Thermodynamic stability of PuO_2 surfaces: Influence of electronic correlations. *Phys Rev B*. 2011;84(19):195469. doi:10.1103/PhysRevB.84.195469.

24. Rák Z, Ewing RC, Becker U. Hydroxylation-induced surface stability of AnO2 (An=U, Np, Pu) from first-principles. *Surf Sci*. 2013;608:180-187. doi:10.1016/j.susc.2012.10.002.

25. Gouder T, Seibert a., Havela L, Rebizant J. Search for higher oxides of Pu: A photoemission study. *Surf Sci*. 2007;601(14):L77-L80. doi:10.1016/j.susc.2007.04.259.

26. Colmenares CA, Terada K. The adsorption of carbon dioxide on uranium and plutonium oxides. *J Nucl Mater*. 1975;58(3):336-356. doi:10.1016/0022-3115(75)90125-7.

27. Arima T, Yamasaki S, Inagaki Y, Idemitsu K. Evaluation of thermal properties of UO2 and PuO_2 by equilibrium molecular dynamics simulations from 300 to 2000K. *J Alloys Compd*. 2005;400(1-2):43-50. doi:10.1016/j.jallcom.2005.04.003.

28. Butterfield MT, Durakiewicz T, Prodan ID, et al. A comparison of hybrid density functional theory with photoemission of surface oxides of δ-plutonium. *Surf Sci*. 2006;600(8):1637-1640. doi:10.1016/j.susc.2005.11.051.

29. Rinehart GH. Design characteristics and fabrication of radioisotope heat sources for space missions. *Prog Nucl Energy*. 2001;39(3-4):305-319. doi:10.1016/S0149-1970(01)00005-1.

30. Theil E, Raymond K. Transition-metal storage, transport, and biomineralization. *Bioinorganic*. 1994:1-35.

31. Scerri ER. *The Periodic Table: Its Story and Its Significance.* Oxford University Press; 2007;239-240.

32. Nakamura K, Ogata T, Kurata M. Analysis of metal fuel/cladding metallurgical interaction during off-normal transient events with phase diagram of the U-Pu-Zr-Fe system. In: *Journal of Physics and Chemistry of Solids*.Vol 66.; 2005:643-646. doi:10.1016/j.jpcs.2004.06.073.

33. *D.O.E Standard Stabilization , Packaging , and Storage of Plutonium-Bearing Materials*. U.S. Department of Energy; 2012.

34. IAEA Safety Reports Series. *Safe Handling and Storage of Plutonium*. VIENNA; 1998.

35. Stakebake JL. The storage behavior of plutonium metal, alloys, and oxide. A

review. *J Nucl Mater*. 1971;38(3):241-259. doi:10.1016/0022-3115(71)90054-7.

36. Page AG, Godbole SV, Deshkar S, Babu Y, Joshi BD. AnalYtische Chemie. *Fresenius Z Anal Chem*. 1977;287(4-5):304. doi:10.1007/BF00634504.

37. Landa A, Söderlind P, Turchi PEA. Density-functional study of bcc U-Mo, Np-Mo, Pu-Mo, and Am-Mo alloys. *J Nucl Mater*. 2013;434(1-3):31-37. doi:10.1016/j.jnucmat.2012.11.033.

38. Wang CP, Fang W, Li ZS, Liu XJ. Thermodynamic modeling of the Mg-Pu and Cu-Pu systems. *J Nucl Mater*. 2009;392(3):525-530. doi:10.1016/j.jnucmat.2009.04.017.

39. Hernandez SC, Holby EF. DFT+U Study of Chemical Impurities in PuO_2. *J Phys Chem C*. 2016;120(24):13095-13102. doi:10.1021/acs.jpcc.6b03469.

40. Periodic Table. http://periodictable.com/Properties/A/LatticeConstants.html. Accessed May 5, 2017.

41. Clementi E, Raimondi DL. Atomic Screening Constants from SCF Functions. *J Chem Phys*. 1963;38(11):2686-2689. doi:10.1063/1.1733573.

42. Cordero B, Gómez V, Platero-Prats AE, et al. Covalent radii revisited. *Dalt Trans*. 2008;(21):2832-2838. doi:10.1039/b801115j.

43. Batsanov SS. Van der Waals Radii of Elements. *Inorg Mater Transl from Neorg Mater Orig Russ Text*. 2001;37(9):871-885. doi:10.1023/A:1011625728803.

44. Hu SZ, Zhou ZH, Robertson BE. Consistent approaches to van der Waals radii for the metallic elements. *Zeitschrift fur Krist*. 2009;224(8):375-383. doi:10.1524/zkri.2009.1158.

45. Dirac PAM. On the Theory of Quantum Mechanics. *Proc R Soc A Math Phys Eng Sci*. 1926;112(762):661-677. doi:10.1098/rspa.1926.0133.

46. Slater JC. The theory of complex spectra. *Phys Rev*. 1929;34(10):1293-1322.

doi:10.1103/PhysRev.34.1293.

47. Teller E. On the stability of molecules in the Thomas-Fermi theory. *Rev Mod Phys*. 1962;34(4):627-631. doi:10.1103/RevModPhys.34.627.

48. Kohn W, Sham LJ. Self-consistent equations including exchange and correlation effects. *Phys Rev*. 1965;140(4A). doi:10.1103/PhysRev.140.A1133.

49. Anisimov VI, Zaanen J, Andersen OK. Band theory and Mott insulators: Hubbard U instead of Stoner I. *Phys Rev B*. 1991;44(3):943-954. doi:10.1103/PhysRevB.44.943.

50. Paier J, Marsman M, Hummer K, Kresse G, Gerber IC, Angyán JG. Screened hybrid density functionals applied to solids. *J Chem Phys*. 2006;124(15):154709. doi:10.1063/1.2187006.

51. Perdew JP, Ernzerhof M, Burke K. Rationale for mixing exact exchange with density functional approximations. *J Chem Phys*. 1996;105(22):9982. doi:10.1063/1.472933.

52. Tran F, Blaha P. Implementation of screened hybrid functionals based on the Yukawa potential within the LAPW basis set. *Phys Rev B - Condens Matter Mater Phys*. 2011;83(23):1-13. doi:10.1103/PhysRevB.83.235118.

53. Adamo C, Barone V. Toward reliable density functional methods without adjustable parameters: The PBE0 model. *J Chem Phys*. 1999;110(13):6158. doi:10.1063/1.478522.

54. Blaha P, Schwarz K, Madsen GKH, Kvasnicka D, Luitz J. WIEN2k - An Augmented PlaneWave + Local Orbitals Program for Calculating Crystal Properties. *WIEN2k*. 2010;1.

55. Ma L, Atta-Fynn R, Ray AK. Elemental and mixed actinide dioxides: An Ab initio study. *J Theor Comput Chem*. 2012;11(3):611-629.

doi:10.1142/S021963361250040X.

56. Tasker PW. The stability of ionic crystal surfaces. *J Phys C Solid State Phys*. 1979;12(22):4977-4984. doi:10.1088/0022-3719/12/22/036.

57. Zhang P, Wang B-T, Zhao X-G. Ground-state properties and high-pressure behavior of plutonium dioxide: Density functional theory calculations. *Phys Rev B*. 2010;82(14):144110. doi:10.1103/PhysRevB.82.144110.

58. Jollet F, Jomard G, Amadon B, Crocombette JP, Torumba D. Hybrid functional for correlated electrons in the projector augmented-wave formalism: Study of multiple minima for actinide oxides. *Phys Rev B - Condens Matter Mater Phys*. 2009;80:1-8. doi:10.1103/PhysRevB.80.235109.

59. Gryaznov D, Heifets E, Sedmidubsky D. Density functional theory calculations on magnetic properties of actinide compounds. *Phys Chem Chem Phys*. 2010;12:12273-12278. doi:10.1039/c0cp00372g.

60. Gay JG. Summary Abstract: Surface energies in d-band metals. *J Vac Sci Technol A Vacuum, Surfaces, Film*. 1984;2(2):931. doi:10.1116/1.572482.

61. Boettger J. Persistent quantum-size effect in aluminum films up to twelve atoms thick. *Phys Rev B*. 1996;53:13133-13137. doi:10.1103/PhysRevB.53.13133.

62. Atta-Fynn R, Ray AK. Bulk and surface properties of β-Pu2O3: A theoretical study using DFT with exact exchange for correlated electrons. *Chem Phys Lett*. 2013;583:42-48. doi:10.1016/j.cplett.2013.07.059.

63. McNeilly CE. The electrical properties of plutonium oxides. *J Nucl Mater*. 1964;11:53-58. doi:10.1016/0022-3115(64)90120-5.

64. McCleskey MT, Bauer E, Jia Q, et al. Optical band gap of NpO2 and PuO_2 from optical absorbance of epitaxial films. *J Appl Phys*. 2013;113(1):13515. doi:10.1063/1.4772595.

65. Prodan I, Scuseria G, Martin R. Covalency in the actinide dioxides: Systematic study of the electronic properties using screened hybrid density functional theory. *Phys Rev B*. 2007;76(3):33101. doi:10.1103/PhysRevB.76.033101.

66. Mott NF. The Basis of the Electron Theory of Metals, with Special Reference to the Transition Metals. *Proc Phys Soc Sect A*. 1949;62:416-422. doi:10.1088/0370-1298/62/7/303.

67. Petit L, Svane A, Szotek Z, Temmerman WM. First-principles calculations of PuO_2 +/- x. *Science (80-)*. 2003;301(5632):498-501. doi:10.1126/science.1086505.

68. Perdew JP, Burke K, Ernzerhof M. Generalized Gradient Approximation Made Simple [Phys. Rev. Lett. 77, 3865 (1996)]. *Phys Rev Lett*. 1996;78(7):1396-1396. doi:10.1103/PhysRevLett.78.1396.

69. Monkhorst HJ, Pack JD. Special points for Brillouin-zon integrations. *Phys Rev B*. 1976;13(12):5188-5192. doi:10.1103/PhysRevB.16.1748.

70. Moten SA, Atta-Fynn R, Ray AK, Huda MN. Size effects on the electronic and magnetic properties of PuO_2 (111) surface. *J Nucl Mater*. 2016;468:37-45. doi:10.1016/j.jnucmat.2015.11.009.

71. Nakamura H, Machida M, Kato M. LDA+U Study on Plutonium Dioxide with Spin-Orbit Couplings. *Nucl Sci Technol*. 2011;2:16-19. doi:10.15669/pnst.2.16.

72. Ao B, Lu H, Qiu R, et al. First-Principles Energetics of Some Nonmetallic Impurity Atoms in Plutonium Dioxide. *J Phys Chem C*. 2015;119(27):14879-14889. doi:10.1021/acs.jpcc.5b02276.

73. Aykol M, Wolverton C. Local environment dependent GGA+U method for accurate thermochemistry of transition metal compounds. *Phys Rev B - Condens Matter Mater Phys*. 2014;90(11):1-18. doi:10.1103/PhysRevB.90.115105.

74. Huda MN, Ray AK. Molecular hydrogen adsorption and dissociation on the plutonium (111) surface. *Phys Rev B*. 2005;72(8):85101. doi:10.1103/PhysRevB.72.085101.

75. Sarsfield MJ, Taylor RJ, Puxley C, Steele HM. Raman spectroscopy of plutonium dioxide and related materials. *J Nucl Mater*. 2012;427(1-3):333-342. doi:10.1016/j.jnucmat.2012.04.034.

76. Konashi K, Matsui H, Kawazoe Y, Kato M, Minamoto S. Defect Structure of Nonstoichiometric Plutonium Oxide. *J Phys Soc Japan*. 2006;75(Suppl):143-145. doi:10.1143/JPSJS.75S.143.

77. Haschke JM, Ricketts TE. Adsorption of water on plutonium dioxide. *J Alloys Compd*. 1997;252(1-2):148-156. doi:10.1016/S0925-8388(96)02627-8.

78. Principles of General Chemistry. *web*. 2017. http://2012books.lardbucket.org/books/principles-of-general-chemistry-v1.0/s27-01-general-trends-among-the-trans.html. Accessed March 1, 2017.

79. Aidhy DS, Liu B, Zhang Y, Weber WJ. Chemical expansion affected oxygen vacancy stability in different oxide structures from first principles calculations. *Comput Mater Sci*. 2015;99:298-305. doi:10.1016/j.commatsci.2014.12.030.

Biographical Information

Shafaq Amdani Moten received her Bachelor of Science with Honors from the University of Texas at Arlington and Master of Science from Northern Illinois University. She also received her Doctor of Philosophy in Physics and Applied Physics, with a concentration in Condensed Matter Physics with application in the Nuclear Material from the University of Texas at Arlington in May 2017.

Dr. Moten is a member of a number of professional and student organizations, including the American Physical Society (APS), Women in Physics (WIP) and the Physics Graduate Student Association (PGSA), of whom she is a founding officer. She is a recipient of the Dean's Award for Outstanding Poster in Physics and the DOE's Science Graduate Fellowship. She is an active member of Center for The Integration of Research, Teaching and Learning (CIRTL) and has completed the Associate level of achievement. More recently, Dr. Moten led a semester long learning community entitled "Strategies for Creating Effective Learning Communities in the Classroom."

Dr. Moten comes from a close-knit family. Her brief foray into managerial work within an HVAC organization convinced her that further studies in alternative energy are her passion. She particularly enjoys teaching and has taught at the Naperville, IL independent school district as a teacher's assistant for special needs in variety of subject matters, as well as college courses in physics at the University of Texas at Arlington. Her current goal is to delve into practical alternative energy sources and focus on a field that works toward a safer nuclear future.